ADDIS ABEBA UNIVERSITY

COLLEGE OF NATURAL SCIENCES

SCHOOL OF EARTH SCIENCES

GEOCHEMICAL INVESTIGATION OF THE BIMODAL VOLCANIC SUITE AT THE WESTERN AFAR MARGIN: THE CASE OF SHEWA ROBIT MARGINAL GRABEN, NORTHERN SHEWA, CENTRAL ETHIOPIA

By:

Kiflom Mulu Gebremeskel

Advisor: Professor Dereje Ayalew

Co-Advisor: Professor Asfawossen Asrat

A Thesis Submitted to School of Earth Sciences of Addis Ababa University for the Partial Fulfillment of the Requirements for the Degree of Masters of Earth Sciences in Geochemistry.

December 2020

ADDIS ABABA, ETHIOPIA

ADDIS ABABA UNIVERSITY

COLLEGE OF NATURAL SCIENCES

SCHOOL OF EARTH SCIENCES

GEOCHEMICAL INVESTIGATION OF THE BIMODAL VOLCANIC SUITE AT THE WESTERN AFAR MARGIN: THE CASE OF SHEWA ROBIT MARGINAL GRABEN, NORTHERN SHEWA, CENTRAL ETHIOPIA

By;

Kiflom Mulu Gebremeskel

Advisor: Professor Dereje Ayalew

Co-Advisor: Professor Asfawossen Asrat

A Thesis Submitted to School of Graduate Studies of Addis Ababa University for the Partial Fulfillment of the Requirements for the Degree of Masters of Earth Sciences in Geochemistry.

December 2020

ADDIS ABABA, ETHIOPIA

ADDIS ABABA UNIVERSITY

COLLEGE OF NATURAL SCIENCES

SCHOOL OF EARTH SCIENCES

GEOCHEMICAL INVESTIGATION OF THE BIMODAL VOLCANIC SUITE AT THE WESTERN AFAR MARGIN: THE CASE OF SHEWA ROBIT MARGINAL GRABEN, NORTHERN SHEWA, CENTRAL ETHIOPIA

By:

Kiflom Mulu Gebremeskel

Approved by Examining Committee:

Dr. Balemwal Atnafu	_____	_____
Head, School of Earth Sciences	Signature	Date
Prof. Dereje Ayalew	_____	_____
Advisor	Signature	Date
Prof. Asfawossen Asrat	_____	_____
Co-Advisor	Signature	Date
_____	_____	_____
Examiner	Signature	Date
_____	_____	_____
Examiner	Signature	Date

I hereby declare that the thesis entitled “Geochemical investigation of the bimodal volcanic suite at the Western Afar Margin: the case of Shewa Robit marginal graben, northern Shewa, central Ethiopia**”** is my original work prepared for the partial fulfillment of the Degree of Master of Science in the graduated School of Earth Sciences, Addis Ababa University during 2020 under the supervision of Prof. Dereje Ayalew and Prof. Asfawossen Asrat. Further, I assure you that this work is not presented and published anywhere else and all the used sources are well referenced and acknowledged.

Kiflom Mulu _____ _____

Signature Date

This is to certify that the above declaration made by the candidate is correct to the best of my knowledge.

Prof. Dereje Ayalew _____ _____

Signature Date

Prof. Asfawossen Asrat _____ _____

Signature Date

Abstract

The study area, Shewa Robit, is situated in the southern end section of the Western Afar Margin. It is located approximately 222 Km northeast of Addis Ababa. In this study, field, petrological and geochemical (major and trace elements) data of the volcanic rocks from the Shewa Robit area are presented and integrated to understand their petrogenesis. The main lithological units of the study area are lower basalt, glassy rhyolite, porphyritic rhyolite, rhyolitic ignimbrite, unwelded tuff and upper basalt. The petrographic study shows that the mafic volcanic products are characterized by aphyric to porphyritic textures with the plagioclase dominant phenocryst, whereas the felsic rocks are dominated by quartz and K-feldspar (sanidine) phenocrysts and glassy groundmass. The geochemical analysis results indicate that the Shewa Robit volcanic rocks are bimodal in composition with a significant compositional gap (between 52.75 and 69.8 wt. % SiO_2) between the mafic and felsic members. It comprises a rock type, including basalts, trachy-basalts (Hawaiite), basaltic-andesite and rhyolites. The mafic volcanic rocks are olivine to quartz tholeiitic whereas the silicic rocks are metaluminous and peralkaline rhyolites. Trace element ratios of the mafic samples show some crustal contamination on samples from the lower basalts. Moreover, the investigated mafic samples from the study area exhibit trace element ratios such as Nb/U (36-48.3), Zr/Nb (6-9.69), Ba/La (11.39-18.31), La/Nb (0.93-1.13) and Ba/Nb (12.3-20.7) and suggest that these lavas are derived from mantle source similar to OIB-type sources. Furthermore, mafic rocks of the volcanic suite are characterized by low CaO/Al_2O_3 ratios (0.47-0.72), enrichments at Ba, depletions at K and flat HREE patterns (Tb_N/Yb_N = 1.55-2.08). These major and trace element data indicate that basalts from the Shewa Robit area were derived from the melting of amphibole-bearing spinel peridotite source. Moreover, mafic and felsic rocks of the studied area are proved to be genetically related by the fractional crystallization process. The variations in major and trace element concentrations and petrographic studies indicate that fractionation of olivine, clinopyroxene, plagioclase, K-feldspar, apatite and Fe-Ti oxide or opaque minerals occurred during the evolution of the Shewa Robit bimodal basalt - rhyolite volcanic suite.

Keywords: Petrogenesis, Western Afar Margin, Bimodal volcanic rocks, Fractional crystallization

Acknowledgment

I would like to express my deepest gratitude to Woldia University for sponsoring me to attend my MSc program at Addis Ababa University. I am also thankful to Addis Ababa University, School of Earth Sciences, for delivering the required knowledge for the requirements of the degree of masters in geochemistry.

My sincere and heartfelt gratitude goes to my advisors Professor Dereje Ayalew and Professor Asfawossen Asrat for their close guidance, limitless support, valuable advice, encouragement, constructive comments and suggestions throughout the research work. I would like to thank them again for their support in suggesting and providing valuable reference materials and their friendly approach during my research work.

My deepest gratitude also goes to all my close friends who I could not mention enough here. Their constant encouragement, expertise and moral support helped me a lot to carry out the successful completion of my research work. My gratitude also goes to the Australian Laboratory Service (ALS) and Addis Ababa University petrographic laboratory professionals (Mr. Wendwossen Sisay) for geochemical data and thin section preparation.

Words cannot express my deepest thanks and gratitude to my parents for giving me the courage and unforgettable support.

Though last but not least I am extremely thankful to the people of Shewa Robit and Debre Sina locality for their hospitality, respectfulness and willingness to give me necessary information during the fieldwork.

Table of Contents

List of Figures

List of Tables

List of Acronyms

ALS	Australian Laboratory Science
a.s.l	Above Mean Sea Level
CFB	Continental Flood Basalt
CIPW	Cross, Iddings, Pirsson and Washington
DEM	Digital elevation model
EARS	East African Rift System
Fig.	Figure
GCDKit	Geochemical Data Kit
GPS	Global positioning system
HFSE	High field strength elements
HREE	Heavy rare earth element
HT1	High Titanium one
HT2	High Titanium two
ICP-AES	Inductively coupled plasma atomic emission spectrometry
ICP-MS	Inductively coupled plasma mass Spectrometry
LILEs	Large Ion lithophile elements
LIPs	Large igneous provinces
LOI	Loss on ignition
LREE	Light rare earth elements
LT	Low Titanium
ME-4ACD81	Multi-element four acid digestion 81
MER	Main Ethiopian rift
MORB	Mid-oceanic ridge basalt
MREE	Medium Rare earth element
NW	Northwestern
OIB	Ocean island basalt
PM	Partial melting
PPL	Plane polarized light

Ppm	Parts per million
REE	Rare earth element
TAS	Total Alkali-Silica
Vol. %	Volumetric percentage
WAM	Western Afar Margin
Wt. %	Weight percent
XPL	Cross polarized light

CHAPTER ONE

INTRODUCTION

1.1 Background

The Ethiopian volcanic province is located at the northern end of the East African Rift System (EARS) (Rooney et al., 2017). It is one of the youngest large igneous provinces (LIPs) on Earth, consisting mainly of flood basalts with a total area of ca. 600,000 km^2 (Mohr, 1983)**.** The lava of the province is thought to have commenced at 45 Ma in the southwestern part (George et al., 1998). Since then, volcanism has occurred almost continuously in the region and the event has been subdivided into different main stages (Peccerillo et al., 2003, 2007). Based on their age, lithology and frequency of volcanic activity, the Ethiopian Cenozoic volcanic province has been generally subdivided into Main Ethiopian Rift (MER), Afar and rift-bounding plateaus (NW, SW and SE plateaus) (Hart et al., 1989; Fig. 1.1).

The volcanic suites in most parts of the northwestern (NW) Ethiopian plateau are bimodal basalt–rhyolite (ignimbrite) with predominantly basalt in composition (Dereje Ayalew and Gezahegn Yirgu, 2003; Dereje Ayalew, 2011). Lavas with such a bimodal compositional distribution are typical of igneous rocks of almost all continental rifts (e.g. Trua et al., 1999; Peccerillo et al., 2003). In most of the continental flood basalt (CFB) provinces (e.g. Karoo, Parana´, Deccan), basalts and rhyolites are genetically linked either through fractional crystallization (FC) combined with varying amounts of crustal assimilation or through partial melting (PM) of underplated basaltic magmas (Dereje Ayalew et al., 2002 and references therein). The origin of the silicic rocks (rhyolites/ignimbrites) in the Ethiopian volcanic province is commonly attributed to fractional crystallization of basaltic magmas with limited crustal contamination (e.g. Gibson, 1972; Barberi et al., 1975; Walter et al., 1987; Gasparon et al., 1993; Boccaletti et al., 1995; Dereje Ayalew et al., 2002). However, a two-stage model involving small degrees of partial melting (PM) of a basaltic underplate to produce the least-differentiated silicic magmas, which in turn undergo moderate degrees of fractional crystallization (FC) to generate the most-evolved silicic rocks has been proposed for the genesis of the Asela-Ziway pantellerites in the MER by Trua et al., (1999).

The present study area is situated in the southernmost part of the Western Afar Margin (WAM). The WAM represents a region of a major fault zone, separating the Afar Depression from the

Ethiopian Plateau. It marks a drastic reduction in topography from ~3000 m to ~100 m (Mohr, 1983) and in crustal thickness from ca. 40 km down to 23-16 km (Hammond et al., 2011). Volcanic rocks along the WAM are also represented by bimodal composition, ranging in age from Oligocene (pre-rift) to Miocene (syn-rift) (Dereje Ayalew et al., 2006, 2018). The volcanic rocks are related to different rifting episodes that occurred during the continental rifting of the region (Ukstins et al., 2002; Wolfenden et al., 2005). They display a younging trend from the northern (Oligocene) to the southern (Miocene) part of the margin, suggesting that the focus of the magmatism has shifted south-ward (Ukstins et al., 2002; Wolfenden et al., 2005). The present study focuses on the bimodal volcanic rocks of the Shewa Robit area from the southernmost of WAM to evaluate their petrogenesis through the integration of petrographic and geochemical data investigations.

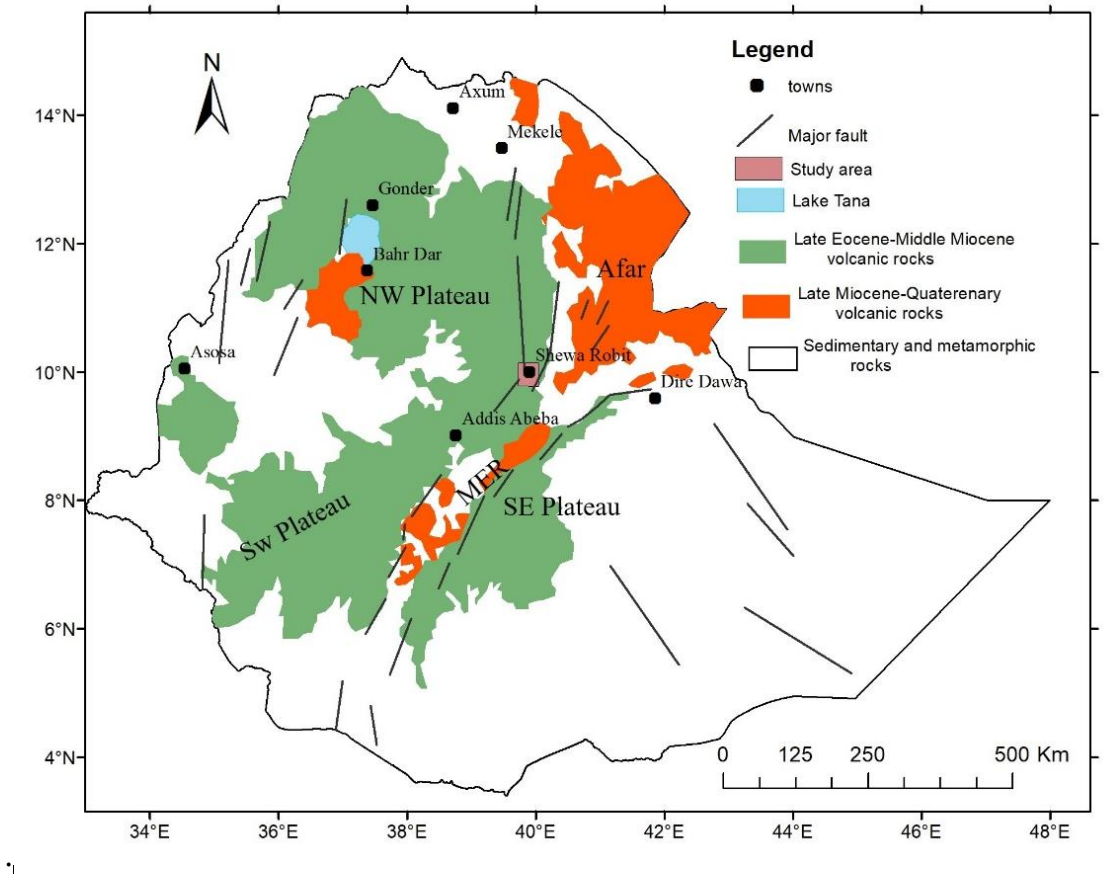

Fig. 1.1: Distribution of main Cenozoic volcanic provinces in Ethiopia (modified after Abbate et al., 2015 and Williams, 2016).

1.2 General Description of the Study Area

1.2.1 Location

The study area is located around Shewa Robit about 222 km northeast of Addis Ababa in the central part of the country within the Northern Shewa Zone of Amhara Regional State. It is situated in the southernmost section of the Western Afar Margin and falls in the Were Illu and Debre Birhan Ethiopian map sheets. Geographically, it is bounded between 1084000 to 1119000N latitudes and 0584000 to 0614000E longitude.

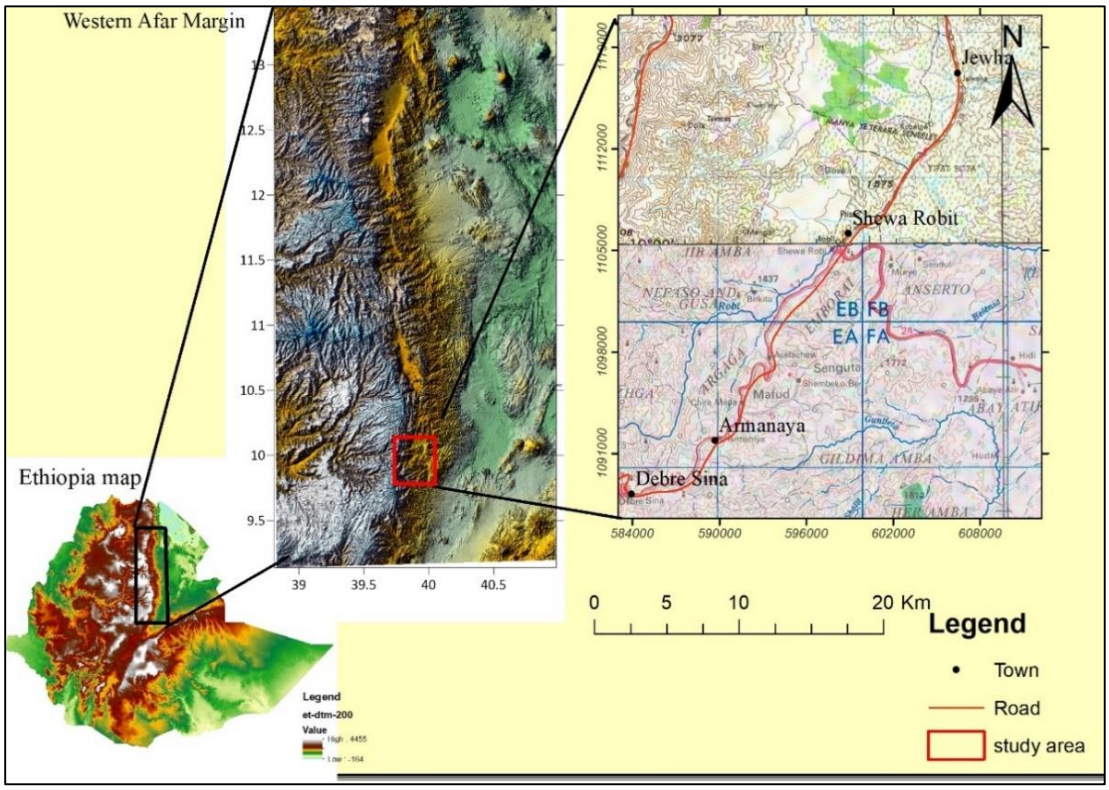

Fig. 1.2: Location map of the study area. The physiographic map of Ethiopia and the western Afar margin is also shown.

1.2.2 Accessibility

The study area can be accessed by a major asphalted road which is running from Addis Ababa through Debre Birhan-Shewa Robit to Dessie. Debre Sina and Shewa Robit are small towns located within the studied area along Addis Ababa-Debre Birhan-Shewa Robi asphalted road at 190 km and 222 km away from Addis Ababa, respectively. All-weather gravel roads branching

from this main road going to Sefed Meda, Agam Ber, Yelen and Kobo and footpaths that connect the surrounding villages to Shewa Robit town are important to visit areas of interest.

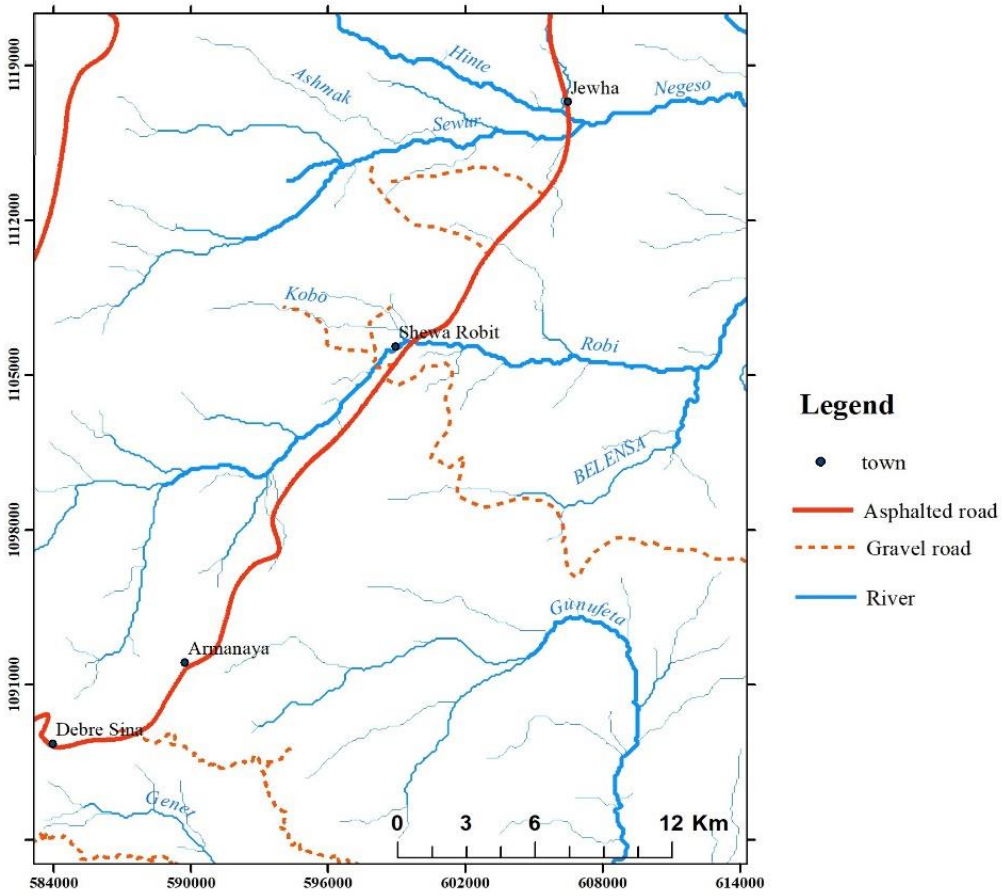

Fig. 1.3*:* Accessibility and drainage map of the study area

1.2.3 Physiography and Drainage pattern

The study area is situated between the central Ethiopia plateau and the Afar Depression. It is characterized by different topographic features such as ridges, hills and flat surfaces formed as a result of the tectonic and volcanic activities (Fig. 1.4). The northwestern and western parts of the study area are mainly characterized by their ridge and hill forming topographic features whereas the central including Shewa Robit town and eastern parts of the study area have relatively flat topographic features. The elevation in the area varies from about 1200 m a.s.l. at the floor of the basin to 3400 m a.s.l. at the peak of the mountain surface.

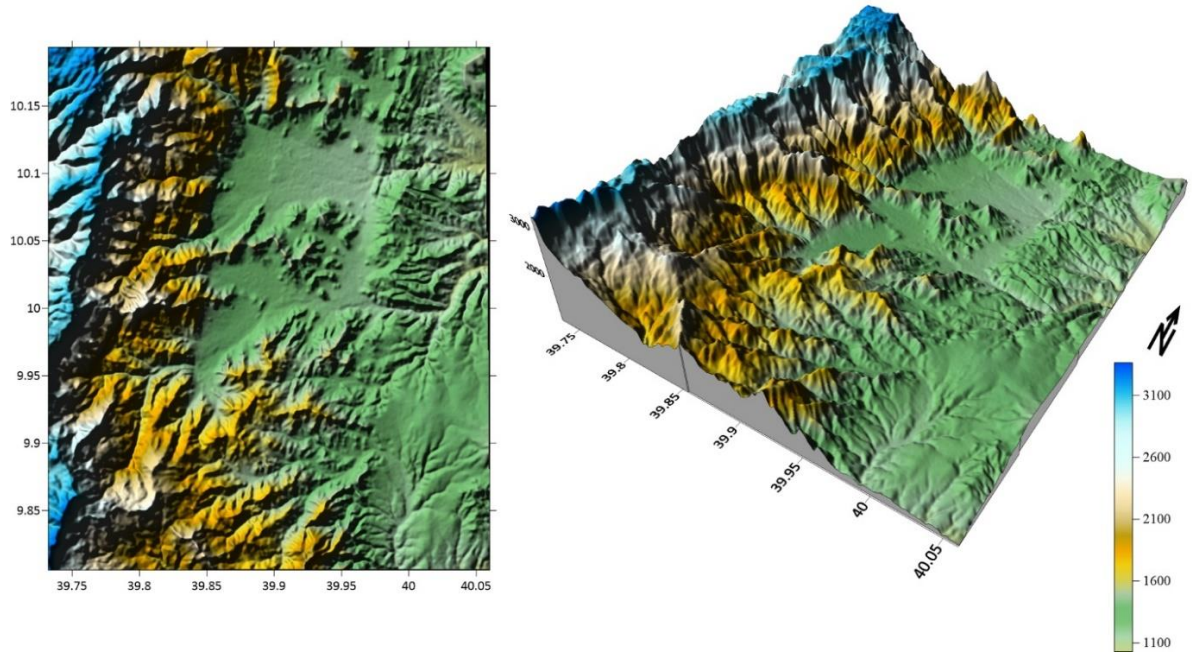

Fig. 1.4: Physiographic map of the study area

The study area is drained by Negeso, Robi, Birkitu, Gunufeta, Jewaha and Sewur main rivers and other small tributaries. All of the main rivers in the area flow towards the east direction of the study area starting from the eastern end of the plateau and show a variation of water flow density due to seasonal variation of the metrology. With the exceptions of Robi and Sewur main rivers, nearly all streams, are seasonal which are filled by water only on the rainy season. Generally, the area is characterized by a dendritic type of drainage pattern (Fig. 1.3).

1.2.4 Climatic Condition

The climate condition of the study area varies from tropical in the western highland to arid in the eastern lowland. The climatic condition of an area is mainly expressed by average temperature and average precipitation. According to Climate-Data.org (https://en.climate-data.org/africa/ethiopia/amhara/shoa-robit-31824/), the study area receives its highest rainfall during the summer season, whereas the least amount of rainfall occurs during the winter season in November. During November the area receives rainfall of about 26 mm on an annual average and in August the precipitation reaches its peak, with an average of 249 mm. June is the warmest month of the year with an average temperature of 27.0 °C / 80.6 °F and December has the lowest average temperature of the year with 19.7 °C / 67.5 °F.

1.2.5 Vegetation

Vegetation coverage of the study area shows variation from place to place. Lands in the southern, southwestern, western and southeastern parts of the study area are densely covered by different vegetation types, whereas central, northern and northeastern parts are sparsely covered. The most widely distributed types of vegetation in the study area include; Podocarpus (zigiba), Junperous Procera (Tid), Shrubs, Bushes and Eucalyptus (Bahirzaf). Eucalyptus in the study area is planted by individual dwellers for some local uses. Lands in the escarpment are sparsely covered by grass and short trees. In addition to these plants, local people cultivate some types of crops on the flat surface of the region. The common types of crops cultivated in the study area are Teff, Bean, Pea, Barley, Sorghum, and Maize. The dissected gorges rarely contain acacia mixed with grass.

1.3 Statement of Problem

The Ethiopian volcanic province is one of the great interesting areas, as it contains the youngest CFB that provides an opportunity to study volcanism related to all stages of continental rift development (Kieffer et al., 2004). The volcanic products are well exposed and preserved along the western margin of the Afar rift (Ukstins et al., 2002; Dereje Ayalew et al., 2006; Rooney et al., 2013). Thus, to understand the complete tectonic and volcanic evolution of the Afar rift system, several studies have been conducted on the Western Afar Margin (e.g. Black et al., 1972; Zanettin and Justin-Visentin, 1975; Chorowicz et al., 1999; Ukstins et al., 2002; Samson Tesfaye et al., 2003; Wolfenden et al., 2005; Dereje Ayalew et al., 2006, 2018; Samson Tesfaye and Weldai Ghebreab, 2013; Rooney et al., 2013; Stab et al., 2016; Williams, 2016; Zwaan et al., 2019). Most of these works have provided a broad framework for the volcanic and tectonic evolution of the western margin of the Afar Depression. By dividing it into five sections, Wolfenden et al. (2005) have carried out geological and structural investigations on the southernmost section of the Western Afar Margin. However, a better understanding of the petrogenetic processes and the petrology and geochemical characteristics of volcanic rocks from each section of the Western Afar Margin remains obscure due to a lack of detailed studies. Thus, in this study, geological mapping (1:50,000) supported by stratigraphic reconstruction and description of field petrologic associations, and geochemical (whole-rock major and trace element) studies of volcanic rocks of the marginal graben from around the Shewa Robit area is conducted. This geochemical-petrologic study aims to shed light on the petrogenetic evolution of the Western Afar Margin volcanics.

1.4 Objectives

1.4.1 General Objective

The main objective of this study is to determine the geochemical, geological and petrological characteristics of the bimodal basalt-rhyolite (ignimbrite) rock units from the Western Afar Margin around Shewa Robit to constrain their petrogenetic evolution.

1.4.2 Specific Objectives

The specific objectives of this research work include;

- To produce a geological map of the area
- To construct a stratigraphic section of the study area
- To describe the petrography of the rock units
- To analayze the petrogenetic relationship between basalt and rhyolite products
- To compare the two volcanic groups in terms of their geology and geochemistry
- To analayze the elemental composition of the rocks with their implication to determine the source, evolution and genesis of the magma

1.5 Methodology

To reach the objectives of the research mentioned above, both field and laboratory (i.e. petrographical studies and geochemical data analysis) techniques have been utilized. Prior to the actual fieldwork, existing technical reports, journals, case studies, maps and textbooks which are relevant to the current study were thoroughly assessed and collected from different sources. Important information like geology, topography, tectonic setting, climatic condition and accessibility of the study area were extracted from these and other existing data.

1.5.1 Field investigation

Following the collection of these secondary data, a detailed field investigation was performed. During the fieldwork, 1:50,000 scale topographic maps of Shewa Robit and Debre Sina were used as a base map. Field traverses were selected primarily to cover the maximum outcrops. Representative fresh samples for each lithological units encountered in the investigated area were collected. Moreover, a proper lithological description like mineral composition and texture, and detail structural data are recorded during the fieldwork. The GPS recording of each lithological

unit was collected to construct the geological map of the area. Photographs have also been taken at representative structures and outcrop features during the fieldwork.

1.5.2 Petrographic analysis

Samples collected from the study area are prepared for further petrographic and geochemical investigations. The number of samples prepared for the petrographic study selected based on their spatial and lithological variation is fourteen (14). Thin section preparation has been carried out in the School of Earth Science at Addis Ababa University of mineralogy and petrographic laboratory. Thin section preparation involves: rock samples were cut using a diamond embedded rock saw and were mounted to glass slides which are later ground down to a final thickness of 30 microns. Finally, each slide was covered with a cover glass. Thus, these prepared thin sections were thoroughly examined under a Leica petrographic microscope in the same institute at the School of Earth sciences petrology laboratory. From the petrographic study, information of petrogenetic significance such as the modal proportion of minerals, grain size diameters, average grain shapes and grain to grain relationship of the phenocrysts are extracted.

1.5.3 Geochemical analysis

Based on the field and petrographic descriptions, a total of 11 fresh samples were selected for whole-rock geochemical analyses. The sample preparation was carried out at the Australian Laboratory Science (ALS) branch at Addis Ababa, Akaki Kaliti, Ethiopia. During sample preparation, the selected samples were broken by hammer into desirable sizes to remove the weathered part from the surface of the rock samples. Then, the samples were dried, crushed to 70 % less than 2 mm, riffled to split off the bulk samples and the splits were pulverized to 93.3% passing 75 microns. The powdered samples (i.e. sealed and packed) were submitted to the ALS commercial geochemical Laboratory in Ireland to determine their concentration of major and trace elements.

From each of the prepared samples, a 0.2 g sample was added to 0.90 g lithium metaborate ($LiBO_2$) flux, mixed well and fused in a furnace at 1000°C. The melt is then cooled and dissolved in 100 ml of 4 % nitric acid (HNO_3) solution. Finally, the solution is analyzed by Inductively Coupled Plasma Atomic Emission Spectrometry (ICP-AES) for major elements and by Inductively Coupled Plasma Mass Spectrometry 81 (ICP-MS 81) for trace elements. Besides, base metal (Ag, As, Cd,

Co, Cu, Li, Mo, Ni, Pb, Sc, Ti, and Zn) contents of samples were analyzed with ICP-AES using four acid digestion. Furthermore, the loss on ignition (LOI) content of each sample is also determined by; a 1.0 g prepared sample is placed in an oven at 1000°C for one hour, cooled and then weighed. The difference in weight before and after heating the sample gives the LOI value of each sample. Further information on the procedure, precision, accuracy, and detection limits of ICP-AES and ICP-MS 81 analyses in the geochemical laboratory of ALS can be found at www.alsglobal.com.

1.5.4 Data computation and processing

All the data collected from the field and laboratory were organized, analyzed, and interpreted using different software programs such as Microsoft Excel 2013, Surfer-10, Petrographic 2 Beta (version 1.0.2), GCDKit 4.1, Arc Map 10.1 and Global mapper 11. The geochemical data computations such as normative calculations and construction of classification, chemical variation, normalized trace and REE multi-element distribution diagrams are performed using the software Petrographic 2 Beta (version 1.0.2) and Geochemical Data Kit (GCDKit version 4.0). Additionally, some analytical data processing is also carried out in Microsoft Excel 2013 and the compilation has been prepared in Microsoft Word 2013. Moreover, the Geological map and cross-section were produced using Surfer-10, Global mapper-11and Arc Map 10.1.

1.6 Review of Previous Works

A number of geochemical studies have been conducted on the Ethiopian volcanic province (e.g. Davidson & Rex, 1980; Brotzu et al., 1981; Seife Michael Berhe et al., 1987; Ebinger et al, 1993; Hofmann et al., 1997; George et al., 1998; Pik et al., 1998,1999; Dereje Ayalew et al., 1999,2000, 2006, 2016, 2018; Kieffer et al., 2004; Furman, 2007; Daniel Meshesha & Shinjo, 2007). Accordingly, volcanism in Ethiopia began in the southwestern part of the country at about ca. 45 Ma and was followed by voluminous flood basalt activity that occurred in both Ethiopia and Yemen at around 30 Ma (Ebinger et al., 1993; George et al., 1998; Hofmann et al., 1997). Most of the geochemical studies have attributed the Ethiopian flood basalt activity to the impact of the Afar plume (e.g. Natali et al., 2011; Pik et al., 1998, 1999). Volcanism in the northwestern Ethiopian plateau has been subdivided into four-stage (Seife Michael Berhe et al., 1987). In ascending stratigraphic order, these are called the Ashange, Aiba, Alage and Termaber. Furthermore, the modern classifications of the Ethiopian plateau flood basalt were done based on the Ti (TiO2)

concentration (Pik et al., 1998; 1999). It is classified into three magma types: two high-Ti groups (HT1 and HT2) and one low Ti group (LT).

Volcanic rocks along the Western Afar Margin (WAM) are range in age from Oligocene to Miocene (Kieffer et al., 2004; Ukstins et al., 2002; Wolfenden et al., 2005). The volcanic products are represented by both acidic and basic composition (Dereje Ayalew et al., 2006). Dereje Ayalew et al. (2006) have presented geochemical data (major and trace elements; Sr, Nd and O isotopic compositions) on the silicic rocks from the western margin of the Afar depression and attempted to constrain their origin and evolution through time. According to the authors, these silicic rocks are interpreted to have been originated through fractional crystallization of the basaltic magmas during the initial phase of the continental rift. A geochemical investigation on felsic volcanic rocks from the central-western Afar margin and adjacent central Afar has also been done by Dereje Ayalew et al. (2018). Some $^{40}Ar/^{39}Ar$ age data and volcano-stratigraphies of volcanic rocks of the eastern margin of northwestern Ethiopian plateau, from the WAM, are obtained from the work of Ukistins et al., (2002) on their study aimed to correlate continental flood volcanic rocks from Ethiopia and Yemen. Dereje Ayalew & Gibson (2009) have also carried out a geochemical investigation on the bimodal magmatic rocks of the central Ethiopian plateau from Northern Shewa zone.

Moreover, the tectonic and geological studies of the southern Red Sea rift/WAM have been carried out by Wolfenden et al. (2005). They have used both new and existing field, remote sensing, geological and geochronological data to understand the tectonic evolution of the region. Their integrated geochronological and structural data show that the rift formation in the southern Red Sea rift/WAM had commenced by 29 Ma, coeval with the last stage eruption of flood volcanism. The works of Ukistins et al. (2002), Wolfenden et al. (2005) and Dereje Ayalew et al. (2006) also show the presence of a decreasing trend in the age of rift-related volcanism along the WAM region from north to south, suggesting that extension locally propagated southward until ca. 11 Ma. In addition to these, the morphology and geology of the Afar depression and its adjacent margins are also studied by many researchers (e.g. Alebachew Beyene & Mohamed Abdelsalam, 2005; Corti et al., 2015).

Because of its complex tectonic environment, several authors have developed various structural evolution models for the Western Afar Margin (WAM). The earliest model involved erosion of

the plateau margin (Mohr, 1962) or block rollover due to crustal creep (Black et al., 1972). Following this, other authors have proposed that extension in Afar is principally accommodated by large-scale detachment faulting (e.g. Chorowicz et al., 1999; Stab et al., 2016; Samson Tesfaye and Weldai Ghebreab, 2013) or by lithospheric flexure caused by magmatic loading (e.g. Wolfenden et al., 2005). Moreover, Zanettin and Justin-Visentin (1975 as cited in Wolfenden et al., 2005) have proposed a three-stage model for the development of the WAM between 15°30′N and 9°30′N that involved first southward and then eastward tilting faulting. Furthermore, numbers of fault-bounded grabens are identified in the middle of the WAM/Ethiopian escarpment (e.g. Samson Tesfaye and Weldai Ghebreab 2013; Abbate et al., 2015; Williams, 2016; Wolfenden et al., 2005). The name of these basins is not always clearly defined, as several authors give different names for these different basins. According to Williams (2016), the major marginal grabens from north to south are Raya, Kobo, Hayk, Borkena and Robit.

Furthermore, Tigel Belayet al. (2009) and Daniel Meshesha et al. (2010) have carried out regional-wise (1:250,000) geological studies on Were Ilu and Debre Birhan sheets, respectively, wherein the study area is included. As outline above, the most important works about the study area include; Ukistins et al. (2002), Samson Tesfaye et al. (2003), Wolfenden et al. (2005), Dereje Ayalew et al. (2006) and Williams (2016). These works have provided valuable data about lithology, structure and geochronology of the volcanic rocks of the study area. Accordingly, the geology of the area is characterized by Oligocene-Miocene bimodal basalt–rhyolite volcanic succession. The lower basaltic lava is dated at 24.59 ± 0.16 Ma (Wolfenden et al., 2005) and is dominantly overlying by ignimbrite formation which spans ages of at least 19.76 ± 0.07 Ma to 14.90 ± 0.06 Ma (Ukstins et al., 2002).

1.7 Significance of the Research

This petrological and geochemical investigation of the bimodal volcanic rocks of the Shewa Robit area will provide a scientific basis for understanding the detailed tectonic and petrogenetic evolution of the area. This study may also give some understanding of the methodology (petrographic and geochemical studies) followed in this research that will be used as a reference framework for the students and other researchers. Besides, the geological map and the stratigraphic section of the study area will serve as a basic source of data for understanding the geological history (tectonic and petrogenetic evolution) of the study area.

1.8 Thesis Overview

The thesis is composed of six chapters. Chapter one presents general information about the area of study, the objectives and methods followed in the research. In chapter two, the regional geological setting of the Ethiopian volcanic rocks as compared to the study area is discussed. Chapter three deals with a detailed description of the lithology and petrographic of the study area. In chapter four, the geochemical results obtained from this study are described. Chapter five presents the discussion and petrogenetic evolution of the Shewa Robit bimodal volcanic rocks. In chapter six, the conclusions reached by this study are summarized. Moreover, recommendations for further study are also presented in chapter six.

CHAPTER TWO

2 REGIONAL GEOLOGY

2.1 Introduction

The earliest volcanism in the East African rift system (EARS) occurred in southwestern Ethiopia, southeastern Sudan, and northern Kenya at 40-45 Ma (Gezahegh Yirgu et al., 2006 and reference therein). Following this, between 31 and 29 Ma, voluminous continental flood basalt (CFB) volcanism was widespread throughout Ethiopia and Yemen (Baker et al., 1996; Hofmann et al., 1997; Pik et al., 1998, 1999; Kieffer et al., 2004; Dereje Ayalew, 2011). About 90 % product of the CFB volcanism was emplaced in the Ethiopian Plateaus, whereas the rest is located on the eastern part of the Red Sea, within Yemen (Baker 1996; Pik et al., 1998). The eruption of the enormous flood basalt volcanism was coeval with northeast-directed extension in the southern Red Sea and Gulf of Aden (Ukstins et al., 2002; Wolfenden et al., 2005). In Ethiopia, the volcanic sequence rests either directly on metamorphic rocks of Precambrian age or Mesozoic sedimentary sequence (Ukstins et al., 2002; Peccerillo et al., 2003, 2007) with various thickness, reaching 2000 m in northwestern Ethiopia and thinning to ~500 m towards both north and south (Furman, 2007). Its products have been estimated to have covered an area ca. 600,000 km^2, with a total volume of ca. 300,000 km^3 (Mohr, 1983).

Most of the flood basalts and associated felsic rocks in Ethiopia have erupted in a short time interval (<5) with the greatest eruption rates occurring from 31 to 28 (Hoffman et al., 1997; Pik et al., 1998; Ukstins et al., 2002). On the bases of geochemical, geophysical, and volcano-tectonic features, the genesis of the Ethiopian continental flood basalts is widely considered to be related to the Afar mantle plume activity (Hofmann et al., 1997; Pik et al., 1998, 1999; Dereje Ayalew et al., 2002; Kieffer et al., 2004; Natali et al., 2011). The CFB is bimodal in composition and is composed of basaltic lavas together with rhyolitic ignimbrites and pyroclastic-fall deposits, and less common basaltic pyroclastic rocks and rhyolitic lavas (Dereje Ayalew et al., 2002, 2011; Kieffer et al., 2004). Generally, the Ethiopian Cenozoic volcanism is subdivided into two successions: the Trap (Tertiary) and the Aden (middle Miocene to Quaternary) Series (Mohr, 1962). The Trap Series represent the whole pile of the Tertiary flood basalt sequence with intercalation of silicic rocks that are exposed on the northwestern, southwestern and Somali

plateaus. The Aden series represents the volcanic rocks in the MER and Afar regions that range in age from Miocene to Quaternary (Blanford 1870; Mohr 1962).

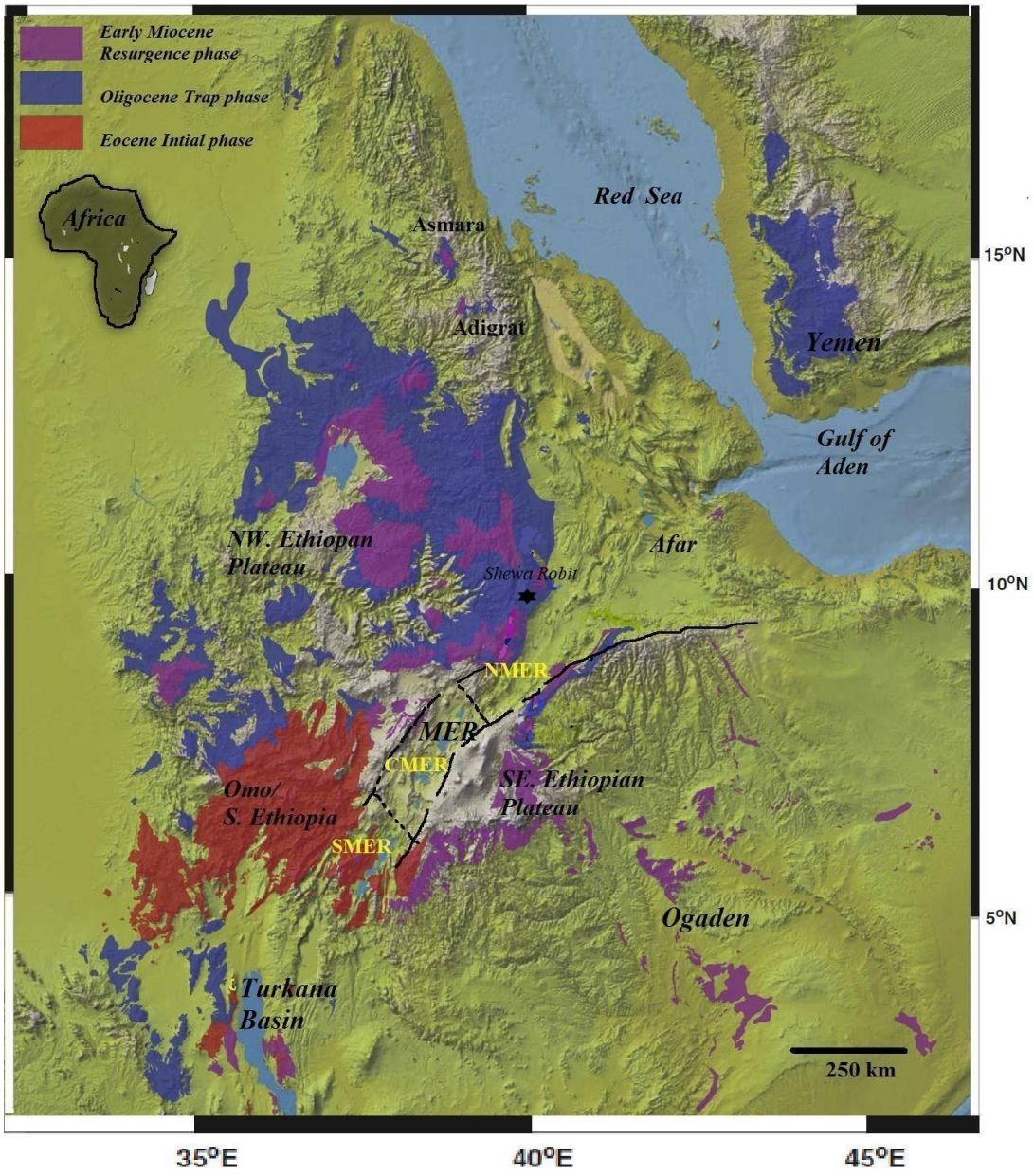

Fig. 2.1: Magmatic activity in Africa and parts of the Arabian Peninsula from 45 to 22 Ma and showing the three broad periods of magmatic activity: (A) Eocene Initial Phase (45–34 Ma), (B) Oligocene Traps phase (~33.9–27 Ma), (C) Early Miocene resurgence phase (26.9 Ma to 22 Ma). (Modified after Rooney, 2017).

Furthermore, the Cenozoic volcanic province of Ethiopia has been categorized into five major provinces based on their lithological development, type of activity, frequency of volcanic centers, and age of eruption (Abbate et al., 2015 and references therein). These are volcanics of the northern plateau, southern plateau, Somali plateau, Afar and Main Ethiopian Rift (MER). The volcanic plateaus (northern, southern and Somali plateaus) together constitute the major part of the Ethiopian volcanic pile (Kieffer et al., 2004; Pik et al., 1998).

2.2 Northwestern Ethiopian Plateau Volcanics

The Northwestern (NW) Ethiopian Plateau is located on the western edge of the tectonically active Main Ethiopian Rift and the Afar Depression (Gani et al., 2007). It is mainly described by Oligocene Pre-rift volcanic rocks overlying by Miocene volcanoes (Mohr and Zanettin, 1988; Pik et al, 1998). In contrast to other typical CFBs (e.g. Deccan, Karoo), the NW plateau flood basalt is composed of several specific volcanic centers that differ both in age and magmatic characters (Kieffer et al., 2004). The flood lava sequence comprises basaltic lava flows, basaltic tuffs, as well as a considerable volume of rhyolitic, trachytic and phonolitic products (Kieffer et al., 2004). Generally, the volcanic succession of the NW plateau is subdivided into Oligocene flood volcanics (Trap Series) comprised of Oligocene – Miocene basalts and rhyolites, the Miocene –Pliocene shield volcanoes, volcanic plugs and domes, and Quaternary volcanic (Kieffer et al., 2004).

Traditionally, the Oligocene – Miocene volcanism of the NW Ethiopian plateau has been subdivided into four stages (Seife Michael Berhe et al., 1987); the First Stage (Ashange, pre-Oligocene), Second Stage (Aiba, 34-30Ma), Third Stage (Alaji, 30-26 Ma) and Fourth Stage (Tarmaber, 25-13Ma). The first three volcanic stages are characterized by the extrusion of flood basalts with inter-beds of pyroclastic rocks of rhyolitic/trachytic compositions while the fourth stage is represented by a central type of eruption. The Ashange basalts are composed of transitional to tholeiitic olivine basalts alternating with subordinate tuffs (Mohr and Zanettin, 1988). The Aiba basalts are a thick cover of flood basalts (200-600m) that erupted unconformably on the Ashange peneplain. The final stage of the flood volcanism, the Alaji series, consists of interbedded layers of aphyric flood basalts and rhyolite (ignimbrite) (Tadiwos Chernet et al., 1998). Compositionally, The Ashange and Aiba series contain dominantly basaltic rocks whereas the Alajae Formation is represented by bimodal rhyolite (ignimbrite) and basaltic volcanism (Mengesha Tefera et al., 1996).

These fissural type volcanics were followed by central type eruptions of alkaline Tarmaber basalts (Kazmin, 1979). This formation represents basaltic shield volcanoes that are emplaced in the Ethiopian plateaus (Mengesha Tefera et al., 1996). They are compositionally bimodal like the flood volcanism and have magmatic similarity with the flood volcanics underlying them, i.e. tholeiitic shields overlie tholeiitic flood basalts and alkaline shields overlie alkaline flood basalts (Kieffer et al., 2004). However, they can be differentiated from the underlying flood volcanics in that they are porphyritic (dominantly plagioclase and olivine), alkaline and enriched in incompatible trace elements (Kieffer et al., 2004).

Furthermore, based on their geochemistry, the Northwestern Ethiopian plateau basalts are classified into three magma types (Pik et al., 1998, 1999): low-Ti basalts (LT), high-Ti1 (HT1) basalts and high-Ti2 (HT2) basalts. They are spatially zoned according to their TiO_2 content (Fig. 2.2). According to the authors, the low-Ti (LT) basalts are predominantly found in the northwestern part of the province and are assumed to be derived from the depleted mantle. They are characterized by relatively flat REE patterns and incompatible trace element concentrations. The High-Ti1 lavas (HT1) constitute the southeastern part of the northwestern Ethiopian plateau and they have trace element compositions intermediate between those of HT2 and LT basalts. The HT2 type of lavas is mainly concentrated in the Lalibela area close to the center of the Afar triangle and represents approximately one-third of the total volume of lavas exposed on the plateau.

2.3 Afar volcanics

The Afar region is a triangular-shaped depression located at the intersection of the Red Sea, Gulf of Aden and the Main Ethiopian Rift (MER) (Wolfenden et al., 2004; Miruts Hagos et al., 2016). Its floor is predominantly covered by volcanic rocks, ranging in age from Miocene to Quaternary (Mohr, 1962; 1983; Mengesha Tefera et al., 1996). Volcanic succession in the Afar region is predominated by basaltic sequences that show a decreasing trend in age and volume from the margin toward the interior of the region (Wolfenden, 2005). Marginal parts of the Afar region are composed of the oldest rock units; Precambrian basement rocks, Mesozoic sediments and Oligocene to Early Miocene basalts belonging to the trap series with minor intercalated silicic units (Alebachew Beyene and Mohamed Abdelsalam, 2005; Mulugeta Alene et al., 2017). The volcanism within the Afar floor has been subdivided into two major stages (Barberi et al. 1975). The first stage that lasted for 20 Mys (from 26 Ma to 6 Ma) includes; the Adolei Basalts, Mabla

Rhyolites, and Dalha Basalts and were formed during the first stage of the continental rifting. The eruption of the Adolei basalts took place in the early Miocene between ~27 and 19 Ma (Barberie et al., 1975), shortly after the initiation of widespread rifting in the Gulf of Aden and the Red Sea (Wolfenden et al., 2004, 2005). The less voluminous phase (the Mabla rhyolites) took place between ~16 and 9 Ma, whereas the Dahla basalts erupted during the late Miocene between 8 and 6 Ma (Lahitte et al., 2003). The second stage volcanism in the Afar region is represented by the Plio-Pleistocene Afar Stratoid Series which covers about two-thirds of the Afar depression (Alebachew Beyene and Mohamed Abdelsalam, 2005). The Afar Stratoid Series are overlaid by the transversal volcanics and marginal rhyolitic centers (<4 Ma), which in turn are followed by the eruption of the Quaternary axial volcanic ranges. Quaternary volcanism in the Afar Depression is mainly confined to magmatic segments within the incipient seafloor spreading zones (Miruts Hagos et al., 2016 and references therein).

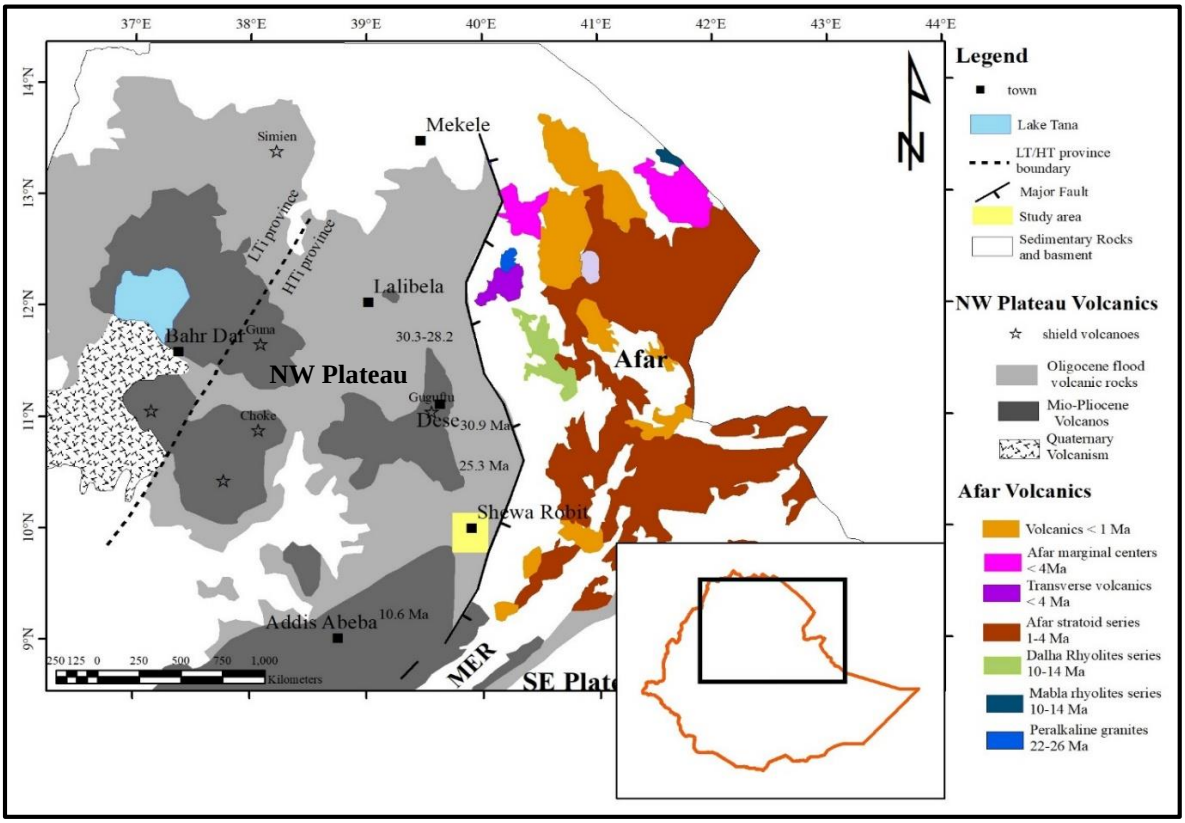

Fig. 2.2: Geological map of the northwestern Ethiopian plateau and the Afar depression with a yellow box showing the location map of the study area. The dividing line between high-Ti and low-Ti basalt province is marked by a dashed line (modified from Dereje Ayalew and Gibson,

2009 and Alebachew Beyene and Mohamed Abdelsalam, 2005). The inset map shows the position of the NW Ethiopian plateau and the Afar region in Ethiopia.

2.4 Geological Setting of the Western Afar Margin

As noted above, the Afar Depression is a triangular-shaped area of rifting at the triple junction between the Nubian, Somalian and Arabian plates (Wolfenden et al., 2004). It is the place where the continental Main Ethiopian Rift and the two oceanic rifts (i.e. Red Sea and the Gulf of Aden rifts) merge forming a rift-rift-rift triple junction. Rift formation in the southern Red Sea had commenced by 29 Ma (Ukstins et al. 2002; Wolfenden et al. 2005), in the whole Gulf of Aden around 34 Ma (Pik et al., 2013 as sited in Dereje Ayalew et al., 2018) and at ca. 18-20 Ma in the Main Ethiopian Rift (Giday WoldeGabriel et al., 1990). In the west, the Afar depression is bordered by the Ethiopian plateau and the fault border formed between these two major domains is widely known as Western Afar Margin (also known as Ethiopian Escarpment) (e.g. Alebachew Beyene and Mohamed Abdelsalam, 2005). The WAM is located west of the present-day location of the triple junction, defining the southernmost end of the Red Sea rift (Wolfenden et al., 2005). The margin marks a physiographic decrease from 3000-3500 m at the ridgeline of the Ethiopian Escarpment to ~160 m in the Afar Depression (Mohr, 1983) and crustal thickness from about 40 km below the Ethiopian Plateau to 15 km or less in the Danakil Depression (Makris and Ginzburg, 1987; Hammond et al., 2011). It is generally characterized by N–S running border faults, right-stepping marginal basins and hilly terrain of faulted blocks (Alebachew Beyene and Mohamed Abdelsalam, 2005; Corti et al., 2015; Fig. 2.3C). The southern termination of the Ethiopian escarpment/WAM is marked by the Ankober border fault system (Fig. 2.3A; Wolfenden et al., 2004, 2005). The Ankober border fault system represents a major fault system that characterizes the structurally complex between the NE trending MER and the N–S trending Red Sea rift (Wolfenden et al., 2005).

The Western Afar Margin preserves a record of flood basalt and bimodal basalt-rhyolite/ignimbrite volcanic rocks spanning from Oligocene (pre-rift) to Miocene (syn-rift) (Dereje Ayalew et al., 2006, 2018). About 50% of the volcanic pile is represented by felsic volcanic rocks that commonly lie towards the top level of the sequence (Dereje Ayalew et al., 2006). The first silicic ignimbrite in the western margin of the Afar depression has erupted at 30.2 Ma and bimodal basalt-rhyolite volcanism continued in parts of the broad flood basalt province until 10 Ma (Kieffer et al. 2004;

Wolfenden et al. 2004). The flood volcanic sequences in the region overlie the Mesozoic sedimentary succession (Hunegnaw et al. 1998), but none of the Mesozoic sedimentary rocks are exposed in the study area. The age of the volcanic rocks along the Ethiopian Escarpment displays a decreasing trend from north to south, indicating shifts in the focus of magmatism rift-ward (Ukstins et al., 2002, Dereje Ayalew et al., 2006). Moreover, these volcanics are related to different rifting episodes that occurred during the continental rifting of the region (Ukstins et al., 2002; Wolfenden et al., 2005) and three stages of rifting each characterized by new phases of magmatism and basin formation have been suggested by Wolfenden et al. (2005).

According to Wolfenden et al. (2005), the first stage of rifting in the Western Afar Margin occurred at ca. 29-26 Ma, after the emplacement of primarily basaltic flood volcanic units and during the emplacement of massive rhyolites and ignimbrites. Basins such as Kemise and Ataye were formed during this stage. These initial rift basins have the form of half grabens. Following this stage of rifting, Stage 2 continued to have occurred between ca. 25 and 20 Ma and it is defined by both basaltic and felsic volcanism. The basaltic rocks have dated between ca. 25 and 7 Ma, whereas the felsic rocks (dominantly ignimbrites) at 20–14 Ma. Stage 3 rifting is dated to have occurred <7 Ma and it is characterized by the emplacement of Dahla series fissural basalt sequences. Following the rifting event, numbers of fault-bounded grabens are developed in the middle of the Ethiopian escarpment (Wolfenden et al., 2005; Samson Tesfaye & Woldai Ghebreab, 2013; Williams, 2016; Fig. 2.3B). The name of these basins is not always clearly defined, as several authors give different names for these different basins. According to Williams (2016), the major marginal grabens from north to south are Raya, Kobo, Hayk, Borkena and Robit (Fig.2.3B). The marginal basins/grabens are some 10-20 km wide and several tens of km in length. They are filled by alluvial deposits of at least Pliocene-Quaternary age (e.g. Kazmin 1972; Chorowicz et al. 1999). However, there is no detailed information on the actual type, thickness and age of the sediments (Samson Tesfaye and Weldai Ghebreab, 2013).

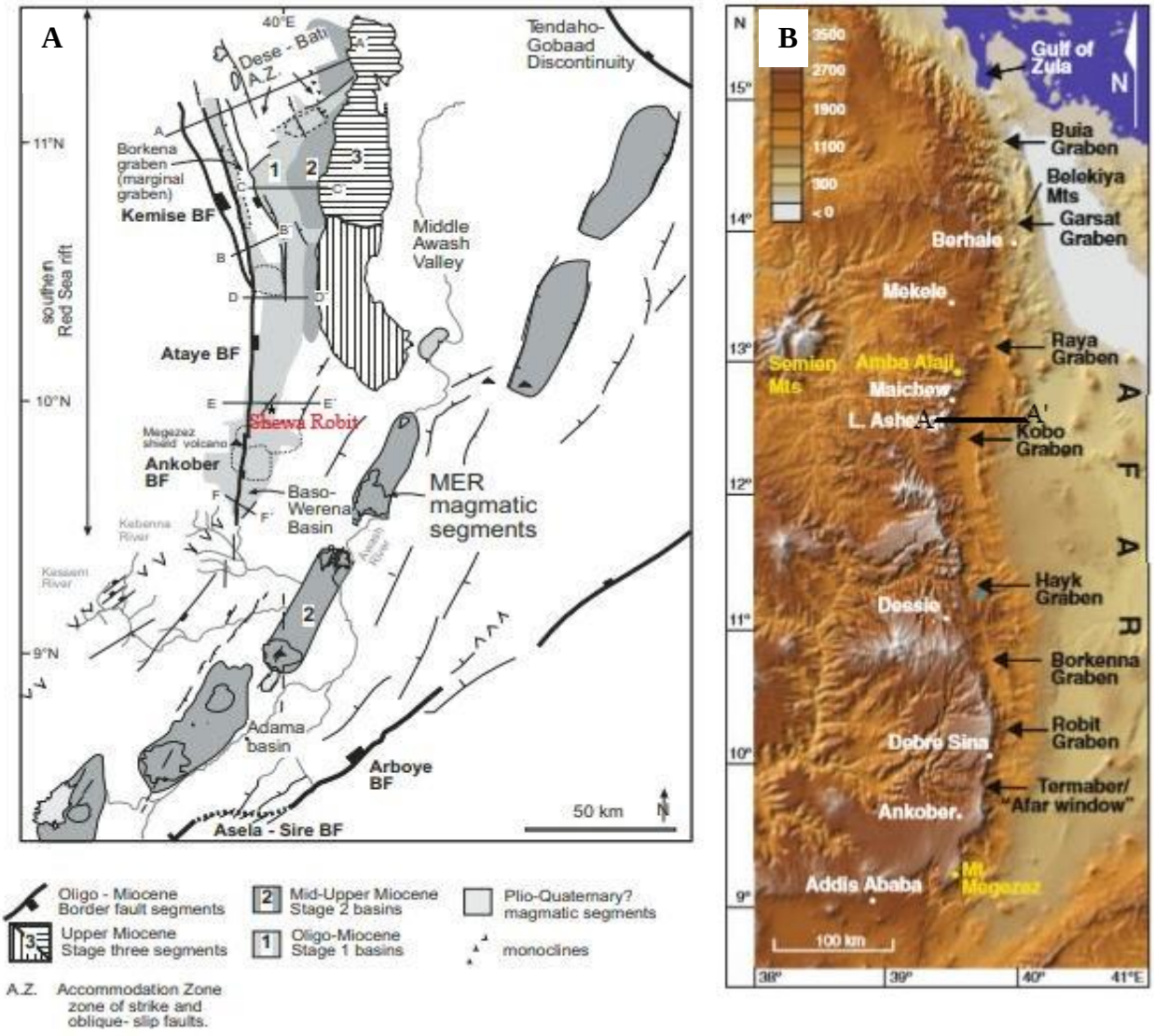
A
40°E
Dese - Bati
A.Z.
Tendaho-
Gobaad
Discontinuity
11°N
Borkena
graben
(marginal
graben)
Kemise BF
Middle
Awash
Valley
southern
Red Sea rift
Ataye BF
10°N
Shewa Robit
Megezez
shield volcano
Ankober
BF
Baso-
Werena
Basin
MER
magmatic
segments
Kebenna
River
Kessem
River
Awash
River
9°N
Adama
basin
Arboye
BF
Asela - Sire BF
50 km
Oligo - Miocene
Border fault segments
Upper Miocene
Stage three segments
Mid-Upper Miocene
Stage 2 basins
Oligo-Miocene
Stage 1 basins
Plio-Quaternary?
magmatic segments
monoclines
A.Z. Accommodation Zone
zone of strike and
oblique- slip faults.
B
3500
2700
1900
1100
300
< 0
Gulf of
Zula
Buia
Graben
Bekekiya
Mts
Garsat
Graben
Berhale
Mekele
Raya
Graben
Semien
Mts
Amba Alaji
Maichew
L. Ashe
Kobo
Graben
Hayk
Graben
Dessie
Borkenna
Graben
Robit
Graben
Debre Sina
Termaber/
"Afar window"
Ankober.
Addis Ababa
Mt.
Megezez
100 km
38°
39°
40°
41°E
C
(a)
(a')
Ethioplan
Plateau
Ethioplan
Escarpment
Marginal
graben
Marginal area of the
Afar Depression
Afar Stratoid
Trap Series
Pre-rift Sedimentary Rocks
Neoproterozoic Basement
Normal fault
3000
2000
1000
m asl
W
E
Km
20
40
60
80
100

Fig. 2.3: (A) Stages of basin development in the southernmost sector of the southern Red Sea and the northern Main Ethiopian Rift (MER). BF = border fault. Numbering refers to stages of basin development in the Kemise, Ataye, Baso-Werena and Adama basins (Adapted from Wolfenden et al., 2005). (B) DEM of the western margin of Afar showing the location of the marginal grabens (Adapted from Williams, 2016). (C) Schematic geological cross-section across the western Afar margin. The trace of the cross-section is shown in Fig. B (Adapted from Corti et al., 2015).

Furthermore, a new volcanic stratigraphy for the southern sector of the Western Afar Margin has been compiled by Wolfenden et al. (2005). It comprises five magmatic episodes: (1) Oligocene rhyolitic formations (e.g., Kemise and Ataye rhyolite formations) (2) Oligo-Miocene basaltic formations (25.0–24.6 Ma) (e.g., Dese basalt formation and Birkitu formation) (3) Lower-mid–Miocene ignimbrites and associated tuffs (20–11.6 Ma) (Shewa Robit ignimbrite formation and the Aliyu Amba ignimbrite formation) (4) Middle-upper Miocene basaltic to intermediate centers (16–7 Ma) (The Burka formation, the Aneno formation, and the Bercha formation) and (5) Upper Miocene fissural basalts (6.6–5.3 Ma) (Dahla Series).

This study is located in the Shewa Robit basin/graben wherein the bimodal basalt-rhyolite (ignimbrite) rock units of the Oligocene-Miocene volcanic units are outcrop. The basaltic rock units are a member of Birkitu formation dated at 24.59 ± 0.16 Ma (Wolfenden et al., 2005) whereas the pyroclastic deposits around the basin/graben are members of Shewa Robit ignimbrite formation dated at 19.76 ± 0.07 Ma to 14.90 ± 0.06 Ma (Ukstins et al., 2002). According to Wolfenden et al. (2005), the lower Miocene Birkitu basaltic formation is emplaced after the initiation of the border fault (Ataye border fault). On the plateau, the topmost part of the mid-Miocene Shewa Robit ignimbrite formation (14.9 ± 0.06 Ma) is subhorizontal where it overlies the flood volcanic units. There is no erosional unconformity on the plateau between the top of the flood volcanic group and the overlying Shewa Robit ignimbrite formation that would suggest removal of section (Wolfenden et al., 2005).

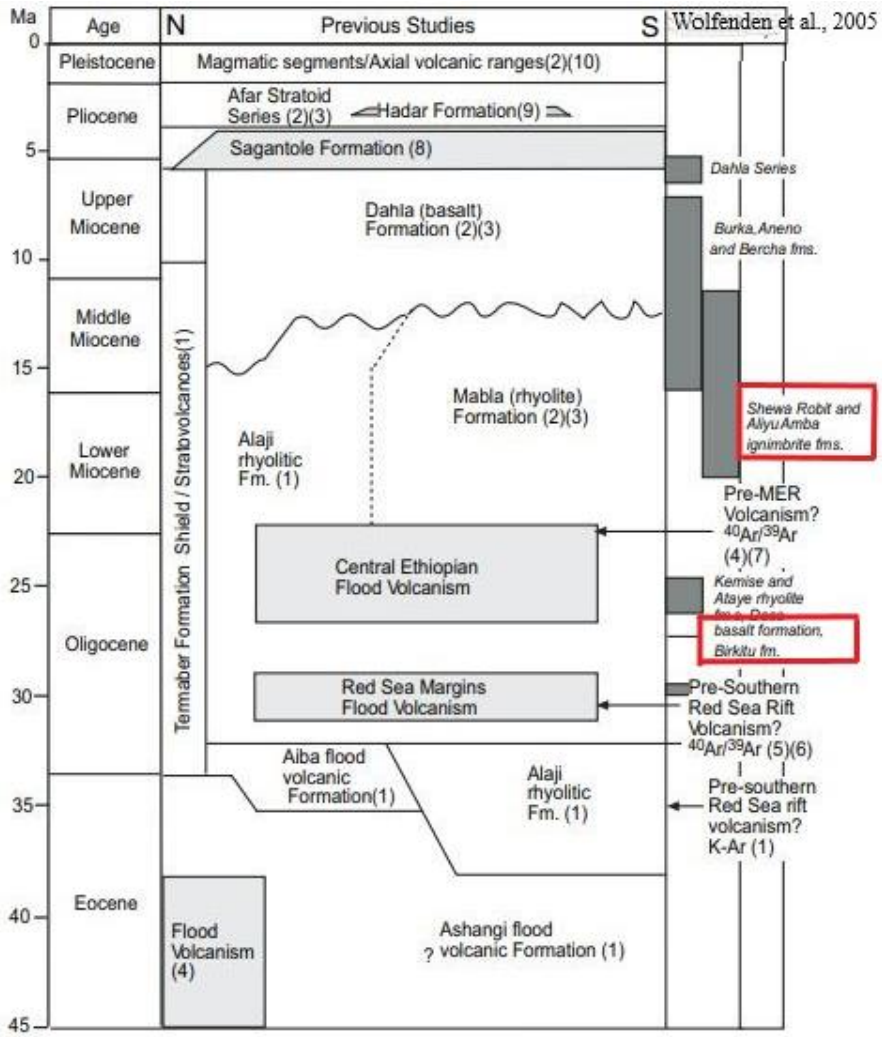

Fig. 2.4: Correlation chart of Cenozoic Ethiopian volcanic rocks (Eocene-Recent) relations in the southern Red Sea and Main Ethiopian rifts. The stratigraphic positions of the studied volcanic rocks are shown by the red box (from Wolfenden et al., 2005).

CHAPTER THREE

3 GEOLOGY OF THE STUDY AREA

3.1 Introduction

The Shewa Robit graben is one of the marginal grabens (Williams, 2016) situated along the southernmost end of Western Afar Margin. The geology of the Shewa Robit basin and its surrounding area contains an abundance of volcanic rocks that are bimodal in their composition. The rock units commonly recognized in the study area are aphyric basalt, porphyric basalt, rhyolitic ignimbrite, glassy rhyolite, porphyritic rhyolite and unwelded tuff. Basaltic rock units collectively dominate the southwestern, southeastern and northern sectors of the study area whereas the felsic rock units make the dominant rock types along the southern, northwestern, east-central and northeastern part of the region. The felsic units are found both as rhyolitic lava flow and as pyroclastic deposits while the basaltic rocks predominantly occur as lava flows often forming flat-laying topography. A considerable portion of the study area is covered by siliceous volcanic rocks. Structural and a few geochronological data of the lithological unit of the study area are integrated into this study from the work of Ukstins et al. (2002) and Wolfenden et al. (2005). According to these studies, the lower basaltic rocks exposed in the study area, particularly within and around the basin, have dated to 24.59 ± 0.16 Ma whereas ignimbrite rocks overlying them have ages ranging between 14.90 ± 0.06 and 19.76 ± 0.07 Ma. In addition to these rock units, undated rhyolitic lava is exposed in the southeastern outskirt of Shewa Robit (Wolfenden et al., 2005). Additionally, there are various geological structures associated with these rock units such as faults, joints and dykes that are recognized during the field observation and from the satellite images. In this chapter, detailed field descriptions, geological map, geological cross-section, as well as composite stratigraphic section and petrographic study of the volcanic rocks from the Shewa Robit area are documented in order to upgrade the geological understanding of the area.

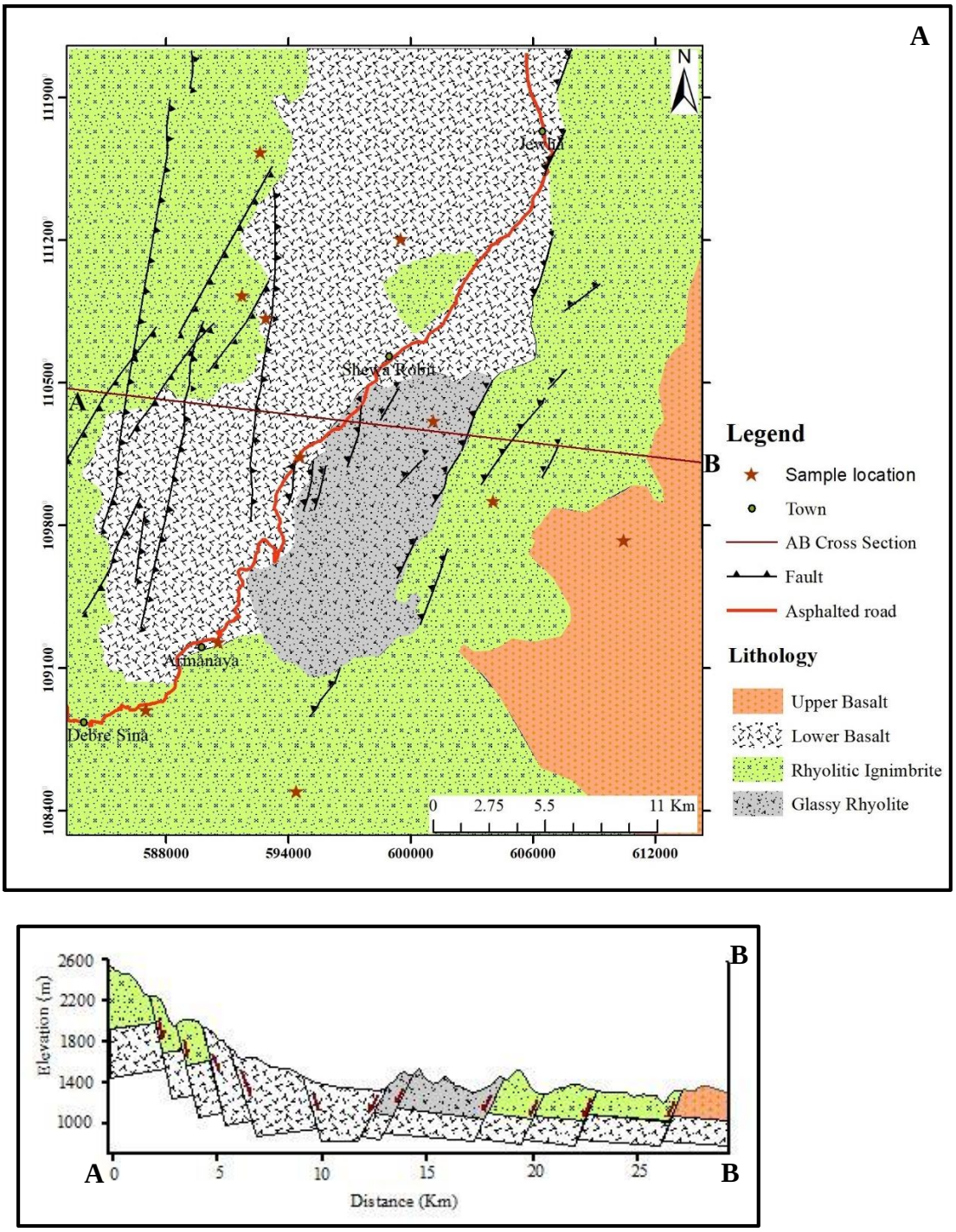

Fig. 3.1: Geological map of the study area (A) and geological crosssection along the line A-B (B).

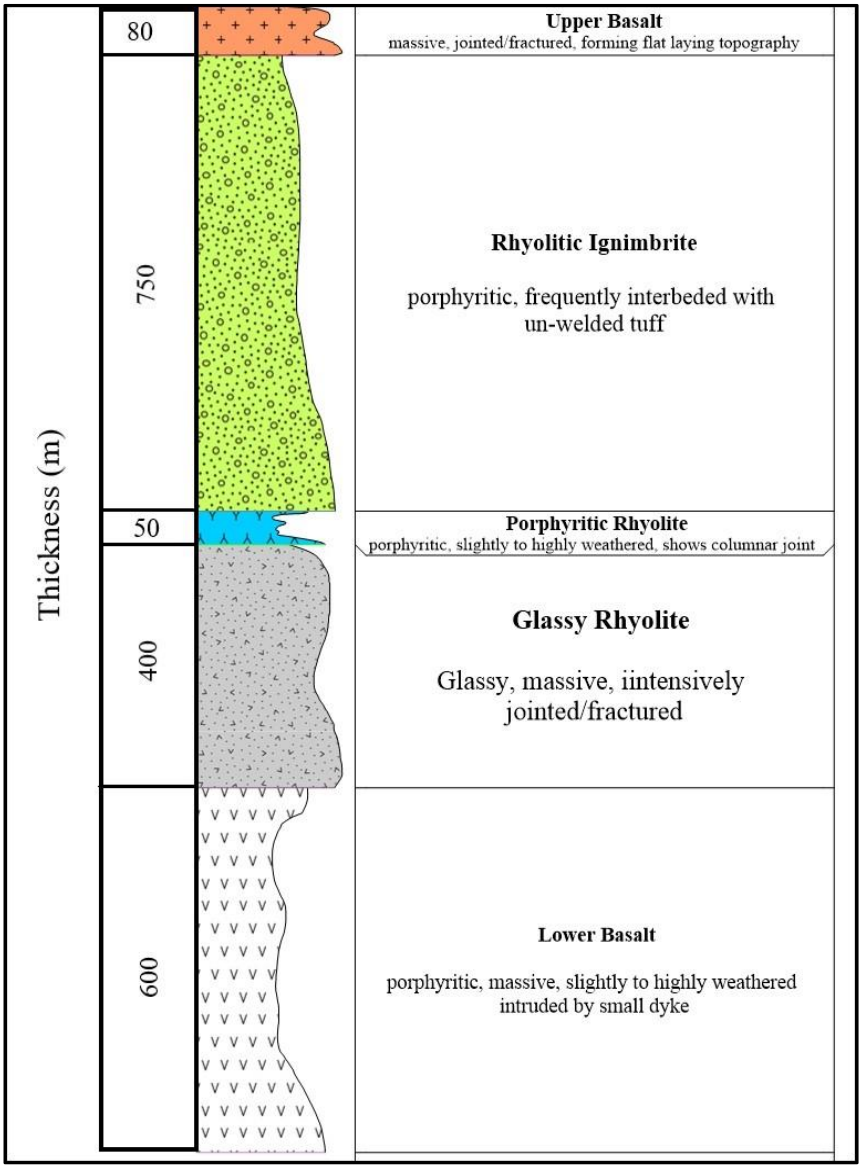

Fig. 3.2: Composite stratigraphic log section of the Shewa Robit area volcanic rocks

3.2 Lithological and petrographic description of the study area

Based on mineral composition, texture and stratigraphic position, various volcanic rocks are recognized in the study area. The main lithological units according to their ages (Ukstins et al., 2002; Wolfenden et al., 2005) and stratigraphic position from the bottom to the top are lower basalt, glassy rhyolite, porphyritic rhyolite, rhyolitic ignimbrite, unwelded tuff and upper basalt. The field observed physical and mineralogical properties, as well as a petrographic description of these lithological units, are described in detail below.

3.2.1 Lower Basalt

This rock unit is mainly exposed in the central, southwestern and northern parts of the study area, particularly within the Shewa Robit basin and its surrounding area. It is exposed mostly forming flat laying topography and partly forming a ridge. According to Wolfenden et al. (2005), this rock unit is the oldest one among the volcanic rocks exposed in the study area and is dated at 24.59 ± 0.16 Ma. It is poorly exposed and most exposures of this unit are found along the road cuts and river channels. The exposed rocks are generally described as slightly to highly weathered, massive, reddish-brown to dark grey (weathered) and black (fresh) colored. In most places, it is found intensively weathered and fractured. Exfoliation weathering is the most common type of weathering which predominantly affecting this rock unit (Fig. 3.3 (B)). The diameter of the exfoliation weathering reaches up to ~50 cm. Moreover, it is also affected by both systematic and non-systematic sets of joints having an average joint space ranging between 2 cm to 20 cm. The systematic joint set observed in this rock unit has an average orientation of N20W/84°/NE. In hand specimen, the basalt is aphyric to sparsely porphyritic and the phenocrysts in the porphyritic rocks are predominated by plagioclase. A relatively small non-persistent dyke of aphanitic basalt (Fig. 3.3 (C)) is found cutting across this unit, particularly in the southwestern part of the study area. The dyke has 0.75 m width, black (fresh), light grey (weathered) colored and nearly vertical with N70E overall orientation.

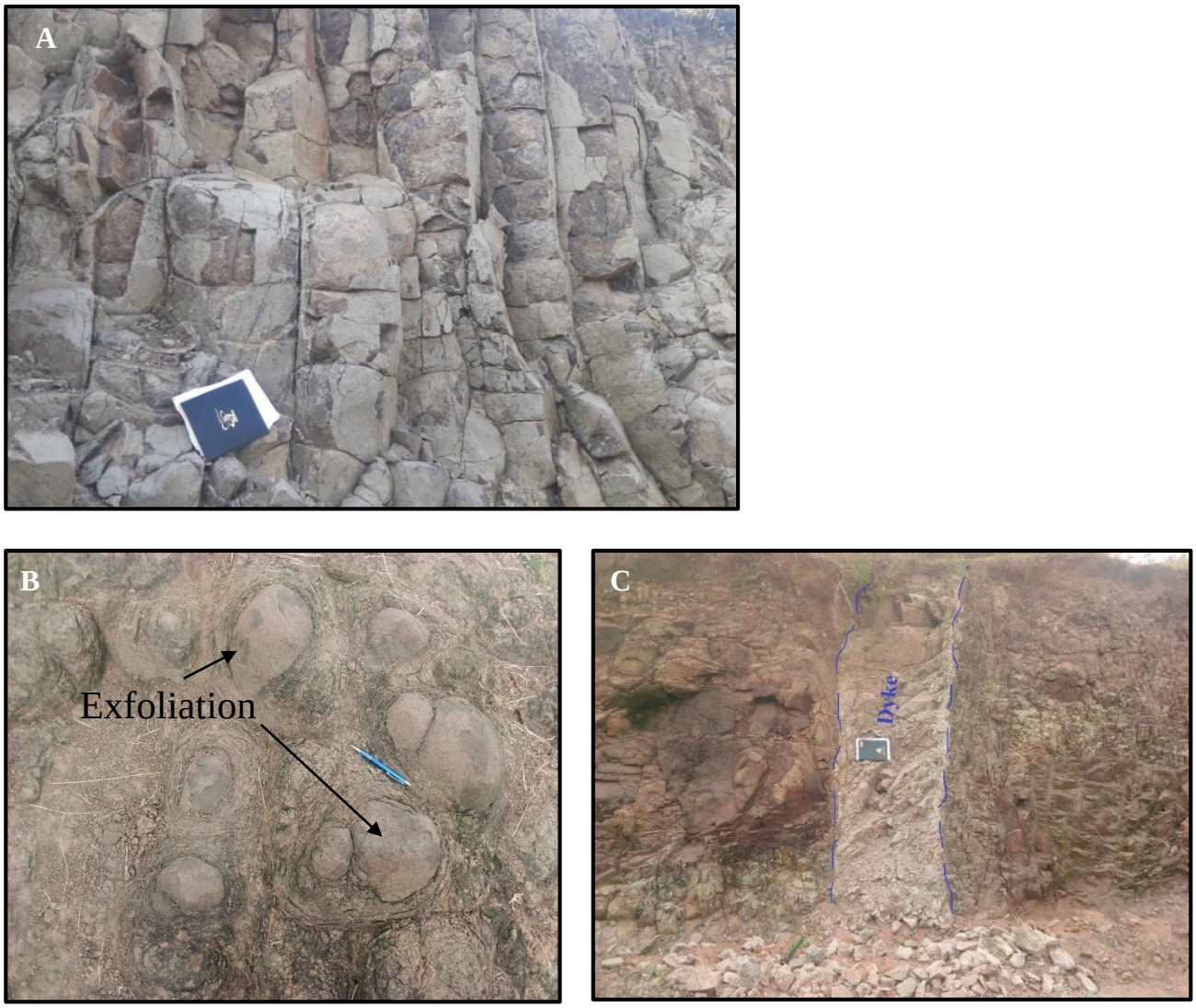

Fig. 3.3: Outcrop photos of Lower basalt. (A) vertical to sub-vertical joints in Lower basalt; (B) Exfoliation weathering on the sparsely porphyritic basalt; and (D) Northeast trending dyke of aphanitic basalt cutting across the sparsely porphyritic basalt.

The petrographic examination of this rock unit indicates that, except for one sample (SR2) which has an aphyric texture, it is porphyritic with micro to mega phenocryst of dominantly plagioclase (max. =~25%) and very few pyroxenes and olivine. The modal composition of the phenocrysts shows that it is composed of 10-25 % (by vol.) plagioclase, 2-5 % (by vol.) clinopyroxene and 2-5 % (by vol.) olivine, whereas 70-85 % (by vol.) of the thin sections are occupied by the groundmass. The plagioclase phenocrysts in the phenocryst assemblage are randomly oriented and frequently exhibit pronounced polysynthetic twinning and compositional zoning. They are

elongated and vary between the euhedral and subhedral shape. In place, megacryt of plagioclase phenocryst is embedded olivine micro-grain, displaying poikilitic texture (sample Y01; Fig. 3.4A). In sample SR5 (Fig. 3.4D), glomerophyric textured phenocrysts of plagioclase, olivine, pyroxene and opaque minerals are embedded in a glassy groundmass. On the other hand, the groundmass in most thin sections is composed of predominantly fine-grained minerals of plagioclase and opaques with reddish-brown and/or dark green colored glass interspersed among the microcrystalline grains (probably altered minerals). For a complete petrographic description of the lower basalt samples, see appendix I.

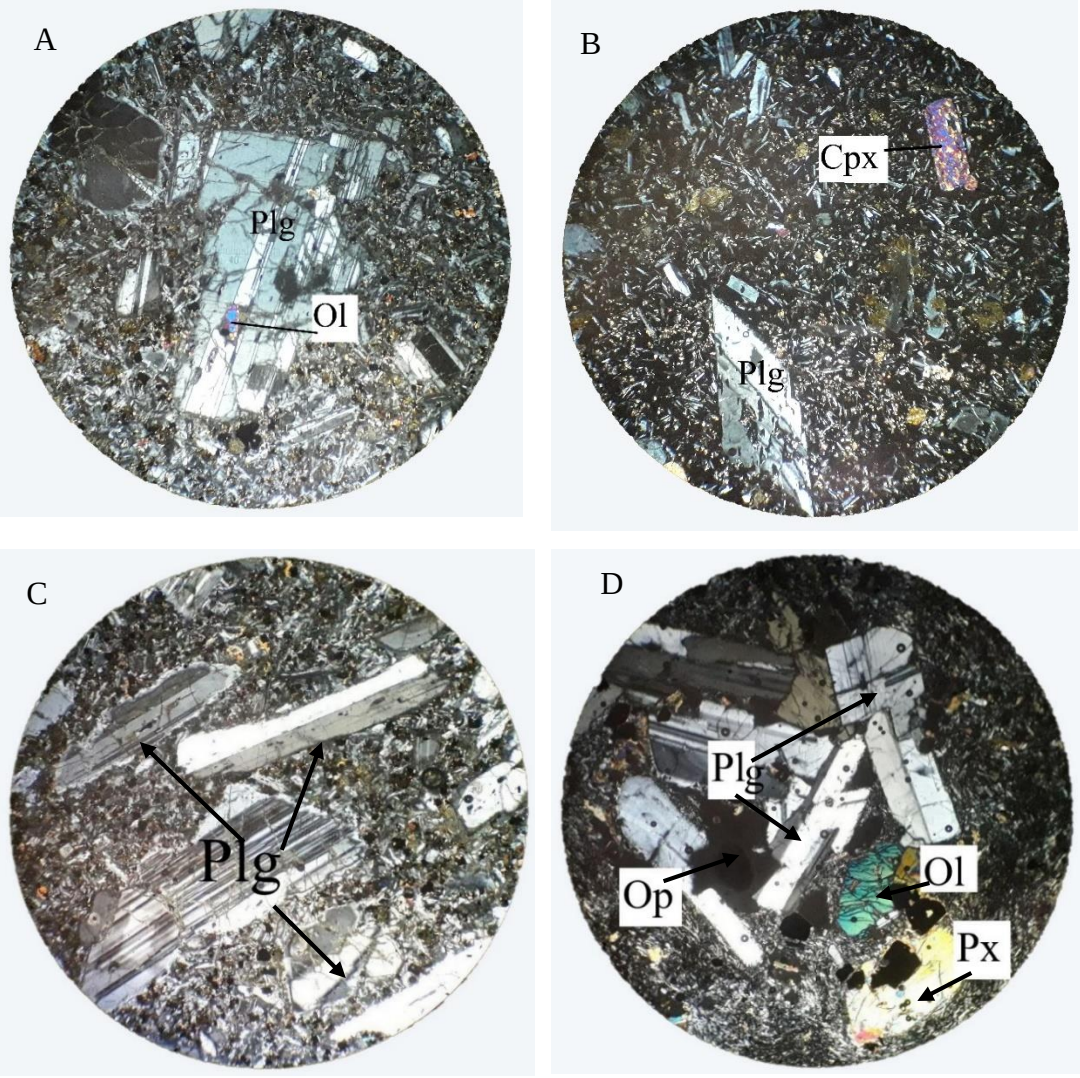

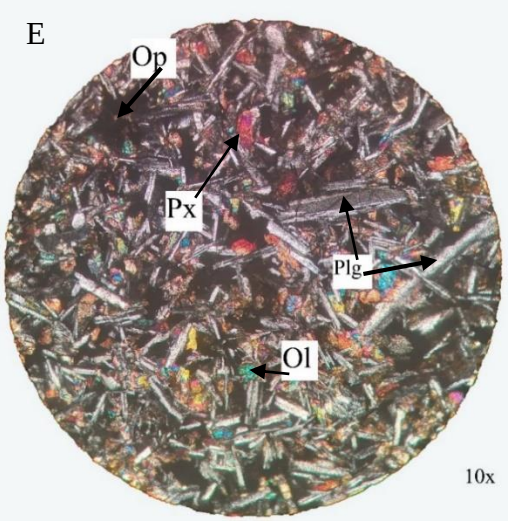

Fig. 3.4: Microphotographs of the Lower basalt samples; (A) Sample Y01: subhedral mega phenocryst of plagioclase crystal showing its diagnostic polysynthetic twinning set in plagioclase and opaque mineral dominated microcrystalline groundmass. It shows a poikilitic texture wherein olivine grain is enclosed by the plagioclase grain. Plagioclase with compositional zoning is also present in the upper-left part of the thin section. (B) Sample AR1: euhedral phenocrysts of plagioclase and pyroxene embedded in a groundmass of fine grained plagioclase and opaque minerals with some dark green interstitial of glassy material. (C) Sample SR14: euhedral to subhedral shaped phenocrysts of plagioclase set in a groundmass composed of fine-grained opaque minerals and some reddish-brown interstitial glassy material. (D) Sample SR5: glomerophyric texture wherein phenocrysts of the sub-euhedral shaped plagioclase, olivine, pyroxene and some opaque (Fe-Ti oxides) are embedded in a glassy groundmass. (E) Sample SR2: intergranular texture wherein the interstices between the plagioclases are filled by Fe-Mg minerals (pyroxene, olivine and opaque mineral). Note that all the photographs, except for one sample (SR2) which is taken at 10x, are taken at 4x magnification in the XPL view. The labels stand for (Plg- plagioclase, Ol- olivine, Cpx-clinopyroxene, Op-opaque (Ti-Fe oxide)).

3.2.2 Glassy Rhyolite

Rhyolitic lava forming ridge-like morphology is exposed close to the southeastern outskirt of Shewa Robit, on the way to Abay Atir village. It has various vertical thickness ranging from 400 to 200 m. The maximum thickness of the rhyolitic lava (~ 400m) is observed in the Insertu ridge located in the southeast of Shewa Robit. The glassy rhyolite is hard, massive, very fine-grained

(glassy texture) and shows a smooth surface. It displays varying colors ranging from dark brown/brown/dark grey on the fresh surface to light brown or dark brown on the outer weathered surface. Within the study area, the glassy rhyolitic rock is best studied along the quarry site located at 0601123 E: 1103127 N. It is widely used by local peoples for the construction purpose in the form of crushed stone, as it has a good physical and chemical quality for concrete and asphalt mix. In nearly all exposers, the glassy rhyolite is seen to be fractured intensively. In place, a systematic joint set is observed with an overall orientation of N35E/80°/SE. Geochronological data of this rock unit is not available, but Wolfenden et al. (2005) have inferred mid-Miocene from the stratigraphic position of the unit.

The petrographic examination of the glassy rhyolite (sample SR7) collected from the quarry site shows that it is made up of nearly entire (>99%) glassy material displaying holohyaline texture (Fig. 3.10). Microcrystalline grains of quartz are rarely observed in this thin section.

Fig. 3.5: Glassy rhyolite outcrop which is strongly fractured and joined with vertical to sub-vertical joints at a quarry site (0601123 E: 1103127 N).

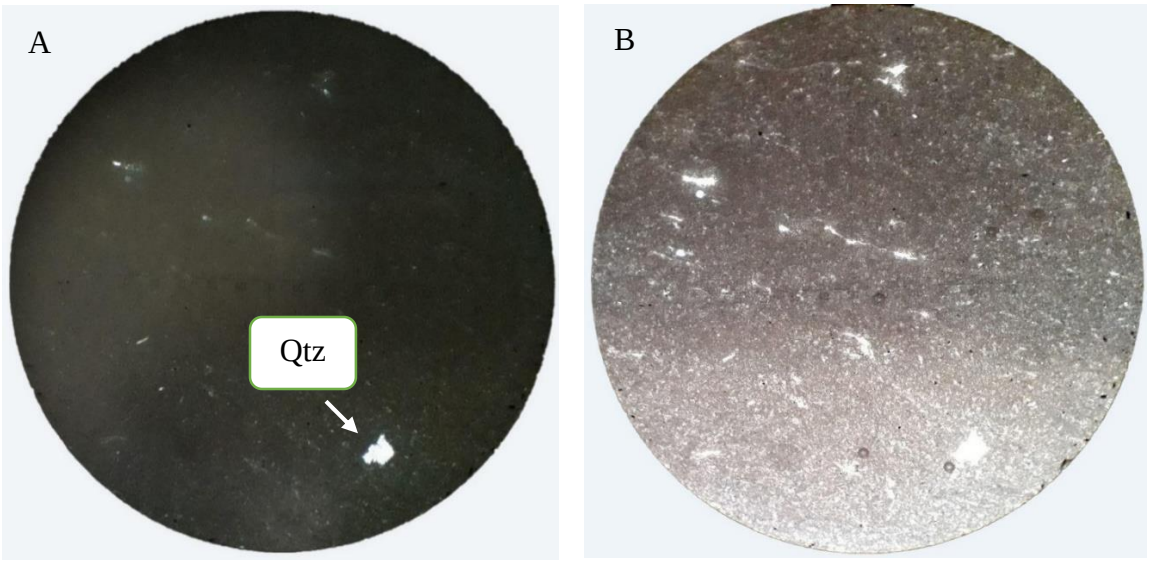

Fig. 3.6: Microphotographs of the glassy rhyolite rock unit under (A) XPL and (B) PPL view for sample SR7 with magnification 4x, location (0601123 E: 1103127 N).

3.2.3 Porphyritic Rhyolite

Rhyolite of porphyritic texture is exposed in the southern parts of the study area, particularly in the eastern part of Debre Sine along the way to Agame Ber village. It is one of the lithological units found in the study area which is not mappable; its areal coverage is below the scale of the geological map. The exposure types of this unit are mainly road cuts and they are described as massive, slightly to highly weathered and forming a relatively moderate steep topography. The porphyritic rhyolite is also described by sparsely porphyritic, light brown color when weathered and whitish/light yellowish color when fresh. Stratigraphically, this rock unit is overlaid by rhyolitic ignimbrite. In place, the porphyritic rhyolite is observed as being highly weathered and fractured. Columnar joints are observed locally developed at the uppermost level of this porphyritic rhyolite. The columnar joints are upright (Fig. 3.13). In hand specimens, the grains of quartz and alkali feldspar minerals, which are later confirmed under the thin section, are visible.

The petrographic analysis of this rock unit shows that it is porphyritic in texture due to the presence of phenocrysts of quartz and K-feldspar set in the glassy groundmass. The modal composition of the phenocrysts shows that it is composed of 5 % quartz and 10 % K-feldspar (sanidine) whereas the rest 85 % is occupied by the glassy groundmass. It shows vetrophyric texture; a type of texture

that refers to a rock that is composed of phenocrysts set in a glassy matrix. Quartz occurs as anhedral in shape while K-feldspar varies between the euhedral and subhedral and shows a simple twin feature.

Fig. 3.7: Porphyritic rhyolite outcrop in the southern part of the study area at (594398 E: 1084934 N) which has columnar joins

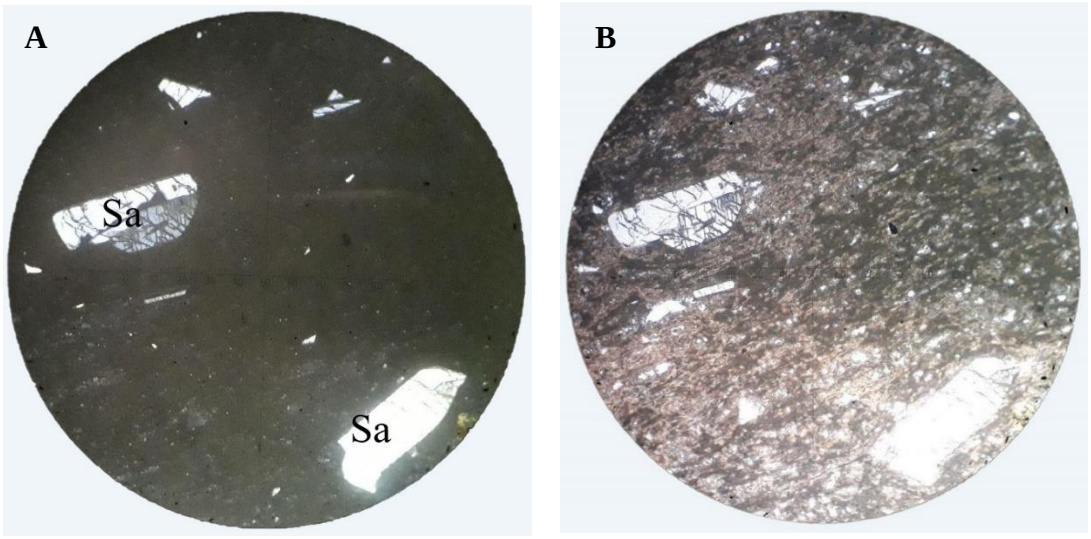

Fig. 3.8: Microphotographs of the porphyritic rhyolite rock unit. Both plates A and B are for sample DC5 under XPL and PPL view with 4x magnifications. The label Sa stands for sanidine.

3.2.4 Rhyolitic Ignimbrite

This rock unit is one of the widely distributed volcanic units in the study area with an areal extent of about 51 % of the total area (see Fig. 3.1 A). It has a variety of colors ranging from grey, pink and reddish-brown fresh color to light grey/pinkish weathered color. Rhyolitic ignimbrite is mainly exposed in the southern, northeastern, central-east and northwestern parts of the study area often forming gentle-steep topography. Stratigraphically, this rock unit is overlaid by the unwelded pyroclastic deposits (unwelded tuff). Northeast of Debre Sina, this rock unit is observed being interlayered with unwelded tuff forming ridge topography. The interlayered deposit in turn is dissected by a medium-sized basaltic dyke. The dyke is deeply weathered with dark brown weathered color. It has ~1.75 m width and N75E/45°/NW overall orientation. The ignimbrite unit is described by grey fresh color, porphyritic texture and incorporated rock fragments. Alkali feldspar, quartz and lithic fragments are visible in the hand specimen and the lithic fragments are highly weathered displaying brown color. Moreover, rhyolitic ignimbrite with vesicular texture is also seen exposed in the southern part of the study area. Rhyolitic ignimbrite with a small number of lithic fragments and more flattened and stretched crystals is seen exposed in the eastern part of the Shewa Robit, particularly along the way to Abay Atir. It forms moderately steep to gentle topographic features.

The microscopic study of this rock unit shows that it is porphyritic with phenocrysts of quartz, K-feldspar (sanidine), rock fragment and opaque minerals. The overall modal proportion of the phenocrysts ranges between 10 and 15 % (by vol.) and constitutes; 3-5 % quartz, 3-10 % K-feldspar (sanidine), 1-2% rock fragments and 1 % opaque minerals. Most of the studied samples show vetrophyric texture (see Fig. 3.10 B, D and E) and one sample shows eutaxitic texture. Quartz and K-feldspar (sanidine) crystals in the phenocryst are generally euhedral to anhedral in shape and are relatively undeformed. The K-feldspar (sanidine) crystals frequently exhibit simple twin features and quartz crystals show some embayments (see Fig. 3.10D). On the other hand, the groundmass is composed of glassy material and some flattened cryptocrystalline minerals. In some thin sections, the flattened fragments show a discontinuous lamination and are aligned around alkali feldspar and quartz crystals (see fig. 3.10 A). Further, rock fragments are also present in small proportions within these thin sections in different shapes and sizes. For a further petrographic description of the rhyolitic ignimbrite samples see appendix I.

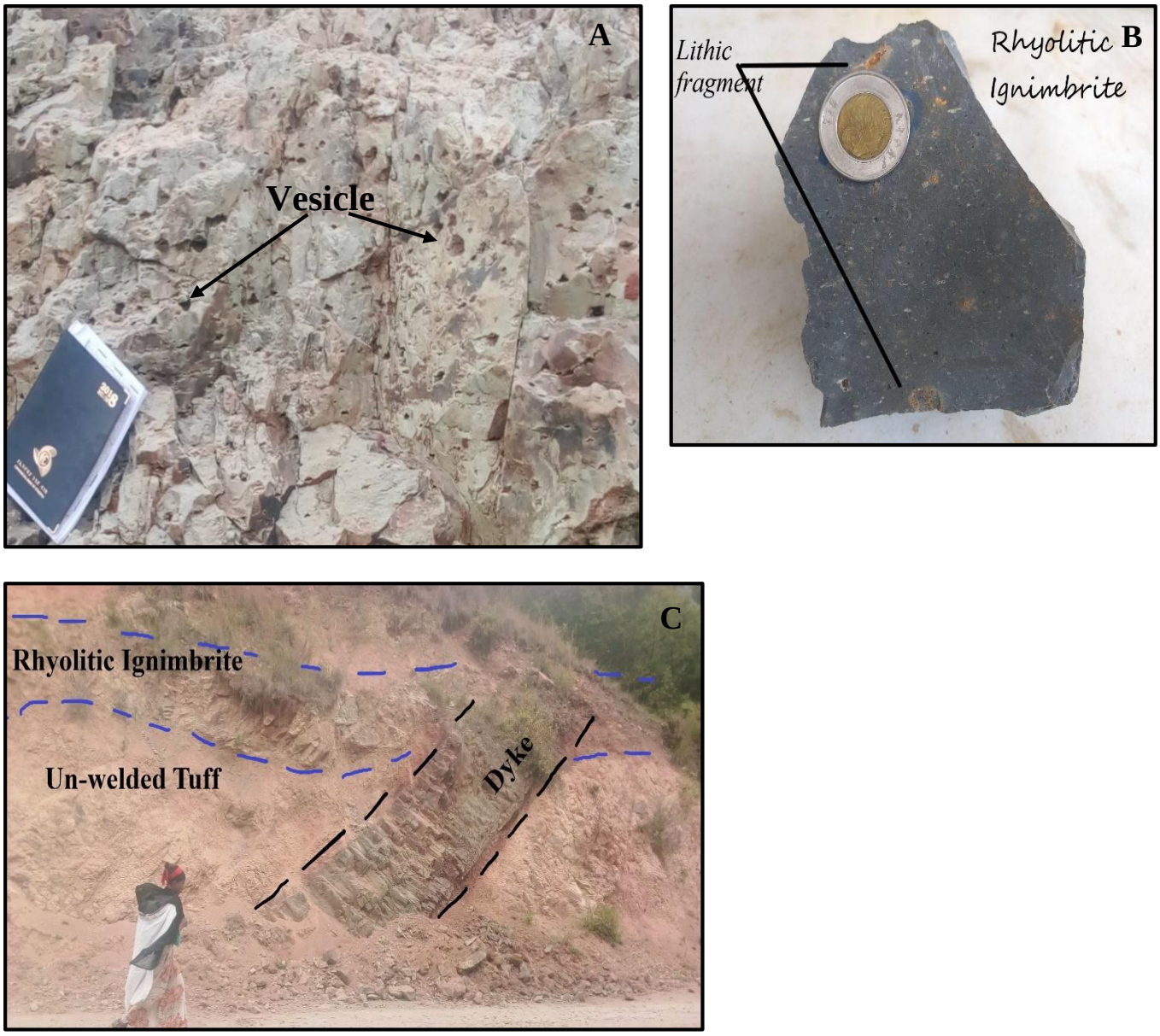

Fig. 3.9: Rhyolitic ignimbrite exposures; (A) A rhyolitic ignimbrite showing vesicles; (B) A rhyolitic ignimbrite hand specimen showing fragments; (C) Northeast trending deeply weathered basaltic dyke cutting across the interlayered pyroclastic deposits (0587687 E: 1088634 N).

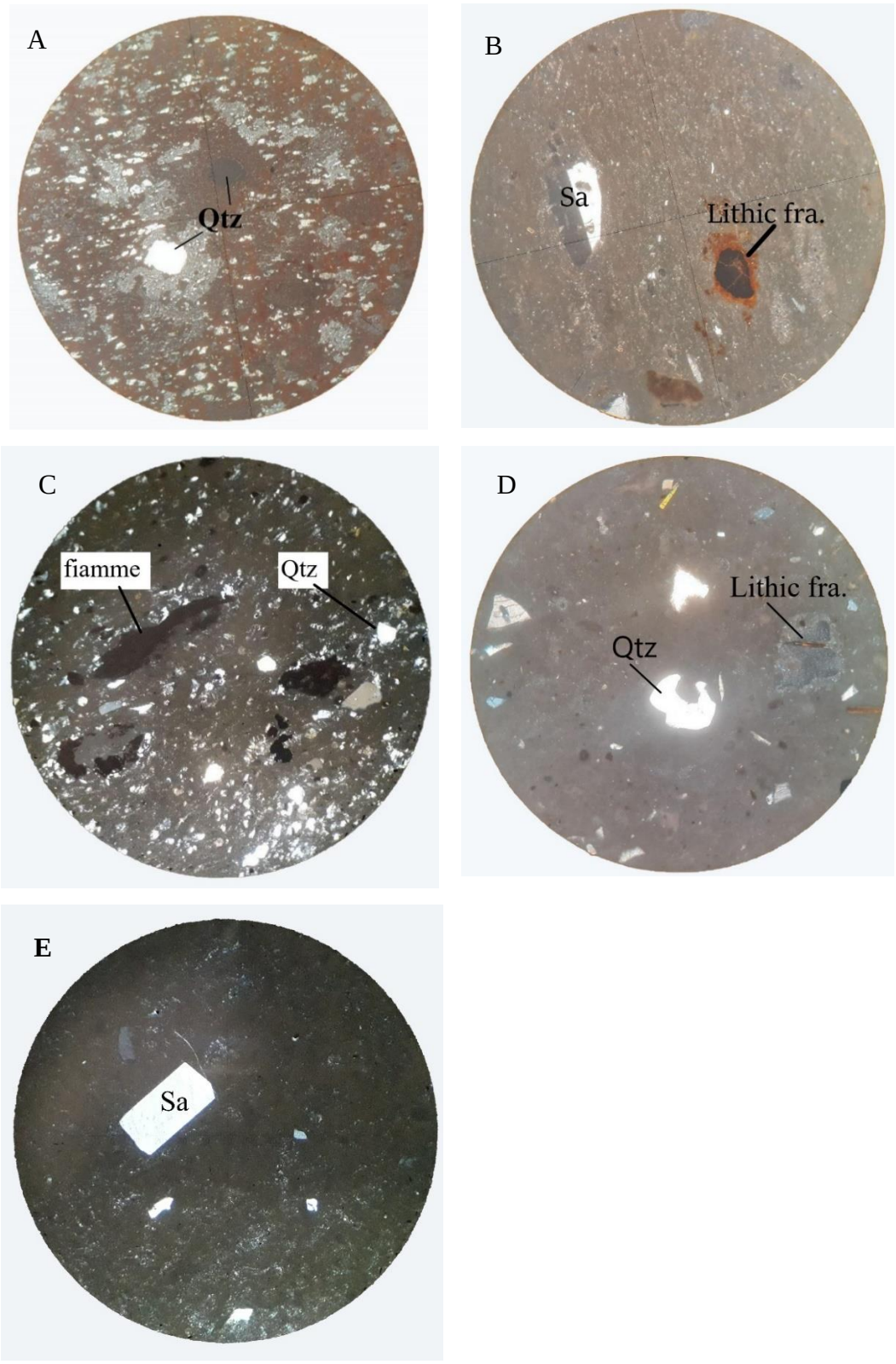

Fig. 3.10: Microphotographs of the rhyolitic ignimbrite rock unit. (A) Sample SR8: subhedral shaped micro-phenocrysts of quartz set in a groundmass composed of glassy material with some

small discontinuous flattened cryptocrystalline minerals. (B) Sample SR10: subhedral phenocryst of sanidine and lithic fragment set in the glassy groundmass showing vetrophyric texture. The sanidine phenocryst shows simple twinning. (C) Sample Y02: flattened fragment of glassy material (i.e. fiamme) with some grains of undeformed quartz, showing eutaxitic texture. (D) Sample SR1: quartz phenocryst showing embayment embedded in the glassy groundmass. It also notes vetrophyric texture. (E) Sample SR9: euhedral-shaped sanidine set in glassy groundmass (i.e. vetrophyric texture). Note that all the photographs are taken at 4x magnification in the XPL view. The labels stand for (Qtz-quartz, Sa-sanidine, Lithic fra.-lithic fragment).

3.2.5 Unwelded Tuff

This unit is mainly exposed in the southern, northeastern and northwestern parts of the study area often forming moderately gentle topography. It commonly occurs interlayered or overlain rhyolitic ignimbrite or/and porphyritic rhyolite units. In the geological map, it is included within the rhyolitic ignimbrite unit as it covers a small area. It is exposed on natural slope faces and along road cuts. In the southern part of the study area, it is exposed with a variety of colors ranging from light brown/whitish to light grey, containing well-sorted medium grain size particles and friable and unconsolidated grains. On the way to Agam Ber village, northeast of Debre Sina, it is dissected by a small dyke of porphyritic basaltic rock (Fig. 3.11). The dyke is well exposed along the road cut with an average width of 1.50 m. It is characterized by black color when fresh and by S25°W/85°/SE overall orientation. The maximum exposure thickness of this unit is about 12 m along the road cut.

In the western part of the study area, along the escarpment, a small extent of unwelded tuffs incorporating rock fragments are observed overlaying the rhyolitic Ignimbrite. The tuff is characterized by light yellowish color, fine to medium grain size, friable to slightly compacted. The rock fragments are ranging in size from a few mm to 2 cm and they are generally black, angular to sub-rounded in shape. Moreover, this rock is affected by closely spaced (about 7 cm) joints that have different orientations.

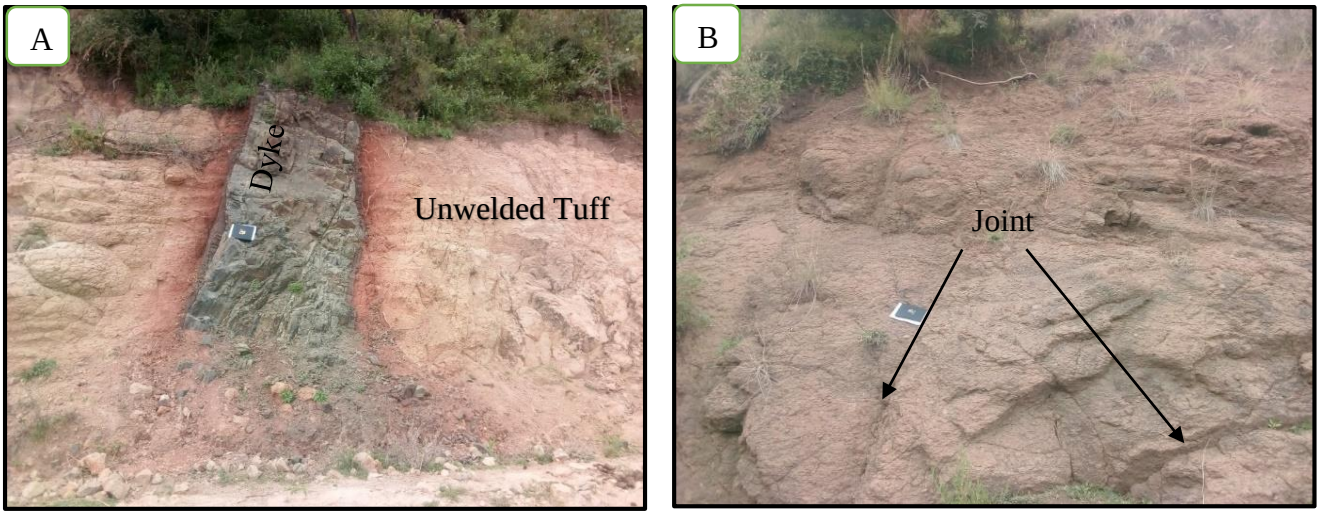

Fig. 3.11: Unwelded tuff outcrop. (**A**) A basaltic dyke crosscutting unwelded tuff (0594314 E: 1084961 N); (**B**) Jointed tuff outcrop from the western part of the study area.

3.2.6 Upper Basalt

This unit is predominantly exposed in the southeastern part of the study area forming relatively flat-lying topography. The weathered and fresh exposures of this basalt are observed along the railway cut and some are studied at natural outcrops. The exposures are generally characterized by black fresh and light gray weathered color, slightly weathered, aphyric texture, compact/massive and hard nature. Moreover, non-systematic joints with a variety of joint spaces are found widely associated with this rock unit. In the investigated area, this rock unit is exposed only its upper section, making it difficult to estimate its total thickness. However, the maximum exposed thickness (about 80 m) of this unit is seen along the railway cut located at 0610483 E and 1097268 N. It covers about ~10 % of the total study area. Moreover, this basaltic unit is the youngest product among the volcanic rocks found in the study area (Wolfenden et al., 2005).

The petrographic investigation of this rock (sample SR6) displays fine-grained identifiable plagioclase laths and opaque and indistinguishable fine grained minerals (brown colored glassy materials). The modal proportion of plagioclase reaches up to 60 % of the total thin section.

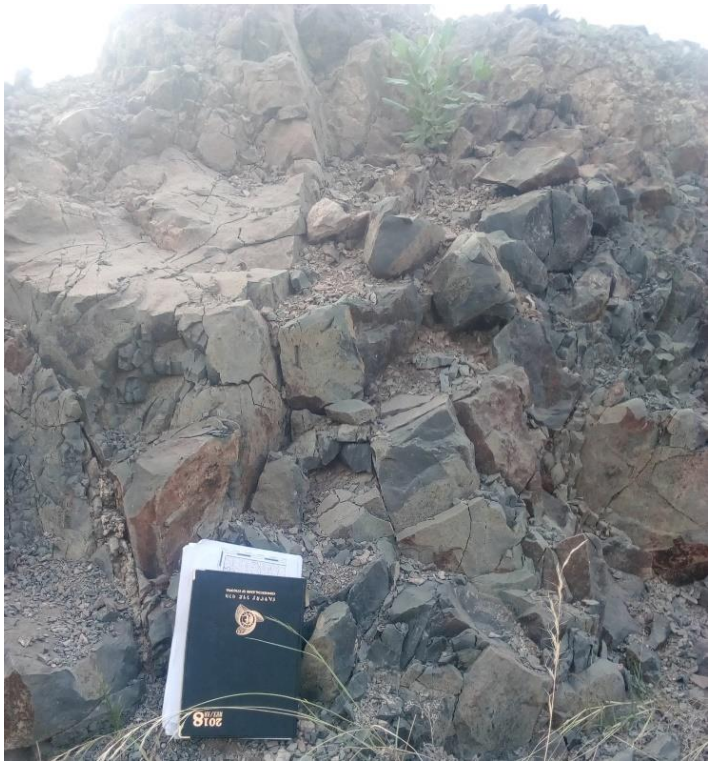

Fig. 3.12: Outcrop photos of upper basalt (location: 0610483E and 1097268N)

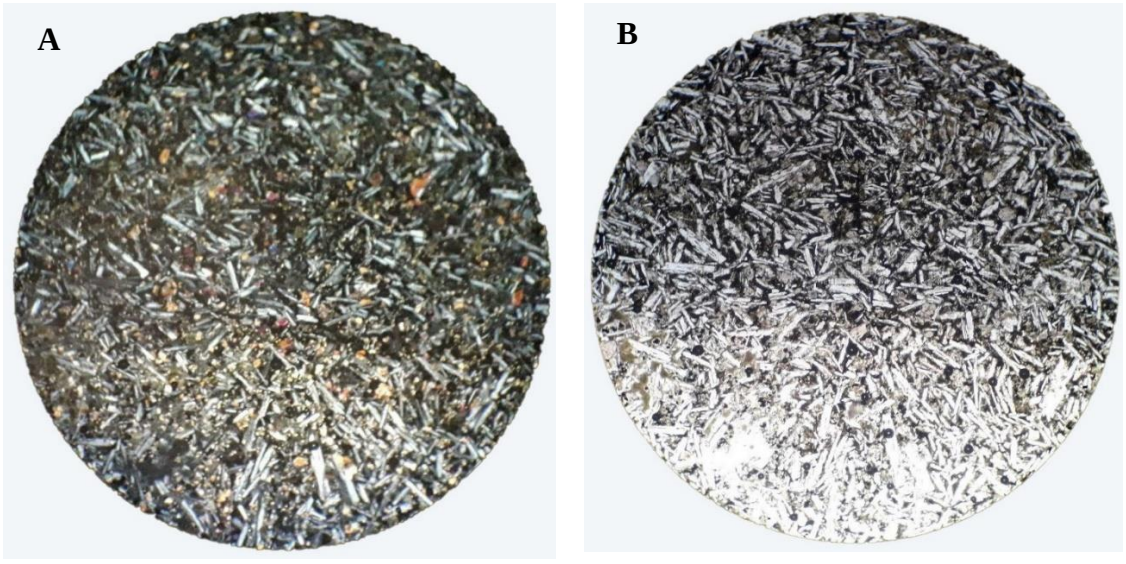

Fig. 3.13: Microphotographs of the upper basalt unit under (A) XPL and (B) PPL view for sample SR6 with magnification 4x.

3.3 Geological Structures

The area of study is characterized by structural features that are considered to have been formed as a result of extensional tectonic processes (Samson Tesfaye & Woldai Ghebreab, 2013; Wolfenden et al., 2005). Faults and joints are the major geological structures mainly found associated with the rocks in the study area. Joints are the common brittle structural features that are identified in nearly all lithological units of the study area. A description like orientations, types and sizes of the joints is given within the respective lithological unit in the description section, whereas the faults are described in detail as follow;

3.3.1 Fault

As noted earlier, the study area is situated along the southernmost section of the Western Afar Margin. The margin is well known to represent the major site of the fault zone (e.g. Wolfenden et al., 2005). The major tectonic structures, mainly normal faults, encountered in the area are formed by the extensional force and are oriented regionally along a general N-S direction (Wolfenden et al., 2005). Along the WAM, the faults are responsible for a series of fault-bounded grabens and Shewa Robit graben (Ataye as per Wolfenden et al., 2005) is one of the marginal grabens which is bounded by different normal faults. The major normal faults in the western part of the study area are formed during the early stage of the regional extension (Wolfenden et al., 2005). These major faults have N-S average strike orientation and are dipping toward the east direction, generally toward the rift. They are cut by NE striking and SE dipping normal faults (see Fig. 3.1). The hanging wall rollover to the border faults is antithetically faulted as illustrated in Fig. 3.1. Satellite image interpretation and previous structural studies (e.g. Wolfenden et al., 2005) show that the antithetic faults are dominantly striking NNE and dip dominantly NW, oblique to the N-S trending border faults. The full data of the major faults identified in the study area are presented in appendix II and their stereonet and rose diagrams are given in Fig. 3.14.

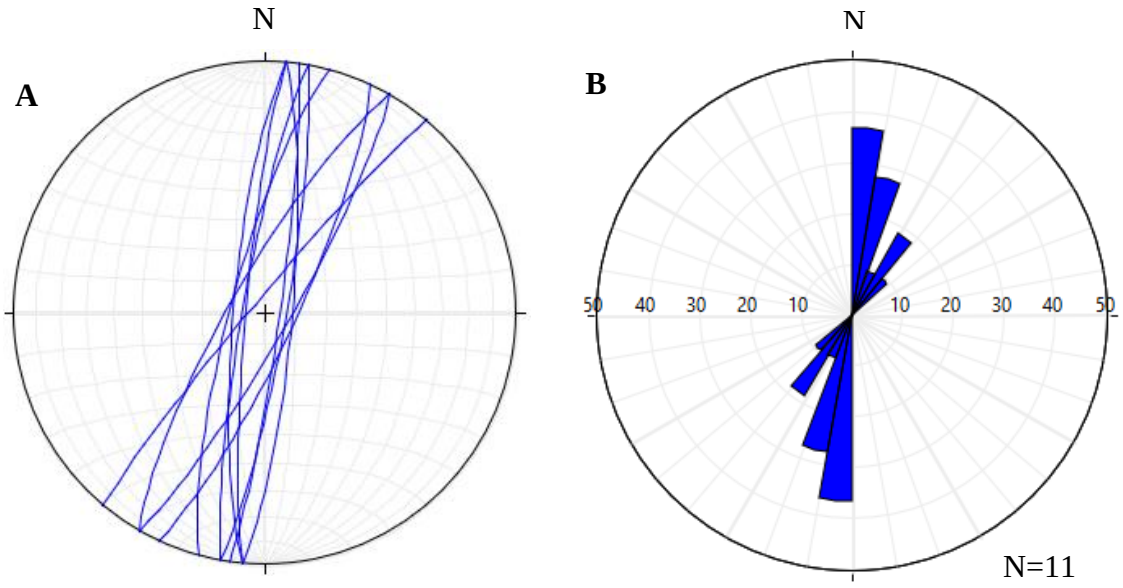

Fig. 3.14: (A) Stereo plot using equal-area projection for normal faults found in the study area on different rock units showing vertical to sub-vertical dip amount, (B) Rose diagram showing N, NNE and some NE trending normal faults

CHAPTER FOUR

4 GEOCHEMISTRY

4.1 Introduction

A total of eleven (11) representative sample (5-mafic and 6-felsic rocks) of volcanic rocks were analyzed for whole-rock geochemistry from the Shewa Robit area. The locations of these representative samples are shown in Fig. 3.1A. The sample preparation was done under ALS (Australian Laboratory Science) services in Addis Ababa, Ethiopia. Major element concentrations of the samples were determined by Inductively Coupled Plasma Atomic Emission Spectrometry (ICP-AES), whereas trace and rare earth element concentrations were determined by Inductively Coupled Plasma Mass Spectrometry 81 (ICP-MS) in Ireland by Australian Laboratory Science (ALS). The details of the analytical techniques used in the present study were already discussed in section 1.5.3 of chapter 1.

The analytical results of whole-rock chemical analyses (major oxides and trace elements including REE), CIPW norms and LOI values for the analyzed samples are given in Tables 4.1 and 4.2. Major element data along with CIPW normative minerals are used to have information about the type of volcanic rocks and to analyze the source and process of magma evolution at a preliminary level. Trace elements are used to further investigate the petrogenesis of the rocks. Except for one sample (DC4) which has a high LOI= 5.7 %, all the analyzed samples have a low LOI (< 2%), suggesting that they are fresh. Thus, the effect of post-emplacement alteration on elemental mobility could be considered only for one sample. Further, obvious correlations between LOI and selected major (Fig. 4.1) and trace elements (not shown) are absent for the studied volcanic rocks, indicating that these elements were not affected by post-magmatic processes. Therefore, all the results of samples are treated as primary for geochemical classification and petrogenetic interpretation. Furthermore, geochemistry of the volcanic rocks of the investigated area is compared with previously published geochemical studies (e.g. Pik et al., 1998, 1999; Dereje Ayalew et al., 2002). Moreover, various types of software such as Microsoft excel 2013, Petrographic 2 Beta (version 1.0.2) and Geochemical Data Kit (GCDKit version 4.0) are used to handle, analyze and generate different geochemical diagrams (e.g. Harker's variation, TAS classification and spidergrams diagrams),

Table 4.1. Major element geochemical analysis result and the CIPW norm of Shewa Robit bimodal basalt-rhyolite samples.

	Basalt					Rhyolite					
sample	SR2	SR6	SR5	Y01	AR1	SR7	SR8	DC4	DC5	SR9	SR1
SiO_2	47.1	47.3	48.3	50.1	52	69.7	69.7	69.9	73.2	75.4	77.7
TiO_2	2.67	3.74	3.21	2.39	2.62	1	1.04	0.31	0.51	0.38	0.38
Al_2O_3	14.05	16.05	14.51	19.55	14.7	13.85	12.45	11.05	11.85	10.8	7.73
Fe_2O_3	15.05	12.8	13.76	9.08	11	4.39	4.44	4.47	3.75	3.72	4.26
MnO	0.22	0.22	0.23	0.14	0.17	0.09	0.1	0.09	0.09	0.1	0.13
MgO	5.63	4.52	5.08	3.14	4.56	0.44	0.43	1.2	0.25	0.14	0.19
CaO	10.1	8.69	9.68	9.17	9.19	1.27	1.23	0.46	0.96	0.2	0.25
Na_2O	2.71	3.6	3.17	3.83	2.87	4.51	4.39	3.49	3.26	4.57	3.39
KO_2	0.42	1.7	0.88	1.23	1.06	4.33	4.55	4.25	4.55	3.58	3.47
P_2O_5	0.44	0.73	0.5	0.51	0.41	0.19	0.18	0.01	0.06	0.03	0.02
LOI	0.65	0.67	0.65	1.38	1.53	0.8	1.59	5.7	1.06	0.92	1.89
total	99.1	100.17	99.99	100.6	100.2	100.66	100.2	100.93	99.64	99.88	99.44
Mg#	42.6	41.1	42.24	40.65	45.09	16.57	16.1	34.72	11.67	6.93	8.12
A/NK	2.9	2.067	2.35	2.56	2.5	1.14	1.02	1.07	1.15	0.95	0.82
A/CNK	0.6	0.68	0.61	0.8	0.65	0.96	0.86	0.98	0.98	0.91	0.79
CIPW norm											
Q	5.76	0	4.34	2.31	9.98	24.13	24.88	30.66	34.59	35.44	46.08
Or	2.48	10.05	5.2	7.27	6.26	25.59	26.89	25.12	26.89	21.16	20.51
Ab	22.93	30.46	26.82	32.41	24.29	38.16	37.15	29.53	27.59	35.62	20.44
An	24.93	22.61	22.76	32.52	24.1	4.76	0.83	1.93	4.26	0	0
Ac	0	0	0	0	0	0	0	0	0	2.69	7.26
Di	10.79	2.77	9.12	1.45	8.06	0	0.68	0	0	0	0.23
Hy	9.02	9.82	8.43	7.15	7.62	1.1	0.76	2.99	0.62	0.35	0.37
Ol	0	0.11	0	0	0	0	0	0	0	0	0
Il	0.47	0.47	0.49	0.3	0.36	0.19	0.21	0.19	0.19	0.21	0.28
Hm	15.05	12.8	13.76	9.08	11	4.39	4.44	4.47	3.75	2.79	1.75
Tn	5.95	8.57	7.24	5.48	5.96	0.21	2.28	0.2	0.08	0.56	0.57
Ru	0	0	0	0	0	0.81	0	0.13	0.38	0.04	0
Ap	1.04	1.73	1.18	1.21	0.97	0.45	0.43	0.02	0.14	0.07	0.05
Sum	98.42	99.4	99.36	99.18	98.61	99.79	98.53	95.24	98.49	98.93	97.53

Normative minerals: Q = quartz; Or = orthoclase; Ab = albite; An = anorthite; Ac = acmite; Di = diopside; Hy = hypersthene; Ol = olivine; Il = ilmenite; Hm = hematite; Tn = titanite; Ru = rutile; Ap = apatite.

Table 4.2: Whole-rock trace element geochemical data for Shewa Robit volcanic rocks.

sample	SR2	SR6	SR5	Y01	AR1	SR7	SR8	DC4	DC5	SR9	SR1
Sc	34	15	30	13	26	3	8	3	2	2	2
V	445	292	305	199	251	44	53	10	17	12	9
Cr	60	<10	60	10	70	10	<10	10	10	<10	<10
Co	47	26	51	23	40	<1	2	<1	<1	<1	<1
Ni	49	16	50	163	27	2	2	1	<1	3	4
Cu	76	4	35	27	53	1	2	<1	<1	2	1
Zn	128	136	116	98	127	122	103	131	160	166	180
Ga	27.5	28.2	29.7	26.2	24	48.7	40.9	40.1	32.4	37	27.9
Rb	17	33	28.5	24.6	26.9	149.5	144	163.5	149.5	165	169
Sr	346	831	577	754	518	253	223	34.2	98.1	25.6	14
Y	24.6	34.6	31.4	28.4	32.6	60.9	52.2	61.5	55	62.6	66.3
Zr	157	358	241	270	204	675	708	1030	735	667	1090
Nb	16.2	45.8	30.5	45	26.6	77.4	78.5	85.5	93.6	77.2	110.5
Cs	0.32	0.21	0.2	0.15	0.19	1.26	0.96	1.4	1.25	0.28	0.38
Ba	287	566	446	577	551	991	897	540	765	376	108.5
Sn	2	3	2	2	2	5	4	10	6	7	8
La	16.6	49.7	33.2	42	30.1	97.9	98	135.5	94.2	109	120.5
Ce	36.6	99.8	68.2	95.3	66	173	156.5	248	187.5	183.5	138.5
Pr	5.19	13.65	9.4	11.3	8.51	21	22.5	31.5	23.8	27.8	30.4
Nd	23.7	58.1	35.5	44.9	36.7	84.5	86.7	119	86.5	103	111
Sm	5.66	12.7	9.1	9	7.59	15.6	15.3	23.4	18.7	20.5	21.3
Eu	1.98	3.36	2.8	2.72	2.3	3.08	3.42	3.1	3.12	3.17	3.78
Gd	6.71	11.2	9.49	9.38	7.56	12.25	12.5	22.8	17.7	19.75	17.75
Tb	1.04	1.55	1.34	1.35	1.15	1.94	1.83	3.55	2.85	2.99	2.74
Dy	6.09	8.39	7.71	7.54	6.7	13.1	12.65	22.3	16.5	17.7	17.25
Ho	1.25	1.67	1.49	1.49	1.31	2.72	2.68	4.48	3.26	3.48	3.36
Er	3.3	3.99	3.8	3.65	3.3	7.29	6.78	13.35	9.67	9	9.58
Tm	0.47	0.56	0.55	0.55	0.53	1.15	1.04	1.94	1.46	1.5	1.53
Yb	2.94	3.28	3.3	3.07	2.86	7.71	7.15	11.6	8.48	8.41	9.91
Lu	0.37	0.5	0.44	0.44	0.38	1.16	1.01	1.77	1.29	1.36	1.5
Hf	4.8	8.4	6.78	6.5	6.7	18.5	17.6	28.3	20.7	18.3	29.8
Ta	0.9	2.4	1.83	2	1.6	4.4	4.4	8.4	6.2	4.8	7.7
Pb	7	5	4	5	10	14	16	17	11	12	9
Th	1.67	4.63	3.52	4.51	3.38	21.4	21.6	21.5	17.9	19.25	23.85
U	0.45	1.03	0.8	0.93	0.62	3.73	3.4	3.91	4.04	1.34	2.16
W	2	1	2	2	1	3	3	4	4	1	2

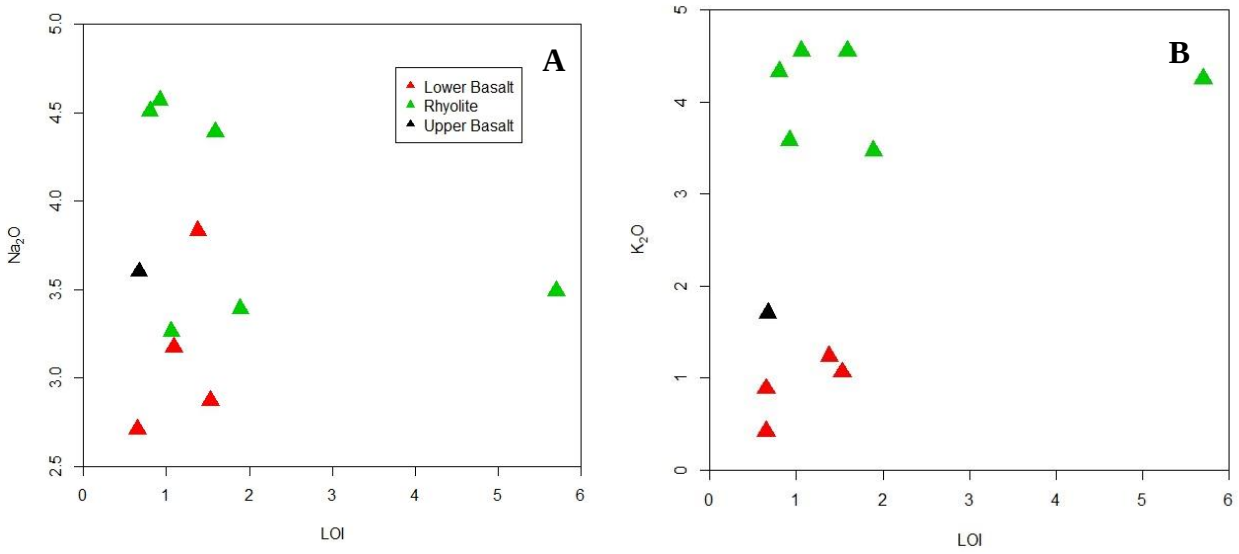

Fig. 4.1: LOI vs. Na_2O and K_2O, showing the effects of alteration.

4.2 Major Element Geochemistry

The analytical results of major element oxides (wt. %) and CIPW norms for the Shewa Robit volcanic rocks are reported in Table 4.1. Before using these major element concentrations in classification and variation diagrams, they are first recalculated to volatile free base compositions. The volatile free base values of the major oxides (given in appendix III) are calculated by normalizing the major element concentration value to 100 % by subtracting the volatile concentration, presented as LOI. Then all the diagrams, descriptions and interpretations of major elements are done using these recalculated (i.e. volatile free basis) results.

The analyzed samples from the study area show wide variations of SiO_2 values, varying from 47.6 to 79.6 wt. %. The basaltic samples are characterized by relatively low to moderate contents of SiO_2 (47.6-52.75 wt. %), high Al_2O_3 (14.28-19.72 wt. %), high Fe_2O_3 (9.16-15.3 wt. %) and intermediate MgO (3.17-5.72 wt. %). Their Magnesium numbers, Mg # = 100 (MgO/(FeO +MgO) (mol. %) (Janousek et al. 2016), range between 40.65 and 45.01, suggesting that the basaltic rocks have undergone a moderate degree of differentiation. The CaO/Al_2O_3 values of the studied samples range from 0.72 to 0.018, being higher for basaltic rocks (0.47-0.72) and lower for rhyolitic rocks (0.018-0.098). According to Pik et al. (1998), TiO_2 is the most important major element for classifying NW Ethiopian flood basalts into three groups (LT, HT1 and HT2). For comparison, some selected major and trace element data of these three basaltic types are presented in appendix

V. The comparison shows that Shewa Robit basalts are geochemically similar to Pik et al.'s (1998) HT1 type of NW Ethiopian flood basalt. On the other hand, the SiO_2 content of felsic rocks ranges from 69.8 to 79.6 wt. %, MgO from 0.14 to 1.26 wt. %, K_2O from 3.56 to 4.62 wt. % and TiO_2 from 0.33 to 1.06. They are relatively enriched in total alkalis ($K_2O + Na_2O$ = 6.86 –8.94 wt. %) and yield relatively uniform K_2O/Na_2O ratios (0.71–1.28). Moreover, the A/NK (molar Al_2O_3/ ($K_2O + Na_2O$)) and A/CNK (molar Al_2O_3/ ($CaO + K_2O + Na_2O$) values of the felsic samples are 0.82-1.15 and 0.79-0.98, respectively, which classify them as metaluminous and peralkaline.

4.2.1 Geochemical Classification

On the total alkali vs. silica (TAS) classification diagram (Le Bas et al., 1986), volcanic rocks from the Shewa Robit area define a typical bimodal (basalt–rhyolite) composition (Fig. 4.2). All felsic samples are rhyolitic in composition with silica content above 69.8 % wt., whereas the mafic samples are plot in basalt, basaltic-andesite and trachy-basalt (Hawaiite) fields. Notably, there is a lack of samples with SiO_2 content between 52.75 wt. % and 69.8 wt. %. Volcanic suites with such a lack/paucity of intermediate rocks (the so-called Daly Gap) have been recognized in many locations of the Ethiopian volcanic province (e.g. Trua et al., 1999; Dereje Ayalew et al., 2002; Peccerillo et al., 2003, 2007; Ronga et al., 2010). The TAS diagram incorporates a dividing line, suggested by Irvine and Baragar (1971), for distinguishing between two types of parental magmas: alkalic and tholeiitic series. Accordingly, the felsic samples from the Shewa Robit area show sub-alkaline nature (tholeiitic), whereas the mafic samples straddle between the alkalic and sub-alkaline (tholeiitic) fields. Form the mafic samples, the sample (SR6) collected from the upper basalt falls in the trachy-basalt (Hawaiite) field and shows alkaline character, whereas the basaltic rocks from the lower basaltic unit have dominantly transitional and tholeiitic characters and most of them fall along the boundary separating the alkaline from the sub alkaline series. Furthermore, the geochemical signature observed in this study confirms the previously proposed bimodal nature of the volcanic rocks in the Western Afar Margin (e.g. Dereje Ayalew et al., 2006).

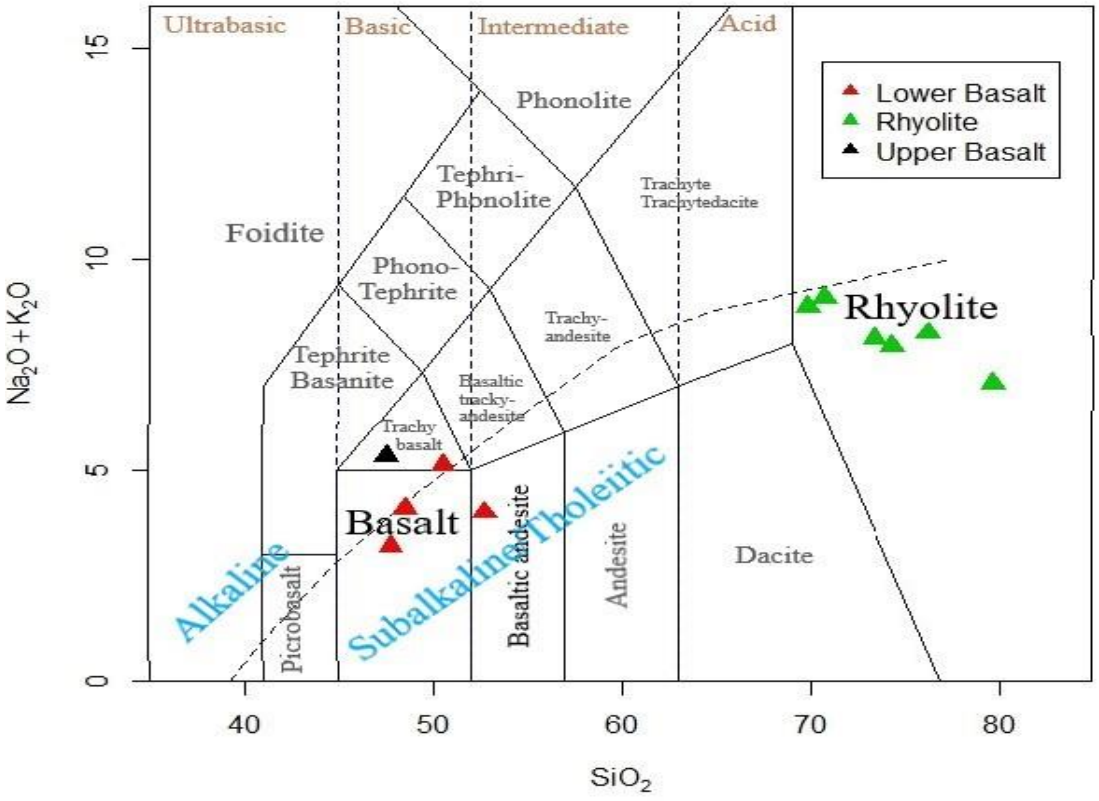

Fig. 4.2: Total alkalis–silica (TAS, Le Bas et al., 1986) classification diagram for Shewa Robit volcanic rocks, showing the bimodal basalt–rhyolite composition. The dividing line between alkaline and tholeiitic rocks is from Irvine and Baragar (1971).

Furthermore, the CIPW-normative compositions of the Shewa Robit volcanic rocks were calculated by using the software known as GCDKit (version 4) and the results are given in Table 4.1. With the exception of one sample (SR6), which is collected from the upper basalt, all the mafic samples exhibit quartz (max. =9.98) and hypersthene (max. = 9.02) normative compositions and are devoid of nepheline normative. Based on this, these mafic samples are grouped under silica-oversaturated basalt (Quartz tholeiite), whereas the other one basaltic sample (SR06) is classified as silica-saturated basalt (Olivine tholeiite) which is characterized by the presence of olivine and hypersthene normative. Generally, basalts from The Shewa Robit area are classified as tholeiitic. On the other hand, all the rhyolite rocks are rich in normative quartz (24.13– 46.07 Wt. %). From the felsic rocks, two samples (SR9 & SR1) have shown a peralkaline affinity which is reflected by the presence of normative acmite ($NaFe^{+3}Si_2O_6$).

4.2.1. Major Element Variation Diagrams

The major element data of the Shewa Robit volcanic rocks reported above in table form can be visualized and compared easily using variation diagrams, which are popularly known as Harker's variation diagrams. Variation diagrams are very important for the identification of magmatic processes responsible for differentiation (e.g. fractional crystallization versus magma mixing) (Wilson, 2007). For the analyzed samples, variation diagrams of major oxides are plotted against SiO_2 content as it shows a wide range of variation (47.6 to 79.6 wt. %) (Fig. 4.2). Fe_2O_3, MgO, CaO, P_2O_5 and TiO_2 exhibit almost negative trends with increasing SiO_2 concentration. Decreasing in Fe_2O_3, MgO, CaO and TiO_2 contents may suggest the separation of ferromagnesian minerals such as olivine, pyroxene and Fe-Ti oxides (e.g. magnetite) whereas the decreasing of P_2O_5 content is indicative of apatite fractionation. On the other hand, Na_2O exhibits scattered distribution against SiO_2 content whereas K_2O and Al_2O_3 display almost inflected trends. The concentration of Al_2O_3 increases up to 50.53 wt. % of SiO_2 and then decreases with increasing SiO_2 whereas the concentration of K_2O increases up to 73.4 wt. % of SiO_2 and then decreases with increasing SiO_2. The inflected trend in any variation diagram is generally taken to indicate either the entry of a new phase during crystal fractionation or loss of phase during partial melting (e.g. Rollinson, 1993). Thus, the inflected trends in Al_2O_3 and K_2O suggest that the fractional crystallization of plagioclase and K-feldspar were important in the last stage of the magma evolution.

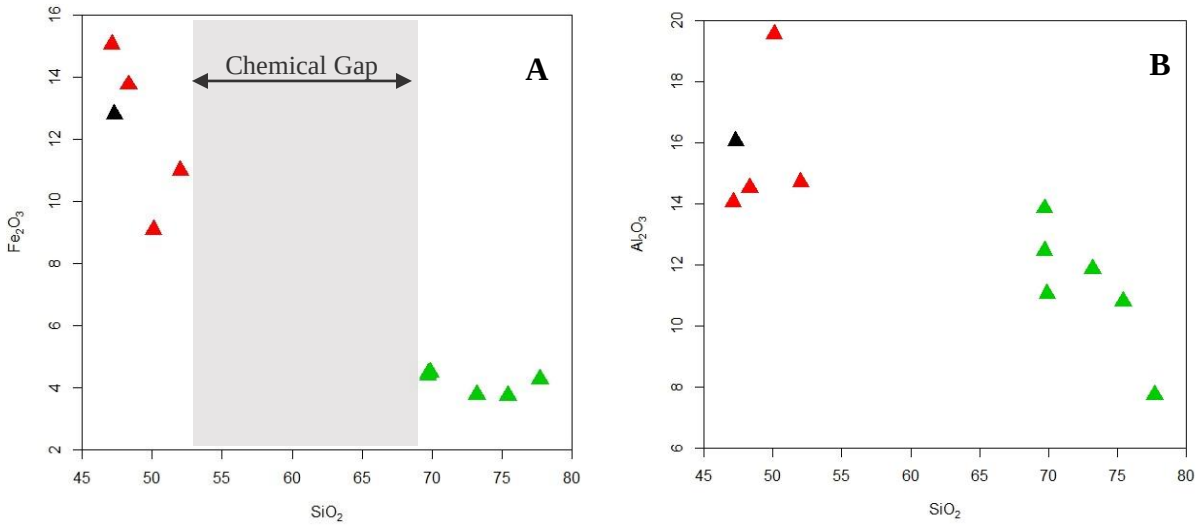

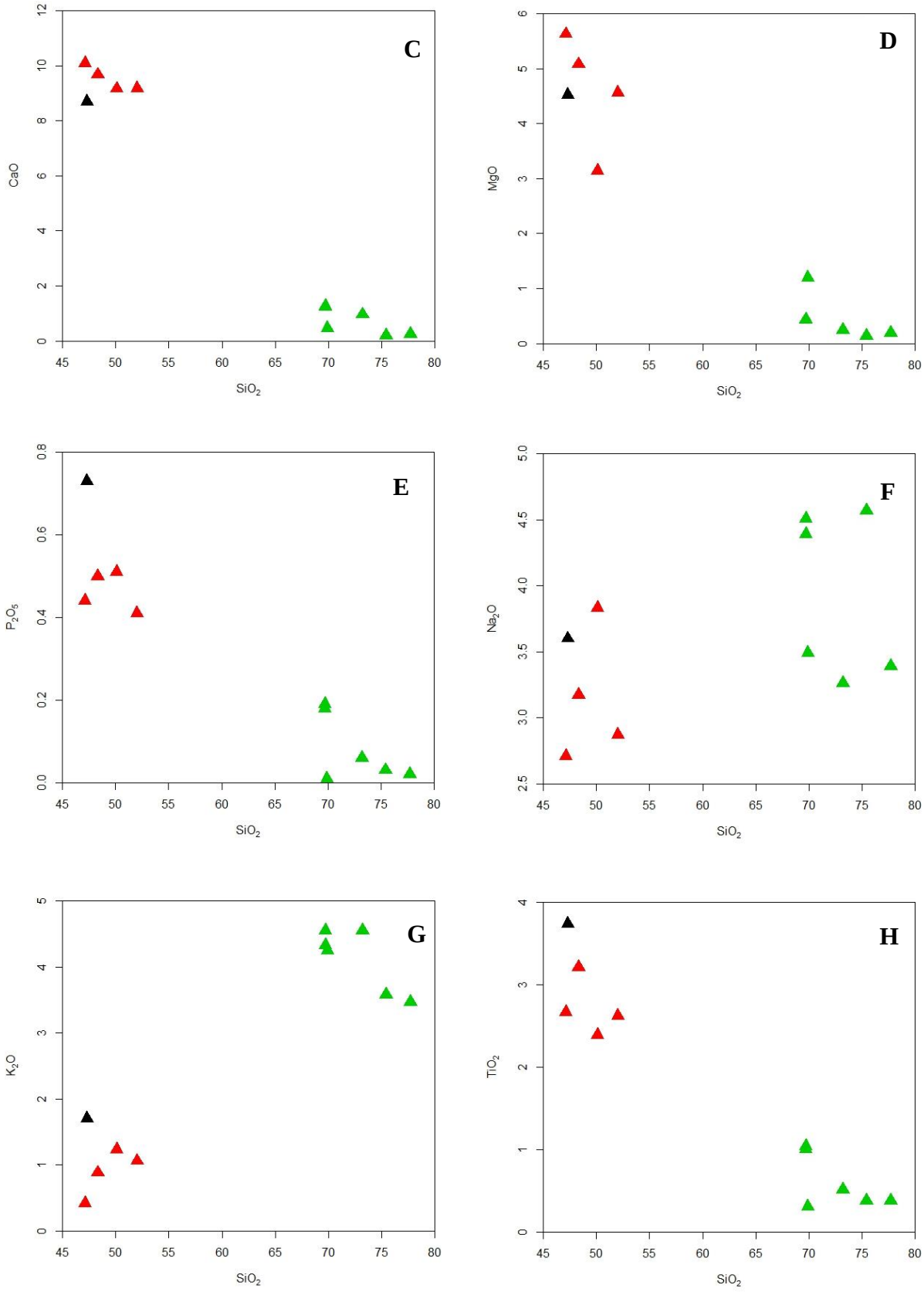
C
CaO
SiO2
D
MgO
SiO2
E
P2O5
SiO2
F
Na2O
SiO2
G
K2O
SiO2
H
TiO2
SiO2

Fig. 4.3: Major element Harker variation diagrams for the volcanic rocks of the Shewa Robit area. Major element concentrations (wt. %) are according to the volatile free base. The gray shaded area in fig. A indicates the SiO_2 gap in the volcanic suite. Symbols are the same as in Fig. 4.1.

4.3 Trace Element Geochemistry

Trace elements are those elements whose concentration level is below 0.1 wt. % in the igneous rocks (White, 2005; Rollinson, 1993). Trace element contents of volcanic rocks from the Shewa Robit area are reported in Table 4.2. Their concentrations are expressed in parts per million (ppm; 1 ppm = 10^{-4} wt. %). The analyzed mafic samples have a relatively higher concentration of compatible elements (Ni = 16-163 ppm, Cr = <10-70 ppm, Co = 23-51 ppm and Sc = 13-34 ppm) than those of highly fractionated silica-rich rocks. However, the concentration of these compatible elements in the mafic rocks are extremely lower than the ranges expected for magmas in equilibrium with mantle sources (Ni> 400-500 ppm and Cr> 1000 ppm; Wilson, 1989, 2007). This suggests that these rocks do not represent primary magmas rather underwent olivine and clinopyroxene fractionation. On the other hand, the highly fractionated silica-rich rocks have very low contents of Ni ≤ 4 ppm, Cr < 10 ppm, Sc ≤ 8 ppm, Sr ≤ 253 and V ≤ 53 ppm, with a concentration below the detection limit for some of the silicic rocks. Furthermore, the concentrations of these compatible trace elements are plotted against SiO_2 in bivariate diagrams (Fig. 4.4). Ni, Cr, V, Sr and Sc exhibit negative correlations with increasing SiO_2. The negative trends of Ni and Cr support the fractionation of olivine ± clinopyroxene, whereas the V and Sr reflect the fractionation of Fe-Ti oxides (e.g. magnetite) and plagioclase, respectively.

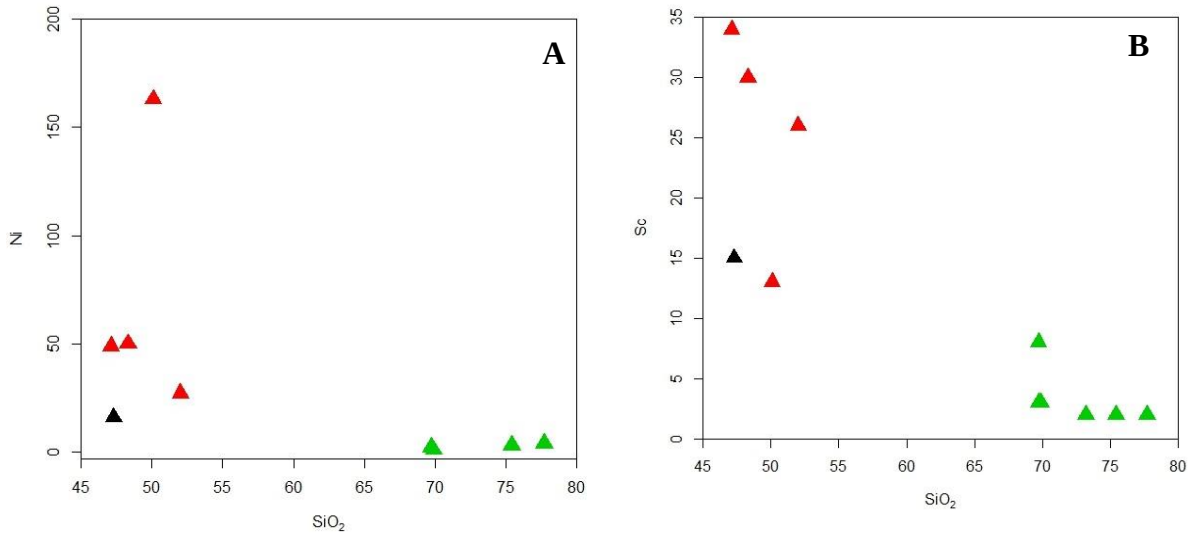

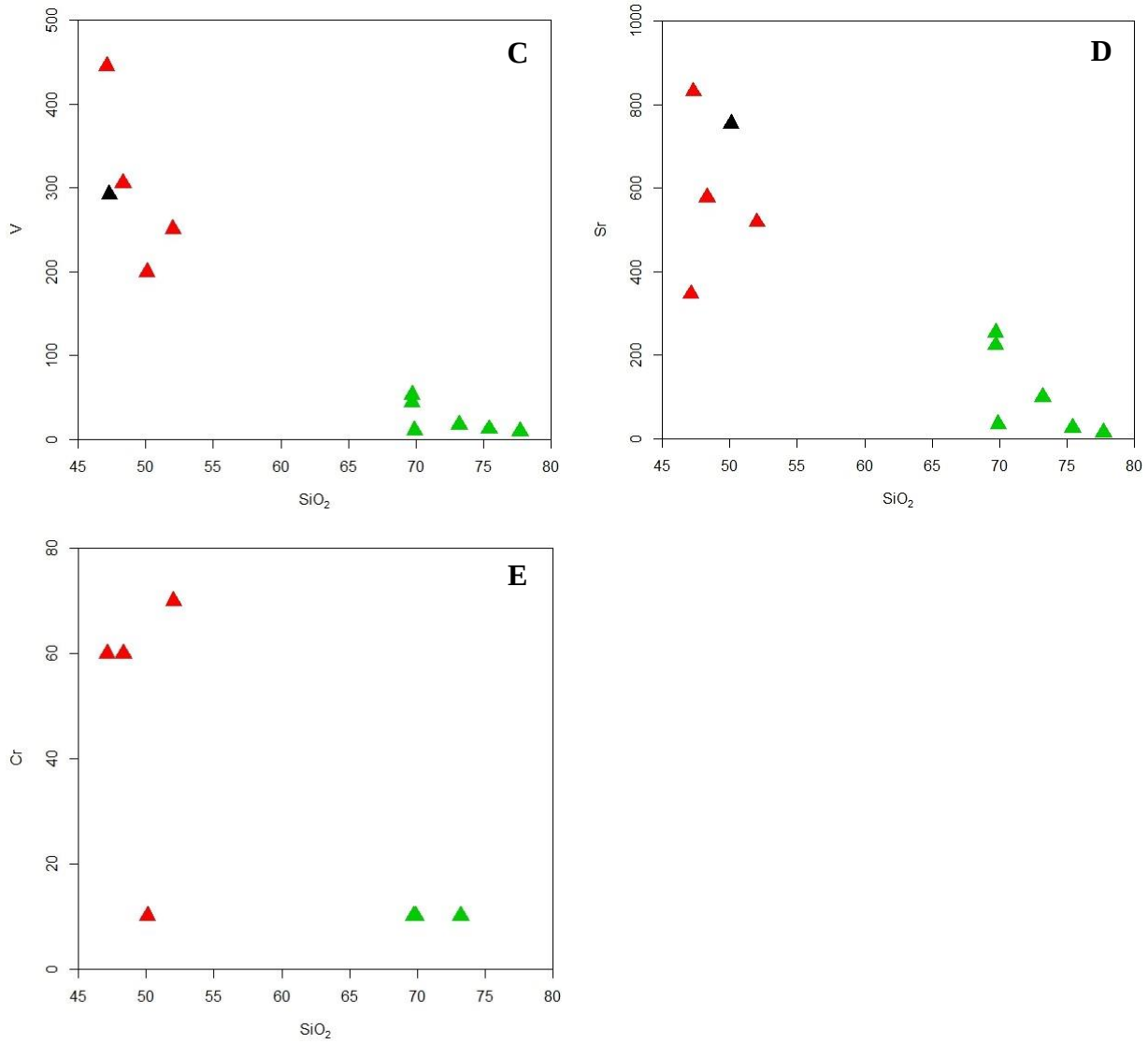

Fig. 4.4: Variation diagram of compatible elements against SiO_2 for Shewa Robit bimodal volcanic suite. The concentration of trace elements is in ppm while the major element (SiO_2) is in wt. %. Symbols are the same as in Fig. 4.1.

The studied samples of bimodal volcanic rocks from the Shewa Robit area also show a great variation in terms of their incompatible trace elements (Table 4.2). Generally, the rhyolitic samples have higher concentration values of incompatible elements compared to mafic samples. Incompatible elements have a low bulk distribution coefficient in the mafic magmas and as the crystallization proceeds they will be concentrated in the highly evolved rocks of a volcanic suite (e.g. Dereje Ayalew et al., 1999; Willson, 2007). Thus, the increment of incompatible trace

element abundance from mafic to felsic rocks within this volcanic suite implies the involvement of the fractional crystallization process in the generation of the rhyolitic rocks.

Further, the variation diagrams for some of the selected incompatible trace elements against SiO_2 are illustrated in Fig. 4.5. Although some scatters are present, Rb, Th, Hf, Nb and Y concentrations generally increase continuously with increasing SiO_2 content throughout the suite. Ba exhibits a positive correlation against SiO_2 for all mafic samples and a negative correlation for rhyolitic samples, displaying an overall inflected trend. The negative correlation of Ba depicted by the silicic rocks suggests that fractionation of K-feldspar was important during their formation. Furthermore, in addition to variations in major element contents (i.e. Ti_2O, Fe_2O_3, P_2O_3 and Si_2O), the northwestern (NW) Ethiopian flood basalt groups (HT1, HT2 and LT) have also shown great variability in their trace element geochemistry (Pik et al., 1998, 1999). A comparison of some incompatible trace element ratios shows that basaltic rocks of Shewa Robit are similar to Pik et al.'s (1998) HT1 type of NW Ethiopian basalt (Fig. 4.6). Similarly, the geographically associated Oligocene-Miocene Ethiopian plateau rhyolites/ignimbrites with these flood basalts have also presented distinct major and trace element compositions (Dereje Ayalew et al., 2002). A comparison of some incompatible trace element ratios shows that the Shewa Robit rhyolites/ignimbrites have trace element ratios similar to Dereje Ayalew et al.'s (2002) Debre Birhan and Wegel Tena rhyolites/ignimbrites (Fig. 4.7).

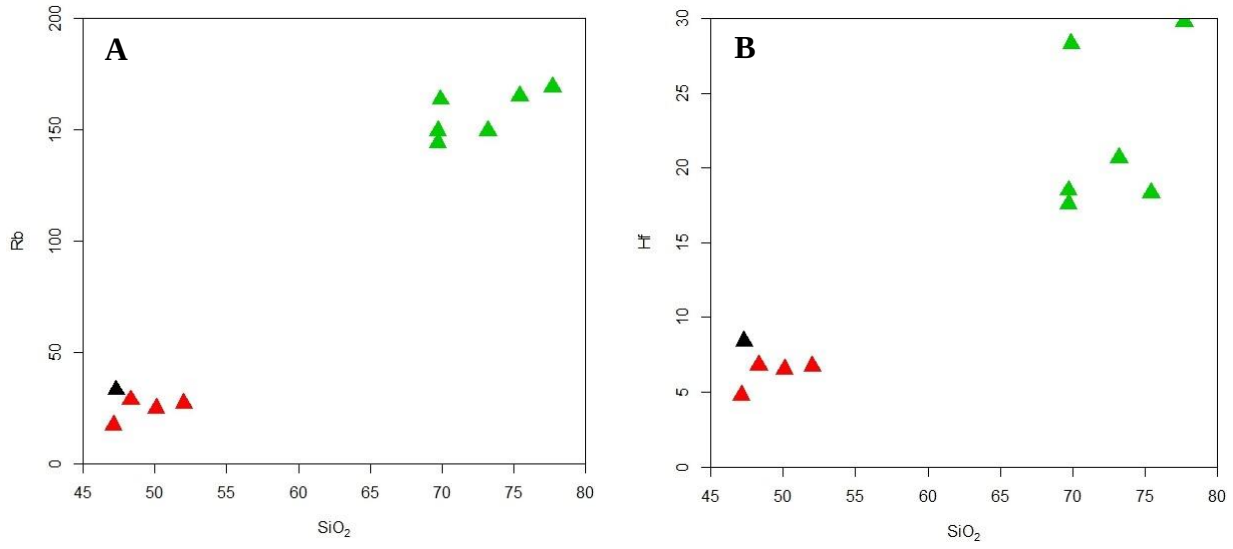

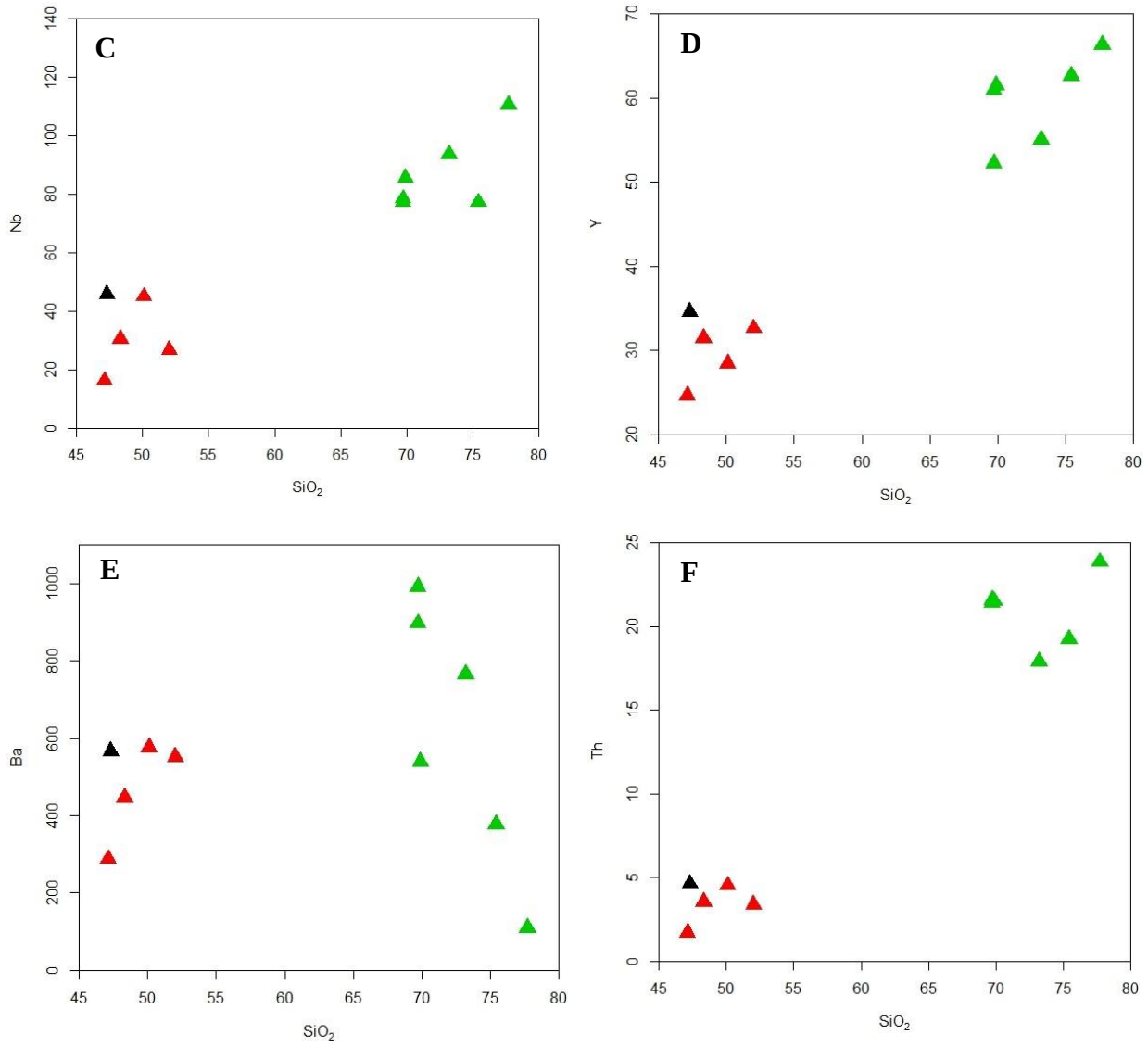

Fig. 4.5: Variation diagram of some selected incompatible trace elements (ppm) against differentiation index SiO_2 (wt. %) for the Shewa Robit bimodal volcanic suite. Symbols are the same as in Fig. 4.1.

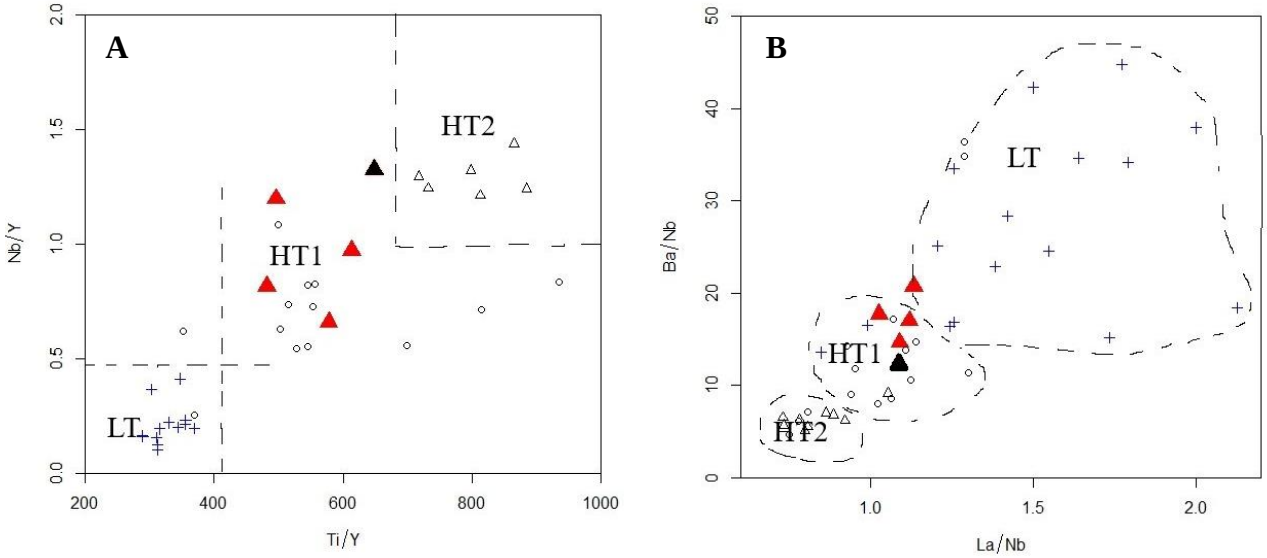

Fig. 4.6: Trace element ratio comparison of the Shewa Robit basalts with the northwestern Ethiopian plateau flood basalt types (LT, HT1, HT2; Pik et al., 1998). (A) Ti/Y versus Nb/Y and (B) Ba/Nb versus La/Nb. It shows the trace element ratios of Shewa Robit basalts are very similar to HT1 basalts. Data and field of LT (+), HT1 (o) and HT2 (Δ) shown for comparison are from Pik et al. (1998). The symbols for this study are as in Fig.4.1.

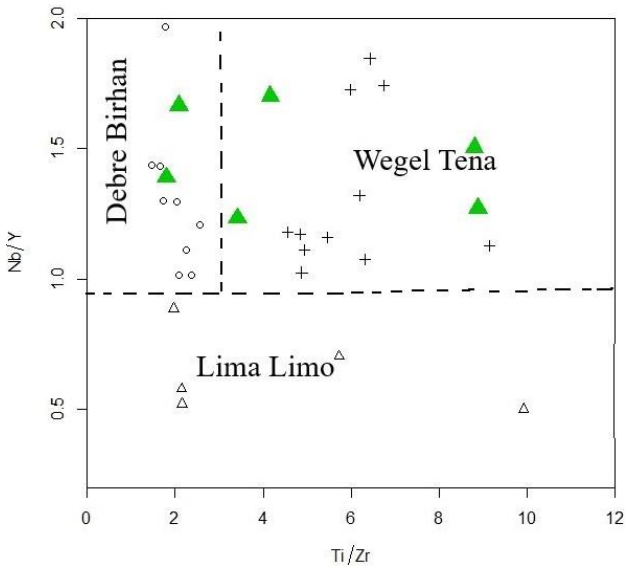

Fig.4.7: Binary plots of Ti/Zr versus Nb/Y comparing the Shewa Robit silicic volcanic rocks with northwestern Ethiopian rhyolites/ignimbrites (after Dereje Ayalew et al., 2002). The data of Wegel Tena (+), Debre Birhan (o) and Lima Limo (Δ) shown for comparison are taken from Dereje Ayalew et al. (2002). The symbols for this study are as in Fig.4.1.

Figure 4.8 shows plots of two highly incompatible trace elements (Zr versus Nb, Hf and Ta). It is well known that plots of two highly incompatible trace elements with similar bulk partition coefficients are very important to ascertain whether all volcanic rocks within a volcanic suite are genetically related or not (e.g. Wilson, 1989; Rollison, 1993; Dereje Ayalew et al., 2018). It can be noticed from Fig. 4.8 that most of the samples define a strong linear trend generally passing through the origin. This suggests that the basalt and rhyolite rocks of the study area are derived from a common source (i.e. they are cogenetic rocks). In addition to this, such variation diagrams are also very important to study the behavior of elements in magmatic evolution by taking Zr as an index.

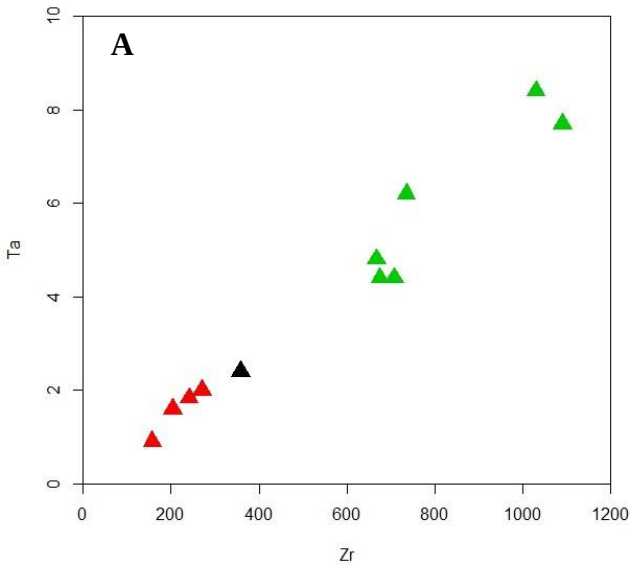

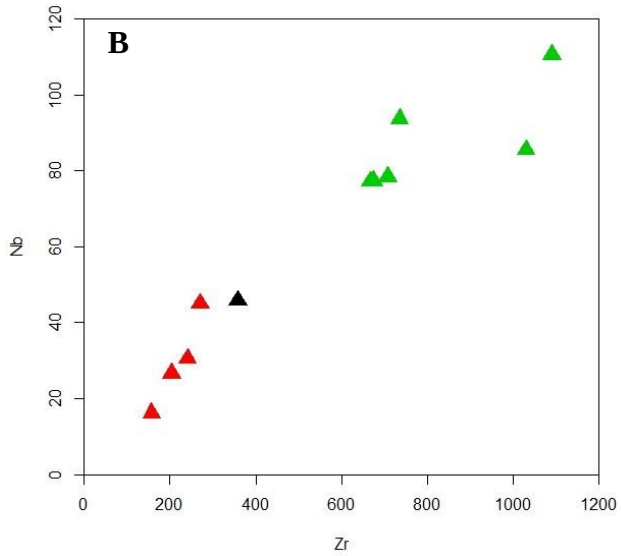

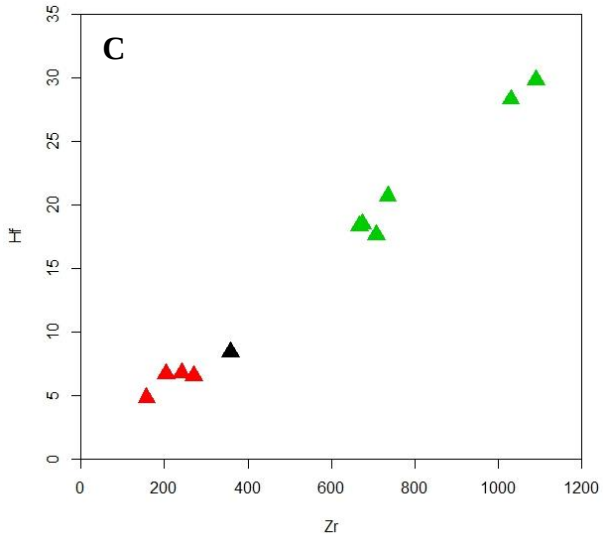

Fig. 4.8: Variation diagrams of some selected trace elements against Zr for the Shewa Robit basalt–rhyolite suite.

In addition to the above plots, bivariate plots of some selected trace elements against the trace element ratio are very important to provide crucial information regarding the fractionation of the volcanic rocks. For samples of silicic volcanic products, Sr and Ba against Rb/Sr are plotted and show negative trends (Fig. 4.9). The negative correlation between Sr and Rb/Sr and the lower Sr contents (Table 4.2) in the felsic samples indicate plagioclase fractionation, whereas the inverse correlation between Ba and Rb/Sr for rhyolites indicates K-feldspar fractionation.

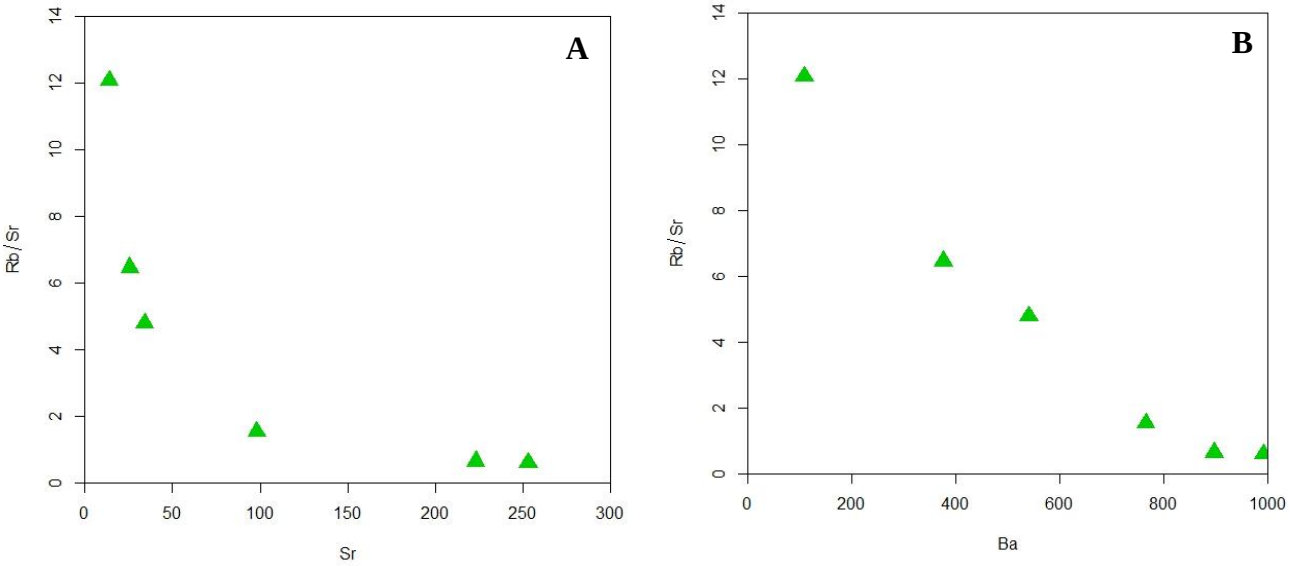

Fig. 4.9: Variation diagrams of Sr and Ba against trace element ratio (Rb/Sr) for the silicic volcanic of the Shewa Robit area. The unit for the Sr and Ba concentrations is in ppm.

4.3.1 Rare Earth Elements (REEs)

The chondrite-normalized (Boynton, 1984) rare earth element (REE) patterns of the analyzed samples are shown in Fig. 4.10 A and B. In this section, the REE analysis of the studied samples is done separately for mafic and silicic rocks. Samples from the mafic rocks show a parallel to the sub-parallel pattern to each other with enrichment in light rare earth elements (LREEs). The enrichment of LREEs with respect to the heavy rare earth elements (HREEs) $(La/Yb)_N$ ranges from 3.81 to 10.2, whereas the HREEs are moderately fractionated with an almost flat pattern ($(Gd/Yb)_N$ = 1.84- 2.76). Notably, none of the mafic samples show a significant anomaly in Eu (Eu/ Eu*=

0.86-0.98), which is explained by the lack of plagioclase fractionation on the early fractionating phases.

The chondrite-normalized REE diagram for the felsic samples also shows strong enrichment in the LREE as compared to HREE (Fig. 4.10B). Their La_N/Yb_N ratio, index of LREE to HREE fractionation, varies between 7.49 and 9.24, suggesting a moderate degree of LREE to HREE fractionation. They reflect well defined moderate to high negative Eu (Eu/Eu*) anomalies varying from 0.41 to 0.75. This is a typical indication for the fractionation of plagioclase feldspar (Hanson, 1980; Rollinson, 1993). Moreover, some rhyolite samples have displayed negative anomalies at Ce which could be due to alteration. Generally, the sum of REEs within the volcanic suite varies from 111.9 to 268.43 ppm in mafic rocks and from 422.29 to 642.29 ppm in felsic rocks.

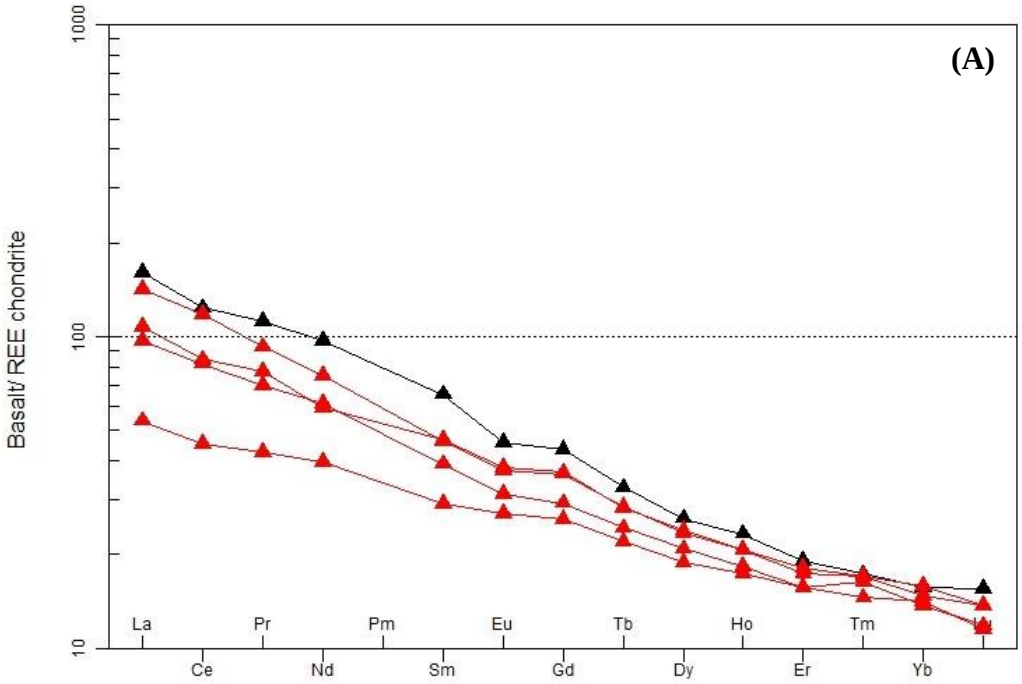

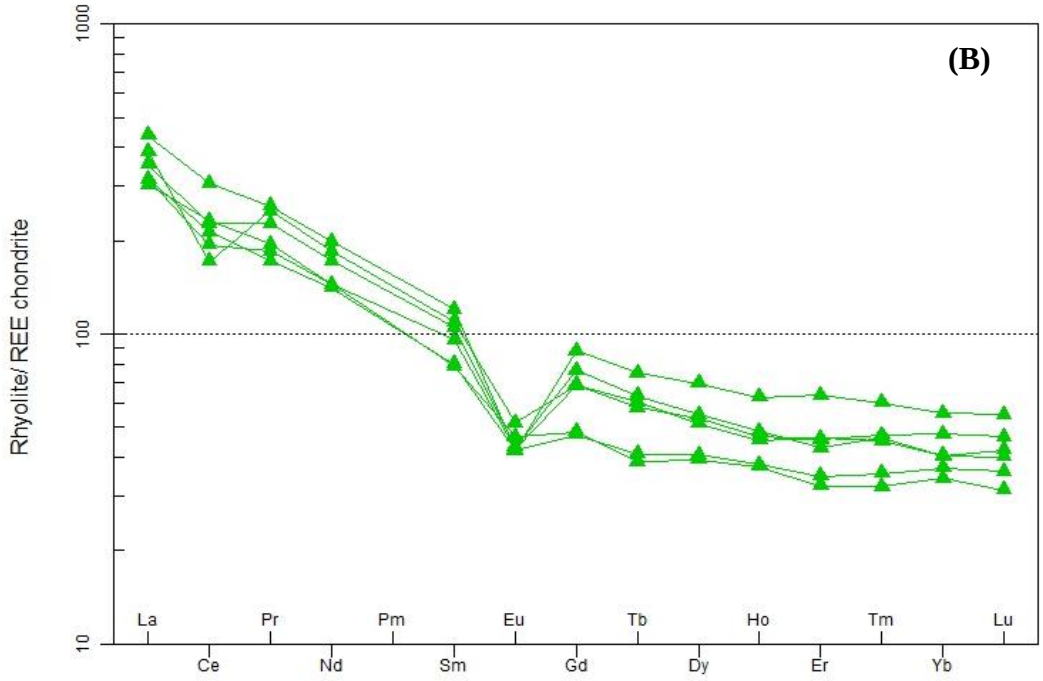

Fig. 4.10: Chondrite-normalized REE patterns of representative samples for basaltic (A) and rhyolitic (B) rocks. Normalization values are from Boynton (1984).

4.3.2 Multi-Element Variation Diagram

Primitive mantle-normalized (Sun and McDonough, 1989) multi-element variation diagrams for the volcanic rocks from the Shewa Robit area are presented in Fig. 4.11 A and B. Elements are arranged in order of decreasing incompatibility from left to right. The multi-element variation diagram of mafic samples shows relative enrichments at Ba, Nb, La, Nd and Pb and negative anomalies at U, Th, K and P. The absence of negative anomalies at Nb in all mafic samples may indicate the absence of a significant crustal contribution during the evolution of the magma. On the other hand, the primitive mantle-normalized multi-element variation diagram for the rhyolite rocks displays similar patterns to each other with marked troughs at Ba, Ce, Sr, P, Ti and Y and positive anomalies at Rb, Th, Pb, Zr and Dy. The slight enrichment and depletion of elements on the multi-element variation diagrams may indicate the involvement and removal of some minerals during the evolution of magma (e.g. Wilson, 1989; Rollison, 1993). The negative anomaly at Ba, Sr, P and Ti indicate the fractionation or removal of K-feldspar, plagioclase, apatite and Fe–Ti oxides (e.g. accessory ilmenite), respectively, during the evolution of magma.

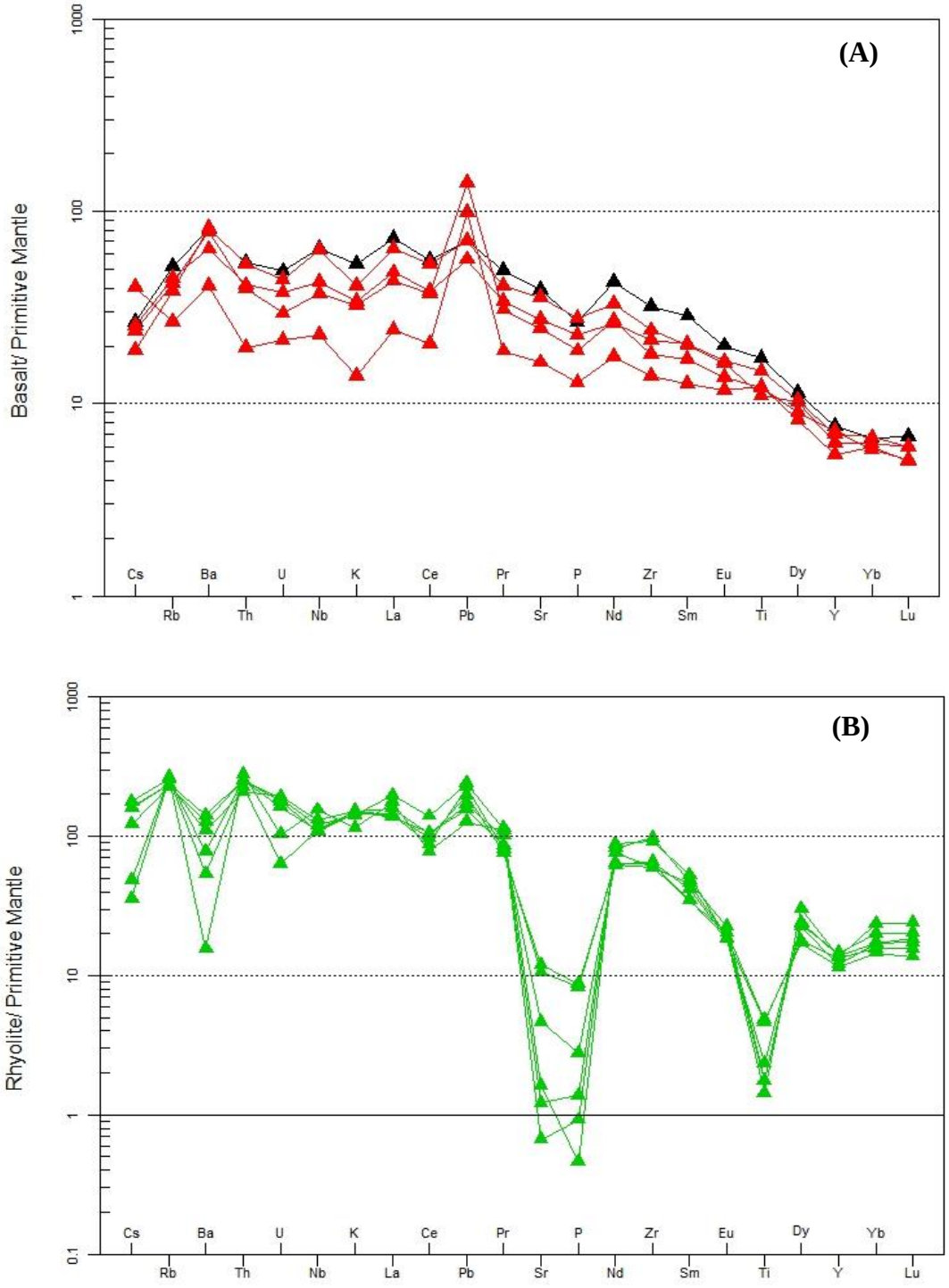

Fig. 4.11: Primitive mantle-normalized multi-element variation diagram for basaltic (A) and rhyolitic (B) rocks. The normalization values are from Sun and McDonough (1989).

CHAPTER FIVE

5 DISCUSSION

5.1 Petrogenesis of Mafic Rocks

Similar to the case of other basaltic rocks, Shewa Robit basaltic rocks were most probably derived from a mantle source. However, the concentration of the compatible elements such as Ni (<163 ppm) and Cr (<10-60 ppm), as well as the MgO contents (3.17-5.72 wt. %) in the mafic rocks are much lower than the ranges expected for magmas in equilibrium with mantle sources (Ni> 400-500 ppm, Cr> 1000 ppm and MgO content between 10 and 15 wt. %; Wilson, 1989, 2007; Dereje Ayalew et al., 2016 and references therein). This suggests that these rocks do not represent primary magmas rather underwent olivine and clinopyroxene fractionation, either in the magma chambers of their parental magma or en route to the surface. The geochemical and petrographic data of the Shewa Robit volcanic rocks show that fractionation of different minerals have occurred during their evolution and the detailed fractionation process is explained below in section 5.2.1.

During their transportation to the surface, mantle-derived magmas can be also modified by the assimilation of crustal materials (Wilson, 1989; Dereje Ayalew et al., 1999). It is noted that crust contaminated or subduction-related volcanic rocks have strong enrichments in LREE and highly incompatible elements on REE and on multi-element variation diagrams, respectively (e.g. Dereje Ayalew et al., 2016). Thus, the higher abundances of highly incompatible elements in the studied basaltic rocks combined with their LREE enrichment (Fig. 4.10A) may indicate either crustal contamination or their derivation from an enriched mantle source. Moreover, ratios of some trace elements such as Ce/Pb, Nb/U, La/Nb and La/Ta are sensitive to contamination and well-defined for primary mantle-derived liquids (Ce/Pb ratio= 25 ± 5 and Nb/U = 47 ± 10, Hofmann et al., 1986; La/Nb ratio < 1.5, and La/Ta ratio < 22, Hart et al., 1989). Mafic rocks from the Shewa Robit basin (lower basalts) have Ce/Pb (5.22-19.06), Nb/U (36-48.3), La/Nb (0.93-1.13) and La/Ta (18.14-21). Their Ce/Pb ratios are lower than the typical mantle range but higher than values for the continental crust (average Ce/Pb = 3.9; Rudnick and Gao, 2003). Additionally, these basalts display positive Pb anomalies in their primitive mantle-normalized trace element diagram (Fig. 4.11A), indicating crustal input in their evolution. However, none of these investigated mafic rocks show negative anomalies at Nb, a distinctive feature of continental crust contaminated magmas (Rollinson, 1993; Dereje Ayalew et al., 2016), in their primitive mantle-normalized multi-element

variation diagram (Fig. 4.11A), These geochemical features indicate some crustal contamination but that contamination does not exert a controlling effect in the evolution of these volcanic rock units. On the other hand, the sample from the upper basalt (sample SR6) has trace element ratios (Ce/Pb =20, Nb/U =44.46, La/Nb =1.08 and La/Ta =20.7) that are typical of the mantle range with no negative anomaly at Nb (Fig. 4.11A), indicating that it is not contaminated by crustal materials.

5.1.1 Magma Generation and Source Rock Characteristics

The ratios of incompatible trace element pairs, such as Ce/Pb and Nb/U, are more useful in identifying differences in magma sources than the absolute abundances of trace elements because fractionation of these pairs during partial melting is minor (e.g. Allegre et al., 1995). The investigated mafic samples from the study area exhibit trace element ratios such as Nb/U (36-48.3), Zr/Nb (6-9.69), Ba/La (11.39-18.31), La/Nb (0.93-1.13) and Ba/Nb (12.3-20.7), which are similar to those observed in modern OIB (Weaver, 1991). This suggests that these lavas are derived from mantle sources that are similar to OIB-type sources at least on the basis of trace element ratios. Moreover, in the Th/Yb vs. Nb/Yb plot of Pearce (2008), basaltic samples from the study area fall on the enriched side of the diagram very close to the values suggested for OIB (Fig.5.1). This further suggested that these basalts are most likely originated from the enriched mantle source like the OIB mantle source. However, none of these studied mafic samples have exhibited trace element ratios typical of a MORB signature, implying that this component plays little or no role in the genesis of these lavas. Furthermore, it is discussed in sections 4.2 and 4.3 of chapter 4 that all the studied basaltic rocks have similar geochemical characteristics to the HT1 type of the northwestern Ethiopian flood basalt. Ethiopian HT1 magmas have OIB-like geochemical signatures and have been interpreted as melts derived from an ascending mantle plume with moderate involvement of upper-crust components based upon their radiogenic isotope signatures (e.g. Pik et al., 1999; Kieffer et al., 2004). However, modeling of the HT1 trace element patterns suggests that these samples may also represent melts of the sub-continental lithospheric mantle that had undergone significant metasomatism associated with an ascending mantle plume (Beccaluva et al., 2009).

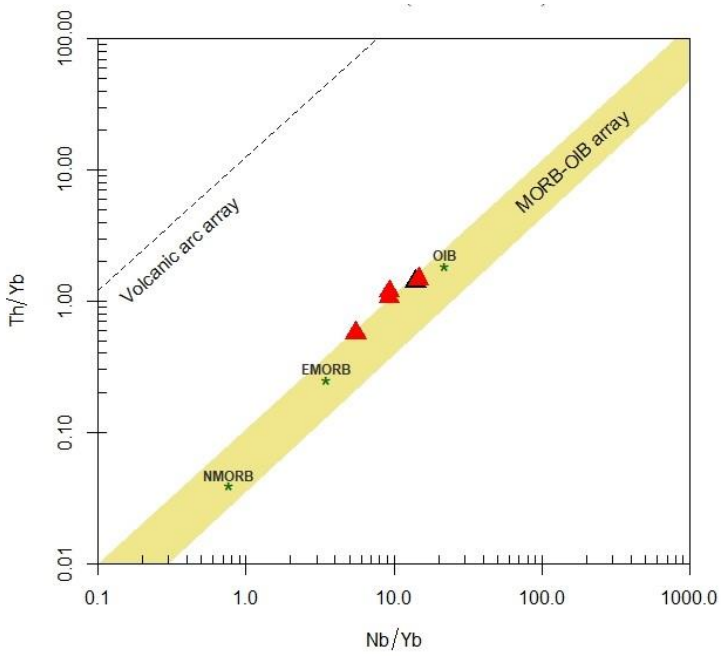

Fig. 5.1: Nb/Yb vs. Th/Yb plot of the basic volcanic rocks of the Shewa Robit area (after Pearce (2008)). It notes the enriched mantle source characteristics of Shewa Robit basics.

On the chondrite-normalized rare earth element (REE) diagram (Fig. 4.10A), the studied basaltic samples display flat HREE patterns (Tb_N/Yb_N = 1.55-2.08) with somewhat elevated HREE concentrations higher than 10-times chondritic values. These geochemical features in combination with relatively low CaO/Al_2O_3 ratios (0.47-0.72) of the basic rocks suggest a mantle source containing spinel rather than garnet (Willson, 2007; Dereje Ayalew et al., 2016). Moreover, in their primitive mantle-normalized multi-element variation diagram (Fig. 4.11A), all the basaltic samples have shown enrichments at Ba and depletions at K. According to Dereje Ayalew et al. (2016 and references therein), such enrichments and depletions are thought to be related to amphibole and/or phlogopite presence in the mantle source. The studied basalts are characterized by higher Na_2O contents than the K_2O contents, indicating that the mantle source contains amphibole rather than phlogopite (Rosenthal et al., 2009 as cited in Dereje Ayalew et al. 2016). In addition to this, the studied basalts have higher ratios of Ba/Rb (15.6-23.4) and Nb/Th (7.8-9.9) and a low ratio of Rb/Sr (0.03-0.05), further indicating that the source region contained amphibole rather than phlogopite (Aydin et al., 2014). Thus, the major and trace element data indicate that basalts from the Shewa Robit area were derived from the melting of amphibole-bearing spinel peridotite source. Because the mineral amphibole is stable only under relatively low temperatures

and pressures, the presence of this mineral implies a shallow mantle source and suggests an origin from the sub-continental lithosphere rather than from the deeper asthenosphere (Kieffer et al., 2004; Daniel Meshesha and Shinjo, 2007; Dereje Ayalew et al., 2016). The lack of significant MREE enrichment in the mafic samples (Fig. 4.10A) suggests that amphibole was present in the residue after partial melting.

Furthermore, it is well known that La is more incompatible than Sm, and thus, on melting, the La/Sm ratios will be highest for the lowest degree of partial melting and would gradually decrease with increasing degrees of partial melting (Wu et al., 2019). Mafic samples from the lower basalts have $(La/Sm)_N$ ratios (1.84-2.49), whereas the sample from the upper basalt have $(La/Sm)_N$ ratio 3.08. This shows that the upper basalt has formed by the lowest degree of partial melting than the lower basalts. Moreover, the ratio of trace elements like Ba/Nb is important to provide information on melting processes and it increases as the degree of partial melting increases (Bougault et al., 1980). The ratio of Ba/Nb is higher in lower basalt (12.8-17.7) than in the upper basalt (12.3), further indicating that the upper basalt has formed by a low degree of partial melting than the lower basalts.

5.2 Petrogenesis of Felsic Rocks

Felsic volcanic rocks, including rhyolite lava, rhyolitic ignimbrite and tuff, are exposed across the study area. In a bimodal volcanic suite, the origin of silicic volcanic rocks has been a major topic of debate for the last several decades (Feyissa et al., 2017; Dereje Ayalew et al., 2018) and various models have been proposed to explain their origin. The three most popular models are: (i) low-pressure fractional crystallization of the associated basaltic magma with or without crustal assimilation (e.g. Baker et al., 2000; Dereje Ayalew et al., 2002), (ii) partial melting of underplated basalt and (iii) partial melting of an old continental crust (crustal anatexis) (e.g. Davies and Macdonald, 1987; Macdonald et al., 1987 as sited in Dereje Ayalew et al., 2018). The role of these processes in relation to the genesis of felsic rocks in the study area are discussed below. However, to arrive at valid petrogenetic conclusions, it is crucial first to ascertain whether all the samples of the suite are cogenetic or not.

To determine whether all the samples of the suite are cogenetic or not, both major and trace element geochemistry are very important (Wilson, 2007). Although the studied rocks have defined two distinct clusters, nearly all of their major elements have defined a good correlation, either positive

or negative, against the differentiation index SiO_2 (Fig. 4.2. (A-H)). This suggests that all of the studied volcanic rocks are genetically related. Moreover, most of the samples have defined a strong linear trend passing through the origin in the bivariate plots of incompatible trace element pairs (Ta, Hf and Nb vs. Zr; Fig. 4.8), suggesting further that the studied volcanic rocks were derived from a common source (Dereje Ayalew et al., 2018). Additionally, the felsic rocks are found in association with the basalts in the same volcanic field with the felsic lavas constrained as being relatively younger, thus it is quite possible that they could have a common origin.

According to Peccerillo et al. (2007 and references therein), magmas formed by melting of crustal rocks preserve or increase LILE/HFSE ratios (e.g. Rb/Nb, La/Nb, Rb/Zr), as LILE are more incompatible than HFSE during crustal anatexis. To assess the possibility of crustal melting for their genesis, the geochemistry of Ethiopian Precambrian rocks that constitute the basement is compared with the chemical result of felsic samples (see Table 5.1). In the Table, trace element ratios of rhyolites/ignimbrites from the nearby volcanic suite (i.e. Debre Birhan and Wegele Tena rhyolites), supposed to be generated by fractional crystallization of basaltic magma (Dereje Ayalew et al., 2002), are also shown for comparison. The comparison shows that Shewa Robit rhyolites have incompatible trace element ratios lower than the average trace element ratios for the Ethiopian Precambrian rocks similar to Debre Birhan and Wegele Tena rhyolites. This implies that felsic rocks of the Shewa Robit bimodal volcanic suite are not originated from partial melting of the crust. Instead, the geochemical features of the rhyolites are consistent with their derivation from mantle-derived basaltic magma by low-pressure fractionation.

Table 5.1: Trace element characteristics of the Shewa Robit rhyolites/ignimbrites compared with Debre Birhan and Wegel Tena rhyolites/ignimbrites as well as with Precambrian rocks of Ethiopia. The number in parentheses corresponds to the number of analyses used to calculate the mean values.

	Rb/Nb	La/Nb	Rb/Zr
Shewa Robit	1.0-2.14	1.0-1.26	0.15-0.24
Debre Birhan	1.01 (9)	0.91 (9)	0.12 (9)
Wegel Tena	1.17 (23)	1.06 (23)	0.16 (23)
Southern and eastern Ethiopia metamorphic rock	7.72 (13)	---------	0.45 (13)

Data sources: Debre Birhan & Wegel Tena, Dereje Ayalew et al. (2002); Southern and Eastern Ethiopia metamorphic rock, Mengist Teklay et al. (1998)

Furthermore, it has been demonstrated by several studies (e.g. Hanson, 1978; Peccerillo et al., 2003; Dereje Ayalew et al., 2018) that a log-log plot of highly incompatible trace element (e.g. Rb) against highly compatible trace element (e.g. Sr) is a powerful tool to discriminate between fractional crystallization and melting processes. This is because both batch and fractional partial melting processes can generate liquids with variable enrichments in incompatible elements, whereas fractional crystallization is much more efficient in producing compatible element depletion than incompatible element enrichment. In the variation diagram of Sr (compatible element) against Rb (incompatible element) (Fig. 5.3A), the studied volcanic rocks show a wide change of Sr concentrations within a limited change in Rb concentrations. This shows that mafic and felsic volcanic rocks of the study area are linked through a fractional crystallization process. This interpretation is also supported by the variation diagram of the element versus element ratio (La vs. La/Yb). In such a diagram, partial melting and fractional crystallization produce contrasting trends (Janousek et al., 2016; Wu et al., 2019; Verma et al., 2020). The felsic rocks fit the fractional crystallization trend (Fig. 5.3B), providing additional evidence for a derivation from a basaltic parent, as previously discussed. Furthermore, it is demonstrated that fractional crystallization is the only process to maintain unchanged ratios of incompatible trace elements (e.g. Zr/Nb) in a suite of volcanic rocks (e.g. Barberi et al., 1975; Wilson, 1989; Kurkura Kabeto et al., 2009; Dereje Ayalew et al., 2018). Thus, the constancy of Zr/Nb (Fig. 4.8B; avg. =~8.5) ratios throughout the studied samples support the inference that fractional crystallization has been the dominant process to occur in their evolution. In addition to this, the sum of REEs within the volcanic suite generally varies from 111.9 to 268.4 ppm in mafic rocks and from 422.3 to 642.3 ppm in felsic rocks. Although the rhyolites differ from the basalts in terms of their depletion in Eu, Ba, Sr, P and Ti, their trace element spider-diagrams (Fig. 5.3B) and chondrite-normalized REE (Fig. 5.3A) patterns still show similarities with those of the basalts. Thus, the parallel to a sub-parallel pattern in the REE and multi-element variation diagrams combined with the increment of incompatible element abundances from mafic to felsic rocks suggest that fractional crystallization was the dominant process in the evolution of the volcanic suite (Dereje Ayalew and Gibson, 2009; Wilson, 2007).

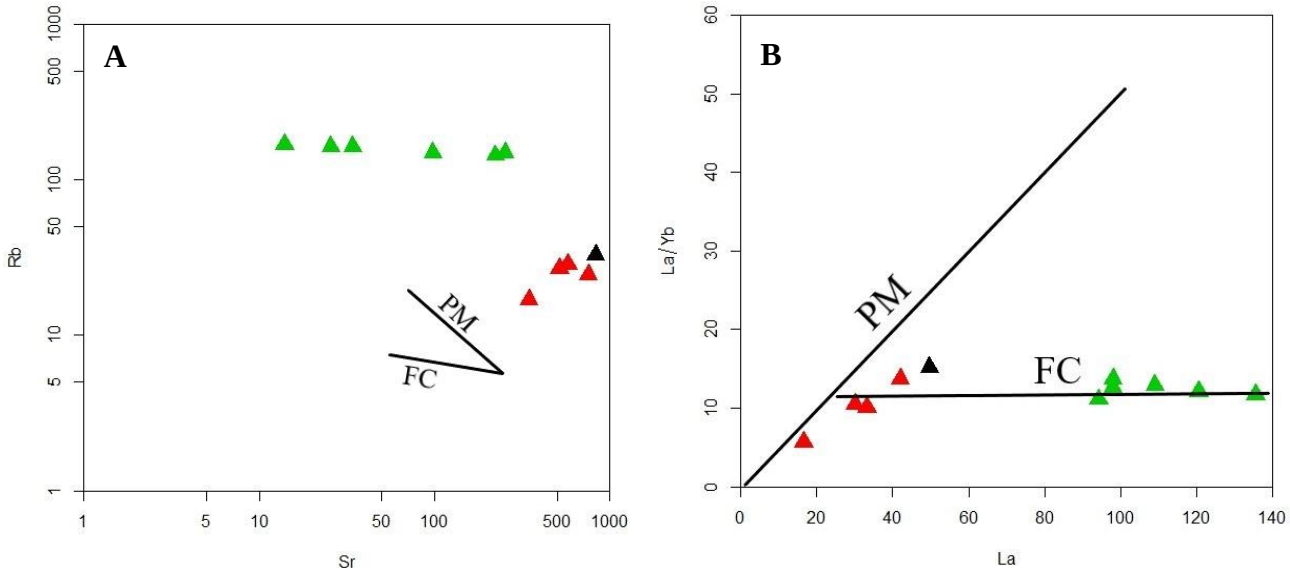

Fig. 5.2: (A) A log-log plot of Sr vs. Rb, displaying a wide variation in Sr concentration interpreted as a fractional crystallization-controlled origin for the rhyolites. (B) La (ppm) vs. La/Yb plot of the Shewa Robit bimodal volcanism. It also notes that the felsic rocks are derived by the fractional process. PM-partial melting, FC-fractional melting

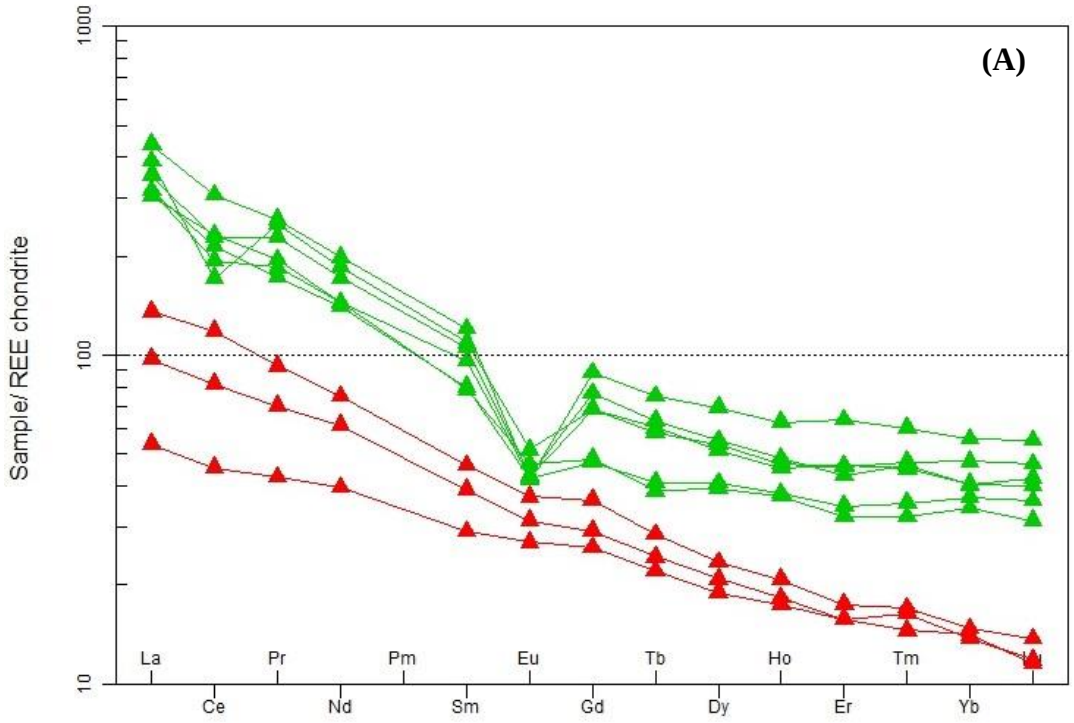

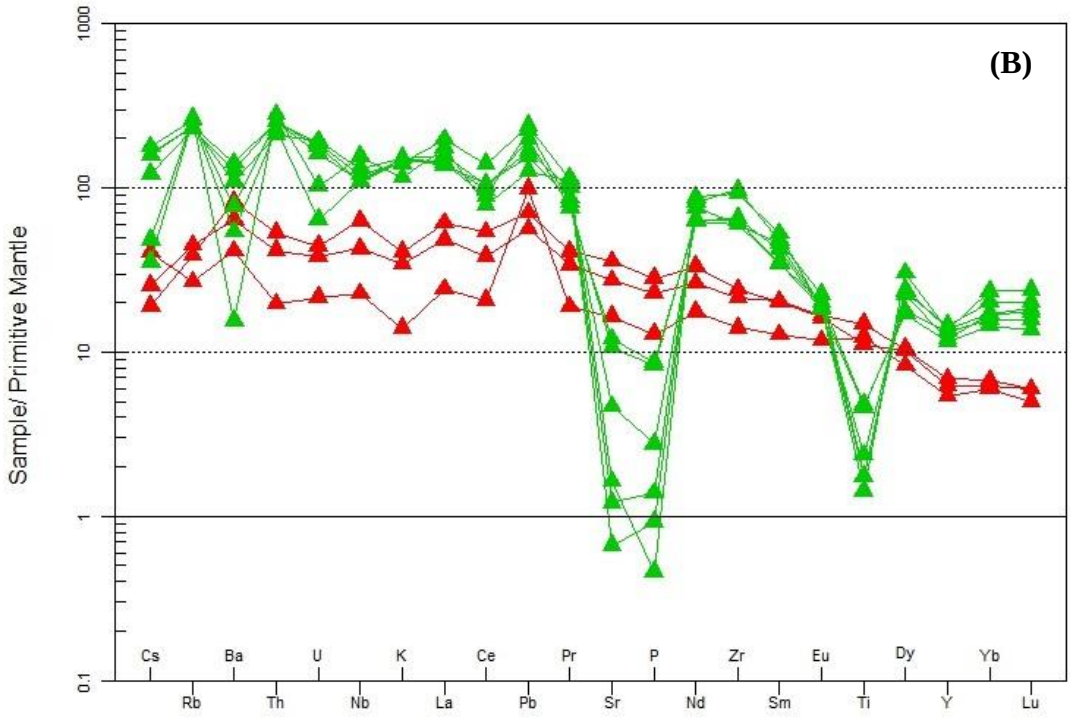

Fig. 5.3: Chondrite-normalized (Boynton, 1984) REE diagram (A) and primitive mantle-normalized (Sun and McDonough, 1989) multi-element variation diagram (B).

5.2.1 Fractional Crystallization

As indicated in Fig. 4.3 (A to H), major element variation diagrams of the studied samples have defined more or less continuous trends, marking the liquid line of descent. This indicates that the geochemical evolution of the volcanic suite is governed by fractional crystallization of different minerals (Dereje Ayalew et al., 2016). The sharp and steep negative correlations of Fe_2O_3, MgO and CaO with SiO_2 indicate that the first phases of crystallizing minerals are Fe- and Mg- bearing mineral phases (olivine and clinopyroxene). Their trends change from steep negative to the gentler slope, implying that Fe- and Mg- bearing mineral removal is less dominant in silicic magma relative to mafic. Following the fractionation of olivine and pyroxene, plagioclase fractionates from the system depicted by the late dropping of the Al_2O_3 trend line after some concentration of SiO_2. The decreasing trend in TiO_2 against SiO_2, indicating that Fe-Ti oxides such as magnetite were involved in the fractionating assemblage. The variation plot of K_2O vs. SiO_2 (wt. %) content depicts an inflected trend with an increasing trend in mafic rocks and decreasing for the most evolved felsic rocks. This indicates that the role of K-feldspar fractionation was important in the

last stage of the magmatic evolution, during the formation of felsic rocks. As suggested in the petrographic section, this is consistent with the presence of euhedral to anhedral phenocrysts of alkali feldspar (sanidine) in the phenocrysts assemblage of felsic samples.

Moreover, the role of the fractionation process in the evolution of the Shewa Robit volcanic rocks is also observed in their trace element geochemistry. The plots of the compatible trace elements (Ni, Cr, V, Sc and Sr) against SiO_2 show a negative correlating line and incompatible trace elements (e.g. Nb, Hf and Ta) against Zr show positive trend lines that favor the fractionation process. The marked decrease in the abundance of compatible trace elements such as Ni (from 163 to <1) ppm and Cr (from 60 to <10) ppm confirms that fractional crystallization of olivine and clinopyroxene has been important in the early evolution of the suite. The basaltic rocks have high concentrations of Sr (831-346 ppm) and V (445–199 ppm), reflecting a lack of significant plagioclase and Fe–Ti oxides fractionation in the early stages of differentiation (Dereje Ayalew & Gibson, 2009). This is also supported by the lack of negative anomaly at Eu, Sr and Ti in their REE plot and multi-element diagrams (Fig. 4.10A and 4.11A). On the other hand, the chondrite normalized REE diagram of rhyolites shows a negative anomaly at Eu that indicates the fractionation of plagioclase feldspar. On their multi-element variation diagram, rhyolitic samples exhibit troughs at Ba, Sr, Ti and P give further evidence for the fractionation of alkali feldspar, plagioclase, Fe-Ti oxides (e.g. ilmenite/magnetite) and apatite from the system.

In summary, the variations in major and trace element concentrations and petrographic observations indicate that fractionation of olivine, clinopyroxene, plagioclase, K-feldspar, apatite and Fe-Ti oxide or opaque minerals has occurred during the evolution of the Shewa Robit bimodal basalt - rhyolite volcanic suite.

CHAPTER SIX

6 CONCLUSION AND RECOMMENDATION

6.1 Conclusion

Based on field observations, petrographic and geochemical data (major and trace elements) obtained in the present study, the following points have been drawn:

- Petrographically, the lower basalts are aphyric to porphyritic with the plagioclase dominant phenocryst, the upper basalt is aphyric dominantly composed of plagioclase and the felsic rocks are porphyritic dominated by quartz and K-feldspar (sanidine) phenocrysts and glassy groundmass.

- The geochemistry result shows that the analyzed rocks are bimodal, which lacks intermediate composition. The rock types include basalts, trachy-basalts (Hawaiite), basaltic-andesite and rhyolites. The lower basalts are tholeiitic to transitional, the upper basalt shows alkaline affinity and the silicic rocks are dominantly sub-alkaline rhyolites.

- The geochemistry result further shows that the two groups of the rocks, mafic and felsic, have the same source. The whole-rock geochemical composition suggests that the Shewa Robit mafic rocks were derived from the melting of amphibole-bearing spinel peridotite source, whereas the rhyolite rocks were derived from the basaltic rocks (i.e. lower basalt) by the fractional crystallization process. The variations in major and trace element concentrations and petrographic studies indicate that fractionation of olivine, clinopyroxene, plagioclase, K-feldspar, apatite and Fe-Ti oxide or opaque minerals occurred during the evolution of the Shewa Robit bimodal basalt - rhyolite volcanic suite.

- Trace element ratios indicate that both basaltic groups (lower and upper basalts) were derived from the same origin and were originated from a common OIB like enriched mantle source but lower basalts show some contamination.

- Geochemical content comparison of Shewa Robit bimodal volcanic suite with the plateau formations shows that all basalts have a very similar geochemical pattern with HT1 type of NW Ethiopia continental flood basalt whereas the trace element ratios of the Shewa Robit rhyolites agree with Debre Birhan and Wegel Tena rhyolites.

6.2 Recommendations

The present study has reached the above conclusions based on field observations, petrographic description and geochemical data interpretations. However, to fully understand the magmatic evolution of the Shewa Robit volcanic rocks, the following studies are recommended for future works:

- Further studies by increasing the amount of sampling and field techniques to map the non-accessible areas
- Isotope geochemistry is a strong tool to understand magma evolution. Hence, more samples for geochemical analysis and isotope geochemistry is suggested for further substantiation of the source and petrogenesis of the bimodal basalt-rhyolite rocks.
- Studies on mineral chemistry are also required to determine the qualitative and quantitative mineral composition of the volcanic rock units.

Reference

Abbate, E., Bruni, P., & Sagri, M. (2015). Geology of Ethiopia: A Review and Geomorphological Perspectives. In P. Billi (Ed.), *Landscapes and Landforms of Ethiopia* (pp. 33–64). Springer Netherlands. https://doi.org/10.1007/978-94-017-8026-1_2

Alebachew Beyene and Mohamed Abdelsalam (2005). Tectonics of the Afar Depression: A review and synthesis. *Journal of African Earth Sciences, 41*(1–2), 41–59.

Allègre, C. J., Schiano, P., & Lewin, E. (1995). Differences between oceanic basalts by multitrace element ratio topology. *Earth and Planetary Science Letters, 129*(1–4), 1–12

Asfawossen Asrat, P. Barbey, J. N. Ludden, Reisberg1, G. Gleizes and Dereje Ayalew (2004). Petrology and Isotope Geochemistry of the Pan-African Negash Pluton, Northern Ethiopia: Mafic-Felsic Magma Interactions during the Construction of Shallow-level Calc-alkaline Plutons. *Journal of Petrology*, *45*(6), 1147–1179.

Aydin, F., Schmitt, A. K., Siebel, W., Sönmez, M., Ersoy, Y., Lermi, A., Dirik, K., & Duncan, R. (2014). Quaternary bimodal volcanism in the Niğde Volcanic Complex (Cappadocia, central Anatolia, Turkey): Age, petrogenesis and geodynamic implications. *Contributions to Mineralogy and Petrology*, *168*(5), 1078.

Baker, J., Snee, L., & Menzies, M. (1996). A brief Oligocene period of flood volcanism in Yemen: Implications for the duration and rate of continental flood volcanism at the Afro-Arabian triple junction. *Earth and Planetary Science Letters*, *138*(1–4), 39–55.

Baker, J. A. (2000). Resolving Crustal and Mantle Contributions to Continental Flood Volcanism, Yemen; Constraints from Mineral Oxygen Isotope Data. *Journal of Petrology*, *41*(12), 1805–1820.

Barberi, F., Ferrara, G., Santacroce, R., Treuil, M., & Varet, J. (1975). A Transitional Basalt-Pantellerite Sequence of Fractional Crystallization, the Boina Centre (Afar Rift, Ethiopia). *Journal of Petrology*, *16*(1), 22–56. https://doi.org/10.1093/petrology/16.1.22

Black, R., Morton, W. H., & Varet, J. (1972). New Data on Afar Tectonics. *Nature Physical Science*, *240*(104), 170–173. https://doi.org/10.1038/physci240170a0

Blanford, W. T. (1870). Observations on the geology and zoology of Abyssinia, made during the progress of the British expedition to that country in 1867-68. (pp. 1–544). Macmillan and co, https://doi.org/10.5962/bhl.title.57004

Boccaletti, M., Getaneh, A., Mazzuoli, R., Tortorici, L., & Trua, T. (1995). Chemical variations in a bimodal magma system: the Plio-Quaternary volcanism in the Dera Nazret area (Main Ethiopian Rift, Ethiopia). *Africa Geoscience Review*, *2*(1), 37-60.

Bougault, H., Joron, J.L., and Treuil, M., 1980. The primordial chondritic nature and largescale heterogeneities in the mantle: evidence from high and low partition coefficient elements in oceanic basalts. Phil. Trans. R. Soc. Lond. A, 297(1431), pp.203–213.

Boynton, W. V. (1984). Cosmochemistry of the Rare Earth Elements: Meteorite Studies. In *Developments in Geochemistry* (Vol. 2, pp. 63–114). Elsevier.

Brotzu, P., Ganzerli-Valentini, M. T., Morbidelli, L., Piccirillo, E. M., Stella, R., & Traversa, G. (1981). Basaltic volcanism in the northern sector of the main Ethiopian rift. *Journal of Volcanology and Geothermal Research*, *10*, 365–382.

Chorowicz, J., Collet, B., Bonavia, F., & Korme, T. (1999). Left-lateral strike-slip tectonics and gravity-induced individualization of wide continental blocks in the western Afar margin. *Eclogae Geologicae Helvetiae*, *92*(1), 149–158.

Corti, G., Bastow, I. D., Keir, D., Pagli, C., & Baker, E. (2015). Rift-Related Morphology of the Afar Depression. In P. Billi (Ed.), *Landscapes and Landforms of Ethiopia* (pp. 251–274). Springer Netherlands. https://doi.org/10.1007/978-94-017-8026-1_15

Daniel Meshesha & Shinjo, R. (2007). Crustal contamination and diversity of magma sources in the northwestern Ethiopian volcanic province. *Journal of Mineralogical and Petrological Sciences*, *102*(5), 272–290. https://doi.org/10.2465/jmps.061129

Daniel Meshesha, Dejene Hailemariam and Abraham Mamo (2010). Geology of Debre Birhan Area. Unpublished technical report, Memoir, 22

Davidson, A., & Rex, D. C. (1980). Age of volcanism and rifting in southwestern Ethiopia. *Nature*, *283*(5748), 657–658. https://doi.org/10.1038/283657a0

Davies, G. R., & Macdonald, R. (1987). Crustal Influences in the Petrogenesis of the Naivasha Basalt--Comendite Complex: Combined Trace Element and Sr-Nd-Pb Isotope Constraints. *Journal of Petrology*, *28*(6), 1009–1031. https://doi.org/10.1093/petrology/28.6.1009

Dereje Ayalew, Gezahegn Yirgu & Pik, R. (1999). Geochemical and isotopic (Sr, Nd and Pb) characteristics of volcanic rocks from southwestern Ethiopia. *Journal of African Earth Sciences*, *29*(2), 381–391. https://doi.org/10.1016/S0899-5362(99)00104-9

Dereje Ayalew (2000). Origin by fractional crystallization of transitional basalt for the Asela-Ziway Pantellerites. Crustal control in the genesis of Plio-Quaternary bimodal magmatism of the Main Ethiopian Rift (MER): Geochemical and isotopic (Sr, Nd, Pb) evidence by Trua et al. (1999). *Chemical Geology*, *168*(1–2), 1–3. https://doi.org/10.1016/S0009-2541(00)00182-0

Dereje Ayalew, Barbey, P., Marty, B., Reisberg, L., Gezahegn Yirgu and Pik, R. (2002). Source, genesis, and timing of giant ignimbrite deposits associated with Ethiopian continental flood basalts. *Geochimica et Cosmochimica Acta*, *66*(8), 1429–1448. https://doi.org/10.1016/S0016-7037(01)00834-1

Dereje Ayalew and Gezahegn Yirgu (2003). Crustal contribution to the genesis of Ethiopian plateau rhyolitic ignimbrites: Basalt and rhyolite geochemical provinciality. *Journal of the Geological Society*, *160*(1), 47–56. https://doi.org/10.1144/0016-764901-169

Dereje Ayalew, D., Ebinger, C., Bourdon, E., Wolfenden, E., Gezahegn Yirgu, & Grassineau, N. (2006). Temporal compositional variation of syn-rift rhyolites along the western margin of the southern Red Sea and northern Main Ethiopian Rift. *Geological Society, London, Special Publications*, *259*(1), 121–130. https://doi.org/10.1144/GSL.SP.2006.259.01.10

Dereje Ayalew and Gibson, S. A. (2009). Head-to-tail transition of the Afar mantle plume: Geochemical evidence from a Miocene bimodal basalt–rhyolite succession in the Ethiopian Large Igneous Province. *Lithos*, *112*(3–4), 461–476.

Dereje Ayalew (2011). The relations between felsic and mafic volcanic rocks in continental flood basalts of Ethiopia: Implication for the thermal weakening of the crust. *Geological Society, London, Special Publications*, *357*(1), 253–264. https://doi.org/10.1144/SP357.13

Dereje Ayalew, Jung, S., Romer, R. L., Kersten, F., Pfänder, J. A., & Garbe-Schönberg, D. (2016). Petrogenesis and origin of modern Ethiopian rift basalts: Constraints from isotope and trace element geochemistry. *Lithos, 258–259*, 1–14. https://doi.org/10.1016/j.lithos.2016.04.001

Dereje Ayalew, Pik, R., Bellahsen, N., France, L., & Yirgu, G. (2018). Differential Fractionation of Rhyolites during the Course of Crustal Extension, Western Afar (Ethiopian Rift). *Geochemistry, Geophysics, Geosystems*, *20*(2), 571–593.

Ebinger, C. J., Yemane, T., Woldegabriel, G., Aronson, J. L., & Walter, R. C. (1993). Late Eocene–Recent volcanism and faulting in the southern main Ethiopian rift. *Journal of the Geological Society*, *150*(1), 99–108. https://doi.org/10.1144/gsjgs.150.1.0099

Ebinger, C., & Sleep, N. (1998). Cenozoic magmatism throughout east Africa resulting from the impact of a single plume. *Nature*, *395*. https://doi.org/10.1038/27417

Feyissa, D. H., Shinjo, R., Kitagawa, H., Meshesha, D., & Nakamura, E. (2017). Petrologic and geochemical characterization of rift-related magmatism at the northernmost Main Ethiopian Rift: Implications for plume-lithosphere interaction and the evolution of rift mantle sources. *Lithos*, *282–283*, 240–261. https://doi.org/10.1016/j.lithos.2017.03.011

Furman, T. (2007). Geochemistry of East African Rift basalts: An overview. *Journal of African Earth Sciences*, *48*(2–3), 147–160.

Gani, N., Gani, M., & Salam, M. A. (2007). Blue Nile Incision on the Ethiopian Plateau: Pulsed Plateau Growth, Pliocene Uplift, and Hominin Evolution. *GSA Today*, *17*(9), 4–11. https://doi.org/10.1130/GSAT01709A.1

Gasparon, M., Innocenti, F., Manetti, P., Peccerillo, A., & Tsegaye, A. (1993). Genesis of the Pliocene to recent bimodal mafic-felsic volcanism in the Debre-Zeyt area, central Ethiopia: Volcanological and geochemical constraints. *Journal of African Earth Sciences (and the Middle East)*, *17*(2), 145–165. https://doi.org/10.1016/0899-5362(93)90032-L

George, R., Rogers, N., & Kelley, S. (1998). Earliest magmatism in Ethiopia: Evidence for two mantle plumes in one flood basalt province. *Geology*, *26*(10), 923–926. https://doi.org/10.1130/0091-7613(1998)026<0923:EMIEEF>2.3.CO;2

Gezahegn Yirgu, Ebinger, C. J., & Maguire, P. K. H. (2006). The Afar volcanic province within the East African Rift System: Introduction. *Geological Society, London, Special Publications*, *259*(1), 1–6. https://doi.org/10.1144/GSL.SP.2006.259.01.01

Gidey Woldegabriel, Aronson, J. L., & Walter, R. C. (1990). Geology, geochronology, and rift basin development in the central sector of the Main Ethiopia Rift. *Geological Society of America Bulletin*, *102*(4), 439-458.

Girson, I. L. (1972). The Chemistry and Petrogenesis of a Suite of Pantellerites from the Ethiopian Rift. *Journal of Petrology*, *13*(1), 31–44. https://doi.org/10.1093/petrology/13.1.31

Giordano, F., D'Antonio, M., Civetta, L., Tonarini, S., Orsi, G., Ayalew, D., Yirgu, G., Dell'Erba, F., Di Vito, M. A., & Isaia, R. (2014). Genesis and evolution of mafic and felsic magmas

at Quaternary volcanoes within the Main Ethiopian Rift: Insights from Gedemsa and Fanta 'Ale complexes. *Lithos*, *188*, 130–144. https://doi.org/10.1016/j.lithos.2013.08.008

Hammond, J. O. S., Kendall, J.-M., Stuart, G. W., Keir, D., Ebinger, C., Ayele, A., & Belachew, M. (2011). The nature of the crust beneath the Afar triple junction: Evidence from receiver functions: crustal structure beneath afar, Ethiopia. *Geochemistry, Geophysics, Geosystems*, *12*(12),. https://doi.org/10.1029/2011GC003738

Hanson, G N. (1980). Rare Earth Elements in Petrogenetic Studies of Igneous Systems. *Annual Review of Earth and Planetary Sciences*, *8*(1), 371–406.

Hanson, Gilbert N. (1978). The application of trace elements to the petrogenesis of igneous rocks of granitic composition. *Earth and Planetary Science Letters*, *38*(1), 26–43. https://doi.org/10.1016/0012-821X(78)90124-3

Hart, W. K., Gidey WoldeGabriel, Walter, R. C., & Mertzman, S. A. (1989). Basaltic volcanism in Ethiopia: Constraints on continental rifting and mantle interactions. *Journal of Geophysical Research: Solid Earth*, *94*(B6), 7731–7748.

Hofmann, A. W., Jochum, K. P., Seufert, M., & White, W. M. (1986). Nb and Pb in oceanic basalts: New constraints on mantle evolution. *Earth and Planetary Science Letters*, *79*(1–2), 33–45. https://doi.org/10.1016/0012-821X(86)90038-5

Hofmann, C., Courtillot, V., Féraud, G., Rochette, P., Gezahegn Yirgu, Ketefo, E., & Pik, R. (1997). Timing of the Ethiopian flood basalt event and implications for plume birth and global change. *Nature*, *389*(6653), 838–841. https://doi.org/10.1038/39853

https://en.climatedata.org/africa/ethiopia/amhara/shoa-robit-31824/

Hunegnaw, A., Sage, L., & Gonnard, R. (1998). Hydrocarbon potential of the intracratonic Ogaden basin, ETHIOPIA. *Journal of Petroleum Geology*, *21*(4), 401–425.

Irvine, T. N., & Baragar, W. R. A. (1971). A Guide to the Chemical Classification of the Common Volcanic Rocks. *Canadian Journal of Earth Sciences*, *8*(5), 523–548.

Janousek, V., Moyen, J.-F., Martin, H., Erban, V., & Farrow, C. (2016). *Geochemical Modelling of Igneous Processes – Principles And Recipes in R Language: Bringing the Power of R to a Geochemical Community*. Springer-Verlag. https://doi.org/10.1007/978-3-662-46792-3

Kazmin, V. (1979). Stratigraphy and correlation of Cenozoic volcanic rocks in Ethiopia. *Reports of Ethiopian Institute of Geological Survey*, *106*, 1-26.

Kieffer, B., Arndt, N., Lapierre, H., Bastien, F., Bosch, D., Pecher, A., Gezahegn Yirgu, Dereje Ayalew, Weis, D., Jerram, D. A., Keller, F., & Meugniot, C. (2004). Flood and Shield Basalts from Ethiopia: Magmas from the African Super swell. *Journal of Petrology*, *45*(4), 793–834. https://doi.org/10.1093/petrology/egg112

Kurkura Kabeto, Sawada, Y., & Roser, B. (2009). Compositional Differences between Felsic Volcanic rocks from the Margin and Center of the Northern Main Ethiopian Rift. *Momona Ethiopian Journal of Science*, *1*(1). https://doi.org/10.4314/mejs.v1i1.46039

Lahitte, P., Gillot, P.-Y., & Courtillot, V. (2003). Silicic central volcanoes as precursors to rift propagation: The Afar case. *Earth and Planetary Science Letters*, *207*(1–4), 103–116. https://doi.org/10.1016/S0012-821X(02)01130-5

Le Bas, M. J. L., Maitre, R. W. L., Streckeisen, A., Zanettin, B., & IUGS Subcommission on the Systematics of Igneous Rocks. (1986). A Chemical Classification of Volcanic Rocks Based on the Total Alkali-Silica Diagram. *Journal of Petrology*, *27*(3), 745–750. https://doi.org/10.1093/petrology/27.3.745

Macdonald, R., Davies, G. R., Bliss, C. M., Leat, P. T., Bailey, D. K., & Smith, R. L. (1987). Geochemistry of High-silica Peralkaline Rhyolites, Naivasha, Kenya Rift Valley. *Journal of Petrology*, *28*(6), 979–1008. https://doi.org/10.1093/petrology/28.6.979

Makris, J., & Ginzburg, A. (1987). The Afar Depression: Transition between continental rifting and sea-floor spreading. *Tectonophysics*, *141*(1–3), 199–214.

Mengist Teklay, Kröner, A., Mezger, K. and Oberhänsli, R. (1998). Geochemistry, Pb-Pb single zircon ages and Nd-Sr isotope composition of Precambrian rocks from southern and eastern Ethiopia: implications for crustal evolution in East Africa. *Journal of African Earth Sciences* 26(2):207-227.

Mengesha Tefera, Tadiwos Chernet and Workineh Haro (1996).Exploration of the geological map of Ethiopia (1:20,000,000). Ethiopian institutes of geological surveys. Unpublished technical report, Addis Ababa, Ethiopia, 83pp.

Miruts Hagos, Koeberl, C., & van Wyk de Vries, B. (2016). The Quaternary volcanic rocks of the northern Afar Depression (northern Ethiopia): Perspectives on petrology, geochemistry, and tectonics. *Journal of African Earth Sciences*, *117*, 29–47.

Mohr, P. 1962. The Ethiopian rift system. Bulletin of the Geophysical Observatory, Addis Ababa 5, 33-62.

Mohr, P. (1983). Ethiopian flood basalt province. *Nature*, *303*(5918), 577–584. https://doi.org/10.1038/303577a0

Mohr, P., & Zanettin, B. (1988). The Ethiopian Flood Basalt Province. In J. D. Macdougall (Ed.), *Continental Flood Basalts* (Vol. 3, pp. 63–110). Springer Netherlands. https://doi.org/10.1007/978-94-015-7805-9_3

Mulugeta Alene, Hart, W. K., Saylor, B. Z., Deino, A., Mertzman, S., Haile-Selassie, Y., & Gibert, L. B. (2017). Geochemistry of Woranso–Mille Pliocene basalts from west-central Afar, Ethiopia: Implications for mantle source characteristics and rift evolution. *Lithos*, *282–283*, 187–200. https://doi.org/10.1016/j.lithos.2017.03.005

Natali, C., Beccaluva, L., Bianchini, G., & Siena, F. (2011). Rhyolites associated to Ethiopian CFB: Clues for initial rifting at the Afar plume axis. *Earth and Planetary Science Letters*, *312*(1–2), 59–68. https://doi.org/10.1016/j.epsl.2011.09.059

Pearce, J. A. (2008). Geochemical fingerprinting of oceanic basalts with applications to ophiolite classification and the search for Archean oceanic crust. *Lithos*, *100*(1–4), 14–48. https://doi.org/10.1016/j.lithos.2007.06.016

Peccerillo, A. (2003). Relationships between Mafic and Peralkaline Silicic Magmatism in Continental Rift Settings: A Petrological, Geochemical and Isotopic Study of the Gedemsa Volcano, Central Ethiopian Rift. *Journal of Petrology*, *44*(11), 2003–2032. https://doi.org/10.1093/petrology/egg068

Peccerillo, A., Donati, C., Santo, A. P., Orlando, A., Gezahegn Yirgu, & Dereje Ayalew (2007). Petrogenesis of silicic peralkaline rocks in the Ethiopian rift: Geochemical evidence and volcanological implications. *Journal of African Earth Sciences*, *48*(2–3), 161–173. https://doi.org/10.1016/j.jafrearsci.2006.06.010

Pik, R., Deniel, C., Coulon, C., Gezahegn Yirgu, Hofmann, C., & Dereje Ayalew, (1998). The northwestern Ethiopian Plateau flood basalts: Classification and spatial distribution of magma types. *Journal of Volcanology and Geothermal Research*, *81*(1), 91–111. https://doi.org/10.1016/S0377-0273(97)00073-5

Pik, R., Deniel, C., Coulon, C., Gezahegn Yirgu, & Marty, B. (1999). Isotopic and trace element signatures of Ethiopian flood basalts: Evidence for plume–lithosphere interactions.

Geochimica et Cosmochimica Acta, *63*(15), 2263–2279. https://doi.org/10.1016/S0016-7037(99)00141-6

Pik, R., Bellahsen, N., Leroy, S., Denèle, Y., Razin, P., Ahmed, A., & Khanbari, K. (2013). Structural control of basement denudation during rifting revealed by low-temperature (U–Th–Sm)/He thermochronology of the Socotra Island basement—Southern Gulf of Aden margin. *Tectonophysics*, *607*, 17–31. https://doi.org/10.1016/j.tecto.2013.07.038

Rollinson, H. R. (1993). Using geochemical data: Evaluation, presentation, interpretation: Longman Group UK Ltd., 352 pp.

Ronga, F., Lustrino, M., Marzoli, A., & Melluso, L. (2010). Petrogenesis of a basalt-comendite-Pantellerite rock suite: The Boseti Volcanic Complex (Main Ethiopian Rift). *Mineralogy and Petrology*, *98*(1–4), 227–243. https://doi.org/10.1007/s00710-009-0064-3

Rooney, T.O., Mohr, P., Dosso, L., Hall, C., (2013). Geochemical evidence of mantle reservoir evolution during progressive rifting along the western Afar margin. Geochimica et Cosmochimica Acta 102, 65–88. https://doi.org/10.1016/j.gca.2012. 08.019.

Rooney, T. O., Lavigne, A., Svoboda, C., Girard, G., Yirgu, G., Ayalew, D., & Kappelman, J. (2017). The making of an underplate: Pyroxenites from the Ethiopian lithosphere. *Chemical Geology*, *455*, 264–281. https://doi.org/10.1016/j.chemgeo.2016.09.011

Rosenthal, A., Foley, S. F., Pearson, D. G., Nowell, G. M., & Tappe, S. (2009). Petrogenesis of strongly alkaline primitive volcanic rocks at the propagating tip of the western branch of the East African Rift. *Earth and Planetary Science Letters*, *284*(1–2), 236–248. https://doi.org/10.1016/j.epsl.2009.04.036

Rudnick, R., & Gao, S. (2003). Composition of the Continental Crust. Treatise Geochem 3:1-64. *Treatise on Geochemistry*, *3*, 1–64. https://doi.org/10.1016/B0-08-043751-6/03016-4

Samson Tesfaye, S., Harding, D. J., & Kusky, T. M. (2003). Early continental breakup boundary and migration of the Afar triple junction, Ethiopia. *Geological Society of America Bulletin*, *115*(9), 1053. https://doi.org/10.1130/B25149.1

Samson Tesfaye & Weldia Ghebreab (2013). Simple shear detachment fault system and marginal grabens in the southernmost Red Sea rift. *Tectonophysics*, *608*, 1268–1279. https://doi.org/10.1016/j.tecto.2013.06.014

Siefemichael Berhe, Berhe Desta, Nicoletti, M., & Mengesha Teferra (1987). Geology, geochronology and geodynamic implications of the Cenozoic magmatic province in W and

SE Ethiopia. *Journal of the Geological Society*, *144*(2), 213–226. https://doi.org/10.1144/gsjgs.144.2.0213

Stab, M., Bellahsen, N., Pik, R., Quidelleur, X., Ayalew, D., & Leroy, S. (2016). Modes of rifting in magma-rich settings: Tectono-magmatic evolution of Central Afar. *Tectonics*, *35*(1), 2–38. https://doi.org/10.1002/2015TC003893

Sun, S., & McDonough, W. F. (1989). Chemical and isotopic systematics of oceanic basalts: Implications for mantle composition and processes. *Geological Society, London, Special Publications*, *42*(1), 313–345. https://doi.org/10.1144/GSL.SP.1989.042.01.19

Tadiwos Chernet, Hart, W.K., Aronson, J.L. and Walter, R.C. (1998). New age constraints on the timing of volcanism and tectonism in the northern Main Ethiopian Rift-southern Afar transition zone (Ethiopia). Journal of Volcanology and Geothermal Research, 80: 267–280.

Tigel Belay, Ilfios, T., Abiy, A., Genet, Y., Teferi, Z., Henok, B., … Tadesse, A. (2009). Geology of the WereIlu Area. Unpublished technical report, Memoir, 25

Trua, T., Deniel, C., & Mazzuoli, R. (1999). Crustal control in the genesis of Plio-Quaternary bimodal magmatism of the Main Ethiopian Rift (MER): Geochemical and isotopic (Sr, Nd, Pb) evidence. *Chemical Geology*, *155*(3–4), 201–231. https://doi.org/10.1016/S0009-2541(98)00174-0

Ukstins, I. A., Renne, P. R., Wolfenden, E., Baker, J., Ayalew, D., & Menzies, M. (2002). Matching conjugate volcanic rifted margins: 40Ar/39Ar chrono-stratigraphy of pre-and syn-rift bimodal flood volcanism in Ethiopia and Yemen. *Earth and Planetary Science Letters*, *198*(3), 289–306. https://doi.org/10.1016/S0012-821X(02)00525-3

Verma, S. K., Acosta Fimbres, K. G., Torres-Sánchez, D., Torres Hernández, J. R., Torres-Sánchez, S. A., & López-Loera, H. (2020). Geochemistry and petrogenesis of oligocene felsic volcanic rocks from the Pinos Volcanic Complex, Mesa Central, Mexico. *Journal of South American Earth Sciences*, *102*, 102704.

Walter, R. C., Hart, W. K., & Westgate, J. A. (1987). Petrogenesis of a basalt-rhyolite tephra from the west-central Afar, Ethiopia. *Contributions to Mineralogy and Petrology*, *95*(4), 462–480. https://doi.org/10.1007/BF00402206

Weaver, B. L. (1991). Trace element evidence for the origin of ocean island basalts. *Geology*, *19*(2), 123-126.

White, W. M. (2005). Geochemistry. John Wiley & Sons.

Williams, F. M. (2016). *Understanding Ethiopia: Geology and Scenery*. Springer International Publishing. https://doi.org/10.1007/978-3-319-02180-5

Wilson, M., (1989). Igneous petrogenesis: a global tectonic approach. *Harper Collins Academic, London*, 466p.

Wilson, B. M. (2007). Igneous petrogenesis: a global tectonic approach. *Springer Science & Business Media.*

Wolfenden, E., Ebinger, C., Yirgu, G., Deino, A., & Ayalew, D. (2004). Evolution of the northern Main Ethiopian rift: Birth of a triple junction. *Earth and Planetary Science Letters*, *224*(1), 213–228. https://doi.org/10.1016/j.epsl.2004.04.022

Wolfenden, E., Ebinger, C., Yirgu, G., Renne, P. R., & Kelley, S. P. (2005). Evolution of a volcanic rifted margin: Southern Red Sea, Ethiopia. *Geological Society of America Bulletin*, *117*, 846–864.

Wu, T., Wang, X., Li, W., Wilde, S. A., & Tian, L. (2019). Petrogenesis of the ca. 820–810 Ma felsic volcanic rocks in the Bikou Group: Implications for the tectonic setting of the western margin of the Yangtze Block. *Precambrian Research*, *331*, 105370. https://doi.org/10.1016/j.precamres.2019.105370

Zanettin, B., & Justin-Visentin, E. (1975). Tectonical and volcanological evolution of the western Afar margin (Ethiopia*)* (pp. 300-309). E. Schweizerb. Verlag.

Zwaan, F., Corti, G., Keir, D., & Sani, F. (2019). A review of tectonic models for the rifted margin of Afar: Implications for continental break-up and passive margin formation. *Journal of African Earth Sciences*, 103649. https://doi.org/10.1016/j.jafrearsci.2019.103649

Appendix I

Petrographic analysis results for lower basalt and rhyolitic ignimbrite samples

Thin section code	Formation	Location (UTM)	Average modal proportion (%)		Average grain shape
Y01	Lower Basalt	0600160 1114008	Plagioclase	25 %	Subhedral
			Groundmass	75 %	Microcrystalline
AR1	Lower Basalt	0590588 1092277	Plagioclase	8 %	Euhedral
			pyroxene	2 %	Euhedral
			Groundmass	90 %	Microcrystalline
SR14	Lower Basalt	0599527 1112042	Plagioclase	25 %	Subhedral
			Groundmass	75 %	Fine-grained opaque minerals+Glassy
SR5	Lower Basalt	0594586 1101372	Plagioclase	13 %	Eu– subhedral
			pyroxene	2 %	Subhedral
			olivine	2 %	Subhedral
			opaque	3 %	Anhedral
			Groundmass	80 %	Glassy material
SR2	Lower Basalt	0592926 1108162	Plagioclase	40 %	Subhedral
			pyroxene	5 %	Anhedral
			olivine	5 %	Anhedral
			opaque	15 %	Anhedral
			Glassy materials	35 %	
SR8	Rhyolitic-Ignimbrite	0604063 1099179	Quartz	5 %	Eu-subhedral
			Sanidine	5 %	Subhedral
			Groundmass	90 %	Glassy+cryptocrytaline flatten grains
Y02	Rhyolitic-Ignimbrite	0602481	Quartz	3 %	Subhedral
			Sanidine	10 %	Subhedral

		1110906	Rock fragment	2 %	Anhedral
			Groundmass	85 %	Glassy material
SR10	Rhyolitic-Ignimbrite	0605485 1105478	Quartz	5 %	Anhedral
			Fiamme	5 %	Flattened shape
			Groundmass	90 %	Glassy material
SR1	Rhyolitic-Ignimbrite	0591756 1109286	Quartz	5 %	Anhedral
			Rock fragment	2 %	Anhedral
			Groundmass	93 %	Glassy material
SR9	Rhyolitic-Ignimbrite	0592646 1116302	Quartz	3 %	Anhedral
			Sanidine	7 %	Euhedral
			Groundmass	90 %	Glassy material

Appendix II

Structural Data

Name		Orientation	
		Strike	Dip
	F1	005	80E
	F2	010	83SE
	F3	008	85SE
	F4	030	82SE
Normal faults	F5	025	80SE
	F6	015	79SE
	F7	010	83NW
	F8	005	84W
	F9	040	86NW
	F10	030	79NW
	F11	005	80W

Appendix III

Recalculated (volatile free basis) major element data for the Shewa Robit bimodal volcanic rocks

	Basalt					Rhyolite					
Sample	SR6	Y01	AR1	SR2	SR5	SR9	SR1	DC5	DC4	SR7	SR8
SiO2	47.61	50.53	52.75	47.87	48.63	76.22	79.68	74.33	73.40	69.86	70.75
TiO2	3.76	2.41	2.66	2.71	3.23	0.38	0.39	0.52	0.33	1.00	1.06
Al2O3	16.16	19.72	14.91	14.28	14.61	10.92	7.93	12.03	11.60	13.88	12.64
Fe2O3	12.88	9.16	11.16	15.30	13.85	3.76	4.37	3.81	4.69	4.40	4.51
MnO	0.22	0.14	0.17	0.22	0.23	0.10	0.13	0.09	0.09	0.09	0.10
MgO	4.55	3.17	4.63	5.72	5.11	0.14	0.19	0.25	1.26	0.44	0.44
CaO	8.75	9.25	9.32	10.27	9.75	0.20	0.26	0.97	0.48	1.27	1.25
Na2O.	3.62	3.86	2.91	2.75	3.19	4.62	3.48	3.31	3.66	4.52	4.46
K2O	1.71	1.24	1.08	0.43	0.89	3.62	3.56	4.62	4.46	4.34	4.62
P2O5	0.73	0.51	0.42	0.45	0.50	0.03	0.02	0.06	0.01	0.19	0.18

Appendix IV

Selected normalized and trace element ratio values.

sample	SR6	Y01	AR1	SR2	SR5	SR9	SR1	DC5	DC4	SR7	SR8
La/Nb	1.09	0.93	1.13	1.02	1.09	1.41	1.09	1.01	1.58	1.26	1.25
Zr/Nb	7.82	6	7.67	9.69	7.9	8.64	9.86	7.85	12.05	8.72	9.02
La/Ta	20.71	21	18.81	18.44	18.14	22.71	15.65	15.19	16.13	22.25	22.27
Rb/Nb	0.72	0.55	1.01	1.05	0.93	2.14	1.53	1.6	1.91	1.93	1.83
Ce/Pb	19.96	19.06	6.6	5.23	17.05	15.29	15.39	17.05	14.59	12.36	9.78
Nb/U	44.47	48.39	42.9	36	38.13	57.61	51.16	23.17	21.87	20.75	23.09
Ba/La	11.39	13.74	18.31	17.29	13.43	3.45	0.9	8.12	3.99	10.12	9.15
Ba/Nb	12.36	12.82	20.71	17.72	14.62	4.87	0.98	8.17	6.32	12.8	11.43
Tb/Yb	0.47	0.44	0.4	0.35	0.41	0.36	0.28	0.34	0.31	0.25	0.26
Nb/Yb	13.96	14.66	9.3	5.51	9.24	9.18	11.15	11.04	7.37	10.04	10.98
Eu/Eu*	0.86	0.91	0.93	0.98	0.92	0.48	0.59	0.52	0.41	0.68	0.76
(La/Yb)N	10.22	9.66	7.1	3.81	6.78	8.74	8.2	7.49	7.88	8.56	9.24
(La/Sm)N	2.46	3.08	2.49	1.84	2.29	3.34	3.56	3.17	3.64	3.95	4.03
(Eu/Yb)N	2.91	2.52	2.29	1.92	2.41	1.07	1.08	1.05	0.76	1.14	1.36
(Gd/Yb)N	2.75	2.47	2.13	1.84	2.32	1.9	1.45	1.68	1.59	1.28	1.41
(Tb/Yb)N	2..08	1.94	1.77	1.56	1.79	1.57	1.22	1.48	1.35	1.11	1.13

Appendix V

Major element and selected trace element data of LT, HT1 and HT2 basaltic groups (From Pik et al., 1998).

Type:	LT							HT1			
Sample:	E166	E168	E171	E178	E181	PM6	E210	E59	E66	E70	E54
SiO_2	50.15	49.95	48.65	49.1	48.63	51.06	47.46	49.85	50.68	48.62	50.33
TiO_2	1.58	2.1	1.88	1.98	1.32	1.8	2.26	3.06	3.99	3.39	3.45
Al_2O_3	15.9	15.3	14.78	15.58	16.5	15.37	17.15	14.38	12.46	14.2	13.82
Fe_2O_3)	11.9	12.03	13.26	13	10.45	12.44	13.66	13.3	14.84	13.54	13.68
MnO	0.19	0.3	0.21	0.18	0.17	0.16	0.17	0.2	0.2	0.22	0.25
MgO	6.42	5.62	5.65	6.41	7.76	5.46	5.96	5.45	4.33	5.1	4.9
CaO	11.53	11.1	11.07	10.7	11.26	10.25	7.69	10.32	8.61	8.84	8.49
Na_2O	2.61	2.82	2.71	2.34	2.91	2.87	3.72	2.63	2.52	3.16	3.3
K_2O	0.27	0.59	0.24	0.27	0.56	0.43	0.58	0.66	1.03	0.89	0.84
P_2O_5	0.17	0.26	0.23	0.25	0.2	0.24	0.34	0.31	0.44	0.89	0.85
Total	101.25	100.93	99.11	100.43	100.44	99.92	99.11	101.12	100.74	100.03	100.72
Mg#	52.76	49.16	46.87	50.51	60.59	47.6	47.46	45.89	37.67	43.82	42.58
CaO/Al_2	0.73	0.73	0.75	0.69	0.68	0.67	0.45	0.72	0.69	0.62	0.61
Y	28.7	39.9	36.1	32.1	26.1	34.7	31	33.2	43.9	38.5	37.9
Nb	6.3	7.7	4.5	6.3	9.5	5.31	6.2	24.2	36	21	21
La	7.9	11.95	7.76	13.37	9.38	8.7	8.8	18.8	29	27	27

HT1		HT2								
E235	E236	E31	E33	E35	E37	E38	E40	E225	E226	E232
48.33	48.11	46.02	46.8	46.92	46.69	47.49	45.95	48.27	44.99	46.15
2.69	2.45	4.02	4.28	4.62	4.99	3.79	3.92	2.62	3.77	4.39
13.96	13.79	7.88	9.95	11.49	10.9	9.38	7.67	9.57	8.11	9.78
13.54	13.35	13.46	14.67	14.07	14.66	12.81	13.74	13.1	13.79	13.1
0.19	0.19	0.18	0.2	0.19	0.18	0.17	0.18	0.18	0.18	0.19
5.44	6.26	14.71	10.6	7.05	6.84	13.61	16.1	13.51	15.97	10
9.4	11.02	9.01	9.81	10.35	9.91	8.81	9.22	10.1	8.68	9.53
2.9	2.59	1.67	2.2	2.46	2.48	1.9	1.55	1.84	1.48	3.25
0.83	0.36	0.86	0.72	0.77	1.11	1.13	0.43	0.41	0.96	1.21
0.41	0.22	0.47	0.43	0.51	0.59	0.45	0.4	0.28	0.44	0.57
1.08	0.87	1.57	1.16	1.56	1.95	1.34	1.05	0.3	1.29	1.41
0.37	0.78	0.32	0.36	0.38	0.76	0.32	0	0.45	0.63	0.27
99.14	99.99	99.13	99.97	99.21	100.12	100.4	99.08	100.63	100.29	99.85